



**Faculty of Science and Technology**

## **MASTER'S THESIS**

Study program/ Specialization:  Master of Science/Offshore Technology (Marine and Subsea Technology)	Spring semester, 2016  Open access
Writer: Malakonda Reddy Lekkala	..... (Writer's signature)
Faculty supervisor: Professor Muk Chen Ong  External supervisor(s): Dr. Jie Wu	
Thesis title: Numerical Simulation of VIV of Risers with Staggered Buoyancy Elements	
Credits (ECTS): 30	
Key words:  Numerical Simulation VIV Riser Staggered Buoyancy elements	Pages: 64  + enclosure: 16  Stavanger, 15 June/2016

# **Numerical Simulation of VIV of Riser with Staggered Buoyancy Elements**

Malakonda Reddy Lekkala

15 June 2016

Department of Mechanical and Structural Engineering and Materials  
Science

University of Stavanger

Advisors: Professor Muk Chen Ong, Dr. Jie Wu

## **Preface**

This thesis is submitted in partial fulfilment of the requirements for the degree of Master of Science (MSc) in Offshore Technology with the specialization Marine and Subsea Technology at the University of Stavanger (UiS), Stavanger, Norway.

It has been completed in cooperation with Dr. Jie Wu, MARINTEK, Trondheim, Norway and under the supervision of Professor Muk Chen Ong, University of Stavanger, during the period January to June 2016.

## Abstract

Steel Lazy Wave Riser (SLWR) is an attractive deep water riser system design, which allows the platform motion to be decoupled from the touchdown point (TDP) of the riser. When subjected to external flow, both buoyancy element and bare riser section may experience Vortex Induced Vibrations (VIV). Such vibrations are the results of the periodic hydrodynamic forces that are induced by the interaction of slender bodies and external fluid flow. If the vibration period is close to the natural period of the system, it can lead to fast accumulation of fatigue damage to the risers and amplified drag loads. The vortex shedding frequency of the buoyancy element is lower than that of the bare riser section due to its larger diameter. These two shedding process will interact and influence the VIV responses. Such interaction depends on many parameters, e.g. buoyancy element dimensions and their arrangement.

Semi-empirical VIV prediction programs, such as VIVANA, SHEAR7 and VIVA are the most commonly used industrial VIV prediction tools. These programs rely on hydrodynamic force coefficient database generated from forced motion test with a rigid cylinder section. However, these database may not be valid for a flexible cylinder with buoyancy elements. Therefore, there are strong needs to obtain force coefficient database, taking into account the influences of the riser and buoyancy element interaction. In present work, the existing riser with staggered buoyancy VIV model test is reviewed. The prediction using VIVANA with default hydrodynamic force coefficient database is evaluated. A new way of obtaining an optimal database directly from VIV tests of a flexible cylinder with staggered buoyancy element is investigated. The hydrodynamic force coefficient database is parameterized and the representative parameters are systematically varied until the predicted frequency, mode and fatigue damage agree well with experimental results. The improvements and uncertainties are also discussed.

## **Acknowledgement**

This master thesis is written by M.Sc. student Malakonda Reddy Lekkala during the spring semester of 2016 at Department of Mechanical and Structural Engineering and Materials Science.

First of all, I wish to thank my supervisor Professor Muk Chen Ong for guiding me through this study. I benefit a lot by his valuable ideas and suggestion. His patience and encouragement are specially appreciated.

I wish to thank my external supervisor Dr. Jie Wu from MARINTEK for patient explanation of basic principles, for providing new ideas, spending time to discuss my problems, providing MATLAB code and helpful support regard the code.

I am grateful to my supportive parents, fellow students and good friends, SS and Neha Reddy. This semester would not have been the same without you.

Thanks to Stavanger for being such a great city to live and study for the past two years.

Malakonda Reddy Lekkala  
June 14, 2016  
Stavanger

# Table of Contents

<b>Preface</b> .....	<b>i</b>
<b>Abstract</b> .....	<b>ii</b>
<b>Acknowledgement</b> .....	<b>iii</b>
<b>List of Figures</b> .....	<b>vi</b>
<b>List of Table</b> .....	<b>ix</b>
<b>Nomenclature</b> .....	<b>x</b>
<b>Chapter 1 Introduction</b> .....	<b>1</b>
1.1 Background and Motivation .....	1
1.2 Purpose .....	2
1.3 Thesis Outline.....	2
<b>Chapter 2 Fundamentals of VIV</b> .....	<b>4</b>
2.1 Introduction .....	4
2.2 Non-dimensional Parameters.....	5
2.3 Vortex Shedding .....	6
2.3.1 Flow Regimes of Flow around a Circular, Smooth Cylinder .....	6
2.3.2 Vortex Formation and Boundary Layer .....	7
2.3.3 Vortex-Shedding Frequency .....	9
2.4 VIV of a Elastically Mounted Cylinder.....	10
2.5 Lock-in.....	11
2.6 Experimental Methods for Investigation of VIV.....	12
2.6.1 Rigid Cylinder Free Oscillation Tests.....	12
2.6.2 Rigid Cylinder Forced Oscillation Tests.....	13
2.7 Methods to Predict VIV.....	15
<b>Chapter 3 VIVANA Software</b> .....	<b>16</b>
3.1 Introduction .....	16
3.1.1 Program Structure .....	16
3.1.2 Analysis Options .....	18
3.2 Method Overview .....	18
3.3 Time Sharing and Space Sharing.....	19
3.3.1 Time Sharing.....	19
3.3.2 Space Sharing.....	20
3.4 Frequency Response Method.....	21
3.5 Hydrodynamic Coefficients.....	22
3.5.1 Added Mass Coefficient.....	22

3.5.2 Excitation Coefficients.....	24
<b>Chapter 4 Description of the Shell Experiment.....</b>	<b>27</b>
4.1 Experimental Setup.....	27
4.2 Experiment Description.....	28
4.2.1 Riser Model Configuration .....	28
4.2.2 Test Arrangement.....	31
4.3 Test Results.....	31
4.3.1 Response Frequency .....	31
4.3.2 Maximum Fatigue Damage.....	33
4.3.3 Response Amplitude .....	34
<b>Chapter 5 VIVANA Simulation with Default Parameters .....</b>	<b>35</b>
5.1 Presentation of Results and Comparison with Experiment results.....	36
5.1.1 Response Frequency .....	36
5.1.2 Maximum Fatigue Damage .....	36
5.1.3 Response Amplitude .....	37
5.2 Uncertainties .....	39
5.2.1 Uncertainties in the Extraction of the Test Results.....	39
5.2.2 Uncertainties in the Default Force Coefficient Parameters .....	39
<b>Chapter 6 Modification of Hydrodynamic Coefficients .....</b>	<b>40</b>
6.1 Default Excitation Coefficient Database in VIVANA .....	40
6.1.1 Change in Range of Non-dimensional Frequency .....	41
6.1.2 Amplitude Ratio Modification .....	43
6.1.3 Excitation Coefficient Modification .....	44
6.2 Procedure to Obtain an Optimal Set of Parameters .....	44
6.2.1 Generating New Set of Excitation Parameters.....	44
6.3 Testing the Algorithm of VIVANA for Bare Riser.....	47
6.4 Testing the Algorithm of VIVANA for a Riser with Staggered Buoyancy Elements ...	51
<b>Chapter 7 Prediction of an Optimal Set of Excitation Parameters .....</b>	<b>55</b>
7.1 Experimental Results.....	55
7.2 VIVANA Analysis Results.....	55
7.3 Discussion and Conclusion.....	62
<b>Chapter 8 Recommendations for Further Work .....</b>	<b>64</b>
<b>References .....</b>	<b>65</b>
<b>Appendix .....</b>	<b>67</b>

## List of Figures

Figure 1 A schematic of SLWR (Jhingran et al., 2012) .....	1
Figure 2 An example configuration of SLWR (Li. & Nguyen., 2010) .....	2
Figure 3 Left: vortex shedding, right: CF and IL motions (Sumer & Fredsøe, 2006) .....	4
Figure 4 Relationship between Strouhal number and Reynolds number (Blevins, 1994) .....	7
Figure 5 Classical vortex patterns behind a fixed cylinder (Sumer & Fredsøe, 2006). .....	8
Figure 6 Boundary layer separation (Sumer & Fredsøe, 2006) .....	8
Figure 7 (a): Prior to shedding of Vortex A, B is being drawn across the wake. (b): Prior to shedding B, Vortex C is being drawn across the wake (Sumer & Fredsøe, 2006).....	9
Figure 8 Motion of cylinder due to vortex shedding (Le Cunff et al., 2002).....	10
Figure 9 The lower figure shows maximum response amplitude in IL and CF direction, while the upper figure shows the corresponding response trajectory at mid-span (Aronsen, 2007). .....	11
Figure 10 Lock in (Sumr & fredsoe, 1997) .....	12
Figure 11 Free oscillation test set-up (Larsen, 2011).....	12
Figure 12 Response amplitudes for three cylinders with different weights (Larsen, 2011) ....	13
Figure 13 An example of CF + IL trajectory (Larsen).....	14
Figure 14 Contours of the CF added mass coefficient (Gopalkrishnan, 1993).....	15
Figure 15 Examples of slender structures that can be analysed by VIVANA (Passano et al., 2015) .....	16
Figure 16 The overall structure of VIVANA (Passano et al., 2015).....	17
Figure 17 Illustration of time sharing process (Passano et al., 2015) .....	20
Figure 18 Space sharing process (Passano et al., 2015).....	20
Figure 19 Contour plot of the CF added mass coefficients based on forced harmonic motions (Gopalkrishnan, 1993) .....	22
Figure 20 Contour plot of the CF added mass coefficients based on forced harmonic motions (Passano et al., 2015) .....	23
Figure 21 The VIVANA model for added mass as a function of frequency for IL response (Passano et al., 2015) .....	23
Figure 22 The VIVANA model for added mass as a function of frequency for CF VIV (Passano et al., 2015) .....	24
Figure 23 Contour plot curves for the IL excitation coefficient (Gopalkrishnan, 1993). .....	24
Figure 24 Contour plot curves for CF excitation coefficient (Gopalkrishnan, 1993) .....	25

Figure 25 Three point excitation coefficient curve for pure IL response (Passano et al., 2015)	26
Figure 26 Three point excitation coefficient curve for CF response (Passano et al., 2015) ....	26
Figure 27 (a) the riser and buoyancy mode (b) the riser during experiments (Jhingran et al., 2012).	27
Figure 28 Test setup and coordinate system; upper: front view; lower: top view (Jhingran et al., 2012).	28
Figure 29 Definition of gap lengths and buoyancy segment lengths (Jhingran et al., 2012) ...	29
Figure 30 The buoyancy modules as half cylinders with central groove to accommodate the riser (Jhingran et al., 2012).	29
Figure 31 Staggered buoyancy configurations over the riser (Rao et al., 2015).....	30
Figure 32 Frequency associated with bare section plotted against flow speed (Rao et al., 2015)	32
Figure 33 Frequency associated with buoyancy section against flow speed (Rao et al., 2015)	32
Figure 34 Max. fatigue damage rate plotted against flow velocity (Rao et al., 2015) .....	33
Figure 35 Reconstructed CF displacements for configuration 2-2 at $U = 1.0$ m/s (Rao et al., 2015)	34
Figure 36 Riser with staggered buoyancy elements model in VIVANA .....	35
Figure 37 Predicted frequency components with default set of parameters (Wu et al., 2016)	36
Figure 38 Predicted fatigue damage with default set of parameters (Wu et al., 2016) .....	37
Figure 39 Predicted CF amplitude with default set of parameters for 2-2 configuration at 1.0 m/s (Wu et al., 2016)	38
Figure 40 Snapshots of CF displacement with default set of parameters for 2-2 configuration at 1.0 m/s (Wu et al., 2016)	38
Figure 41 Strouhal number as a function of Reynolds number (Larsen C M et al., 2009) .....	40
Figure 42 Black curve: default CF excitation coefficient curve at particular non-dimensional frequency in VIVANA, Blue curve: after amplitude modification, red curve: after excitation coefficient modification (Yin et al., 2015).....	41
Figure 43 Parameterization of the excitation coefficient curves.....	41
Figure 44 Algorithm showing how to obtain an optimal set of excitation coefficient parameters	46
Figure 45 Fatigue damage comparison for different sets of excitation coefficient parameters	48
Figure 46 Comparison of accumulated fatigue damage between Test no. 2197 and default case.	49

Figure 47 Comparison between the contour curves of A) default set of parameters and B) set of parameters for Test no. 2197. ....	50
Figure 48 Fatigue damage comparison for different sets of excitation coefficient parameters	52
Figure 49 Comparison of max. accumulated fatigue damage between Test no. 2430 and default case.....	53
Figure 50 Comparison between contour curves of default set of parameters (left plot) and set of parameters for S-Test no. 2430 (right plot) .....	54
Figure 51 Fatigue damage comparison for different sets of excitation coefficient parameters	56
Figure 52 Fatigue damage for test cases that showed similar behaviour. ....	57
Figure 53 Fatigue damage comparison for S-Test no. 3827. ....	58
Figure 54 Predicted CF A/D with optimal set of parameters for 2/2 configuration at 1.0 m/s	59
Figure 55 Comparison between measured response frequency and predicted response frequency .....	60
Figure 56 Comparison between measured fatigue damage, fatigue damage for optimal set of parameters and for default set of parameters. ....	61
Figure 57 Contour plot for optimal set of parameters. ....	61

## List of Table

Table 1 Configurations of buoyancy modules (Jhingran et al., 2012) .....	30
Table 2 Pipe model properties (Rao et al., 2015).....	31
Table 3 The summary of $S_t$ for bare riser and staggered buoyancy riser (Rao et al., 2015) ....	33
Table 4 Default set of parameters from VIVANA (Passano et al., 2015).....	42
Table 5 Default set of parameters (Passano et al., 2015) .....	43
Table 6 Default set of excitation coefficient parameters (Passano et al., 2015) .....	45
Table 7 New sets of excitation parameters for different modification factors for a riser with staggered buoyancy elements. ....	45
Table 8 New sets of excitation parameters for different modification factors for a bare riser.	47
Table 9 Bare riser model properties. ....	48
Table 10 Specified criteria for selecting the best set of parameters. ....	49
Table 11 Set of parameters which gave good prediction to the default parameters.....	49
Table 12 Response values for the default set of parameters and Test no. 2197.....	50
Table 13 New sets of excitation parameters for different modification factors for a bare riser. ....	51
Table 14 Properties of the Riser with staggered buoyancy elements for VIVANA analysis. .	52
Table 15 Specified criteria for selecting the best set of parameters. ....	53
Table 16 Set of parameters which gave good prediction to the default parameters.....	53
Table 17 Response values for the default set of parameters and Test no. 2197.....	54
Table 18 Extracted values from experiment for 2/2 configuration at 1.0 m/s (Figure 34 ) ....	55
Table 19 Test cases that showed similar behaviour with the experiment. ....	57
Table 20 Specified criteria for selecting an optimal set of parameters .....	57
Table 21 Optimal set of parameters with their modification factors.....	58
Table 22 Results from VIVANA for S-Test no. 3827 .....	58
Table 23 Comparision between experimental results and VIVANA analysis for different flow speeds for 2/2 configuration with an optimal set of excitation parameters. ....	60
Table 25 Comparision between experimental and VIVANA analysis results .....	63

# Nomenclature

## General

- Symbols are generally defined where they appear in the text for the first time
- Only the most used symbols are listed in the following section
- Symbols and identifiers are kept unique, as far as practical
- Over-dots signify differentiation with respect to time.

## Abbreviations

CF	Cross Flow
CFD	Computational Fluid Dynamics
DNV	Det Norske Veritas
FEM	Finite Element Method
IL	In Line
Max.	Maximum
RMS	Root Mean Square
RIFLEX	Static and Dynamic Analysis Program for Slender Marine Structures
SCR	Steel Catenary Riser
SLWR	Steel Lazy Wave Riser
TDP	Touch Down Point
VIV	Vortex Induce Vibration
VIVANA	Vortex Induced Vibrations Analysis Program

## Roman Symbols

A	Response Amplitude
$\left(\frac{A}{D}\right)_{IL/CF}$	Amplitude ratio for IL or CF
$\left(\frac{A}{D}\right)_{Ce=0}$	Amplitude when excitation is equal to zero
C	Damping coefficient matrix
Ca	Added mass coefficient
$C_D$	Drag coefficient
$C_{e,IL/CF}$	Excitation parameter
$C_H$	Hydrodynamic damping matrix
$C_S$	Structural damping matrix
D	Cylinder diameter
$f_0$	Natural frequency of the structure
$f_{osc}$	Oscillation frequency
$f_v$	Strouhal frequency
$\hat{f}$	Dimensionless frequency

$K$	Stiffness matrix
$m$	mass per unit length of the cylinder
$m^*$	Mass ration
$M$	Mass matrix
$M_H$	Hydrodynamic mass matrix
$M_S$	Structural mass matrix
$r$	Displacement
$\dot{r}$	Velocity
$\ddot{r}$	Acceleration
$R$	external load
$Re$	Reynolds number
$S_t$	Strouhal number
$U$	Current velocity
$V_r$	Reduced velocity

### Greek symbols

$\rho$	Density of fluid
$\nu$	Kinematic viscosity of the fluid
$\omega$	Frequency



# Chapter 1 Introduction

## 1.1 Background and Motivation

As oil and gas exploration ventures into harsher environment, engineers are faced with the appal task of developing new practical riser designs for these new developments. In recent years, Steel Lazy Wave Riser (SLWRs) have provided engineers with riser solutions for a wide variety of field configurations and challenging environment. SLWRs combine the fatigue characteristics of flexible risers with the robustness of conventional Steel Catenary Risers (SCRs). A SLWR is a special SCR with segment of length equipped with external buoyancy modules, where the upward buoyancy force is greater than its downward gravity forces. The SLWR system as shown in Figure 1, depends on buoyancy section in the riser to provide flexibility and enhanced fatigue life. A typical SLWR consists of three segments, namely hang-of catenary, the buoyancy catenary and the touch down catenary as illustrated in Figure 2.

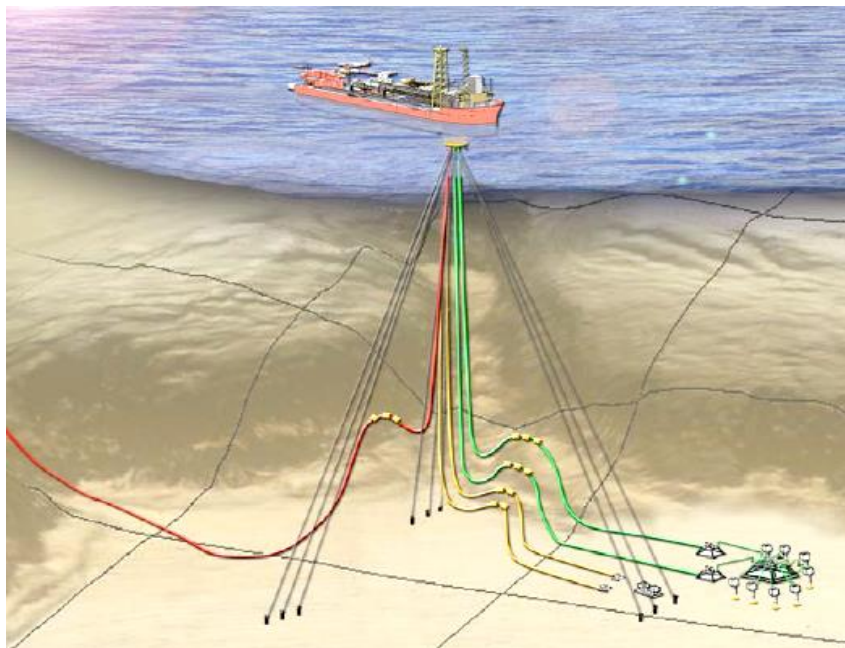


**Figure 1 A schematic of SLWR (Jhingran et al., 2012)**

When current flows over SLWRs, current will lead to separated flow and vortex shedding. These vortices will again lead to periodic forces on structures that may result in horizontal and vertical oscillations. This phenomenon is known as Vortex-Induced Vibrations (VIV) which may lead to accumulation of damage due to fatigue. While considering the VIV fatigue damage, the buoyancy sections of SLWRs becomes critical.

The motivation of the present work is that we still do not have full understanding of VIV of slender marine structures. Various empirical models for prediction of VIV do not give same results, and different experimental methods give diversing conclusions. The effect of change in excitation coefficients are included in empirical models, but the attempt to obtain optimal set of parameters is not defined due to lack of data. Hence an attempt is made to obtain an optimal set of excitation coefficient parameters for VIV prediction.

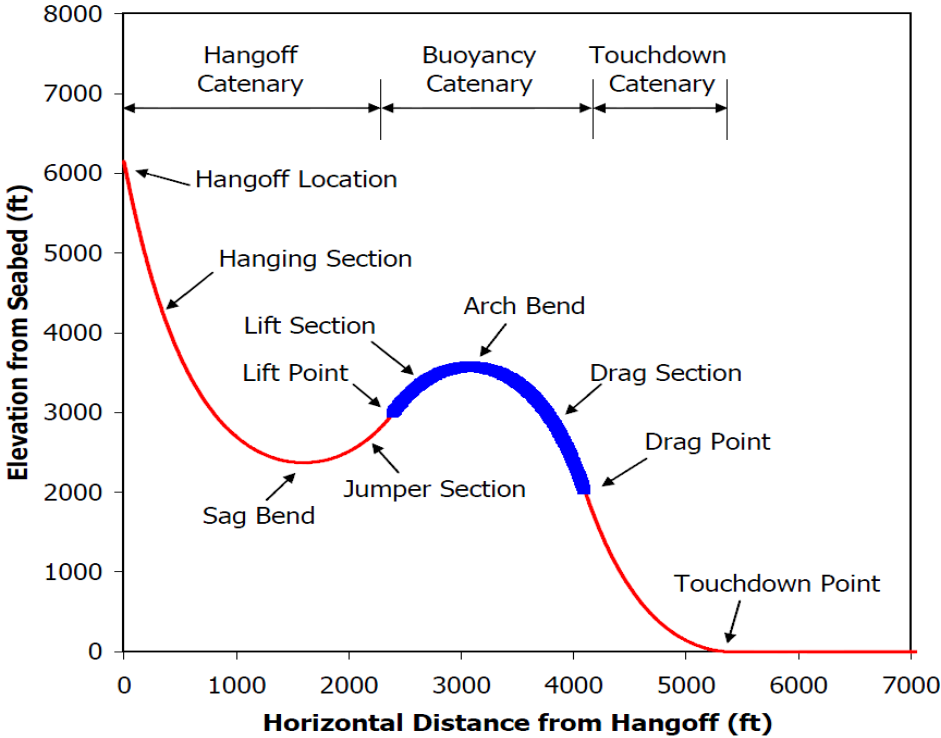


Figure 2 An example configuration of SLWR (Li. & Nguyen., 2010)

**1.2 Purpose**

The purpose of this thesis is to study VIV of a riser with staggered buoyancy elements. Obtain hydrodynamic force coefficient data from experiments and improve present prediction practice.

**1.3 Thesis Outline**

The thesis is divided into the following chapters:

Chapter 2 gives brief overview of the VIV phenomenon and defines some key parameters used in this study. Different experimental methods and studies for investigation of VIV are addressed and a brief introduction to numerical methods for VIV is given.

Chapter 3 a detailed description of the semi-empirical model VIVANA and its controlling parameters.

Chapter 4 gives an overview of the Shell riser VIV tests with staggered buoyancy elements at MARINTEK offshore ocean basin and presents the results.

Chapter 5 presents the VIVANA simulation and compares the experimental results and VIVANA results with default set of parameters and investigate the limitations in the program.

Chapter 6 develops an automatic approach to obtain an optimal set of prediction parameters using information from model tests.

Chapter 7 evaluates the optimal set of parameters for the prediction of VIV of riser with staggered buoyancy elements and gives the discussion and conclusion on the results.

Chapter 8 presents and highlights the contribution from the thesis, and discusses further work following the work performed during this thesis.

# Chapter 2 Fundamentals of VIV

## 2.1 Introduction

Slender marine structures such as risers, anchor lines and free spanning pipelines exposed to ocean currents may experience oscillating motions or vibrations. These vibrations are caused by forces from vortices that shed from both sides of the structure. This phenomenon is called Vortex Induced Vibrations (VIV). The vortex shedding is related to a full periodic cycle of the shedding process. This means that two vortices are shed per cycle, one from each side of the structure as shown in Figure 3. The general requirement for VIV occurrence is that vortex shedding frequency is close to an eigen frequency of the structure.

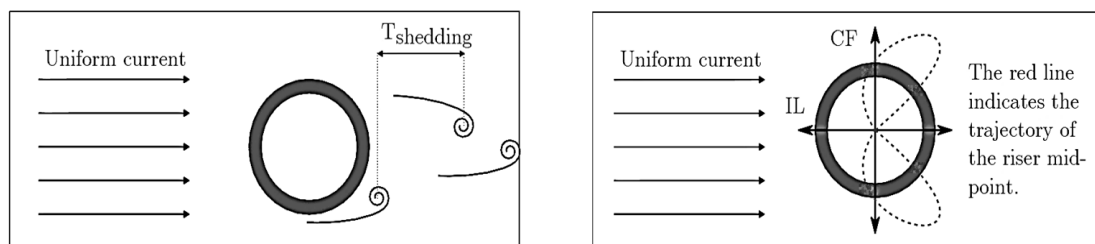


**Figure 3 Left: vortex shedding, right: CF and IL motions (Sumer & Fredsøe, 2006)**

When the vortex shedding frequency of the structure matches with one of the eigen frequencies, the structure starts to oscillate. The structure will experience a lift and a drag force. In relative to the flow, they are defined in local In-Line (IL) – parallel to the incoming flow, Cross-flow (CF) – perpendicular to the incoming flow. This is shown in Figure 3. The lift force will have the same frequency as the vortex shedding, while drag forces will oscillate with twice the frequency. VIV is a vibration at resonance and the vortex shedding frequency will increase for increasing current velocity. As the IL frequency is twice the CF frequency, the structure will start to oscillate at a lower reduced velocity than CF. Pure IL response is important to free-spanning pipeline. But, it is not relevant to deep water riser where combined IL and CF response is of concerned.

In the ocean, the currents usually change direction, magnitude and their velocity profile will never be uniform. To predict a correct current profile is probably the most critical part in the model setup. Experiments and measurements must be performed, but these are not sufficient to get accurate current profiles. Due to variation in the current profile and diameter changes of the riser, multiple modes of the riser can be excited into VIV. This makes VIV prediction of deep water riser more complex than that for risers in shallow water.

## 2.2 Non-dimensional Parameters

A large number of dimensionless parameters are used to describe the vortex induced vibration phenomenon. In the following the parameters used in this thesis are defined.

### **Reynolds number Re:**

Reynolds number is defined as the ratio of inertia force to the friction force acting on the cylinder. This parameter is used to describe the flow pattern behind the cylinder in uniform currents.

Reynolds number at a position along the structure is given as

$$Re = \frac{\text{inertia force}}{\text{friction force}} = \frac{U \times D}{\nu} \quad (1)$$

where U is flow velocity, D is diameter of cylinder,  $\nu$  is kinematic viscosity.

### **Strouhal number $S_t$ :**

This parameter is used to address the vortex shedding frequency for a fixed cylinder in a constant flow.

$$S_t = \frac{f_v \times D}{U} \quad (2)$$

### **Reduced velocity:**

The reduced velocity becomes useful when a structure starts to vibrate due to VIV. The reduced velocity gives the range of velocities that VIV can occur. For each eigen frequency of the structure, the reduced velocity can be determined. For all reduced velocities, vortex shedding will appear but it is often coupled with the amplitude of the vibration. For different values of reduced velocity, the vibration amplitude reaches maximum and becomes “lock-in”. The reduced velocity is given as follows:

$$V_r = \frac{U}{f_0 \times D} \quad (3)$$

where,

$f_0$  = natural frequency of the structure.

### **Non-Dimensional frequency:**

It is used as a controlling parameter for excitation force coefficients and added mass. This is defined as

$$\hat{f} = \frac{f_{osc} \times D}{U} \quad (4)$$

where,

$f_{osc}$  = oscillation frequency

### **Roughness ratio:**

This parameter is used to describe the cylinder surface,

$$\text{Roughness ratio} = \frac{k}{D} \quad (5)$$

where k is surface roughness

### **Mass ratio:**

This is defined as

$$m^* = \frac{\text{mass per unit length of the cylinder}}{\text{fluid density} \times \text{model width}^2} = \frac{m}{\rho \times D^2} \quad (6)$$

The mass ratio is a measure of relative importance of buoyancy and added mass effects on the cylindrical model. It is often used to measure the susceptibility of lightweight structures to the flow-induced vibration.

### **Displacement Amplitude Ratio A/D:**

The displacement amplitude A/D is used to describe displacement amplitude in free vibration experiments and oscillation amplitude in forced oscillation experiments. (Jhingran, Zhang et al., 2012)

$$\left(\frac{A}{D}\right)_{IL/CF} \quad (7)$$

where  $f_{osc}$  is the actual oscillation frequency. IL represent In-Line and CF represents Cross-Flow

## **2.3 Vortex Shedding**

Vortex shedding occurs when an unsteady oscillating flow takes place at certain conditions when a fluid flow around a body, especially around blunt structures. Vortices are generated behind the body of the structure and dissociate periodically from either side of the body which results in formation of Von Karman Vortex Street. Due to periodic shedding, an asymmetrical flow pattern develops around the body and will change the pressure field distribution behind the body. The periodically varying load that arises from the alternatively varying shedding induces vibrations with the same frequency as the frequency of the vortex shedding. After dispersion from the body, the regular pattern of the vortices moves further downside of the structure and the energy is consumed by the viscosity of the flow and pattern gets dissolved.

### **2.3.1 Flow Regimes of Flow around a Circular, Smooth Cylinder**

Vortex shedding from a smooth circular cylinder is a function of Reynolds number. Approximate division of the flow regimes based on Reynolds number is given as follows (Miau et al., 2011)

- Subcritical regime -  $300 < Re < 1.5 \times 10^5$  .
- Transitional regime -  $1.5 \times 10^5 < Re < 3.5 \times 10^5$
- Supercritical regime -  $Re > 3.5 \times 10^5$ .

Experiments have shown that there is a conjunction between Strouhal number and Reynolds number (Dahl et al., 2010). These experiments shows that Strouhal number becomes nearly constant in sub-critical regime ( $3 \times 10^2 < Re < 1.5 \times 10^5$ ). This Strouhal number is also strongly dependent on cylinder surface roughness. This surface roughness influences where the separation of flow occurs around the cylinder and in turn the Reynolds number regime. This states that, if surface is rough, then a low Re is required to enter into critical regime. In general, Reynolds number related to risers is in sub-critical region which corresponds to  $St_t = 0.2$  as shown in Figure 4.

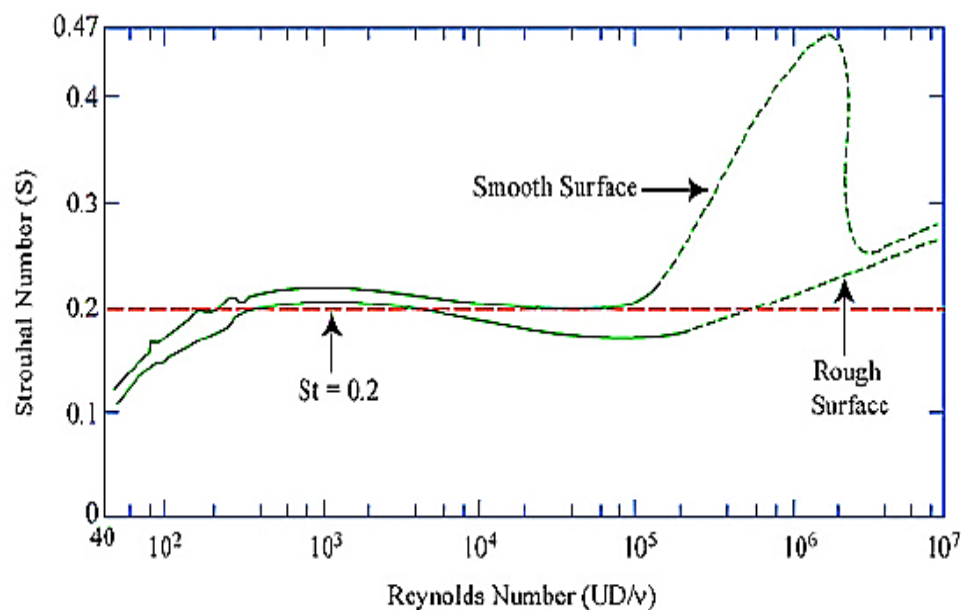


**Figure 4 Relationship between Strouhal number and Reynolds number (Blevins, 1994)**

Vortex shedding appears in all these flow regimes with different patterns. Figure 5, approximately shows how the vortex pattern changes with Reynolds number. One should be aware that the division of flow regimes based on Reynolds number ranges are not definite. Disturbances may have serious effect on the flow and change the Reynolds number ranges on which various flow regimes are seen. Disturbances that may influence the flow may be inflow turbulence, surface roughness and shape imperfections of the cylinder.

### 2.3.2 Vortex Formation and Boundary Layer

The boundary layer is the layer in which the flow is increased from zero at the body surface to the free stream velocity at some distance away from the surface as shown in Figure 6. The fluid field can be categorized into two types (Sumer & Fredsøe, 2006).

- a) Outside the boundary layer where the viscosity is negligible and the flow can be determined by potential theory, i.e. Bernoulli theory is applicable (Figure 6A).  
 b) Near the body surface where the velocity gradient is normal to the surface of the body is large and shear stress are large enough that cannot be neglected (Figure 6B).

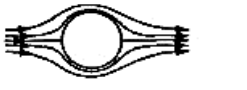
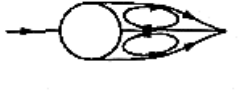
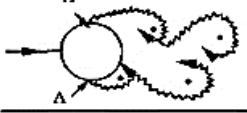
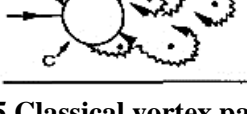
	No separation. Creeping flow	$Re < 5$
	A fixed pair of symmetric vortices	$5 < Re < 40$
	Laminar vortex street	$40 < Re < 200$
	Transition to turbulence in the wake	$200 < Re < 300$
	Wake completely turbulent. A: Laminar boundary layer separation	$300 < Re < 3 \times 10^5$  Subcritical
	A: Laminar boundary layer separation B: Turbulent boundary layer separation; but boundary layer laminar	$3 \times 10^5 < Re < 3.5 \times 10^5$  Critical (Lower transition)
	B: Turbulent boundary layer separation; the boundary layer partly laminar partly turbulent	$3.5 \times 10^5 < Re < 1.5 \times 10^6$  Supercritical
	C: Boundary layer com- pletely turbulent at one side	$1.5 \times 10^6 < Re < 4 \times 10^6$  Upper transition
	C: Boundary layer comple- tely turbulent at two sides	$4 \times 10^6 < Re$  Transcritical

Figure 5 Classical vortex patterns behind a fixed cylinder (Sumer & Fredsøe, 2006).

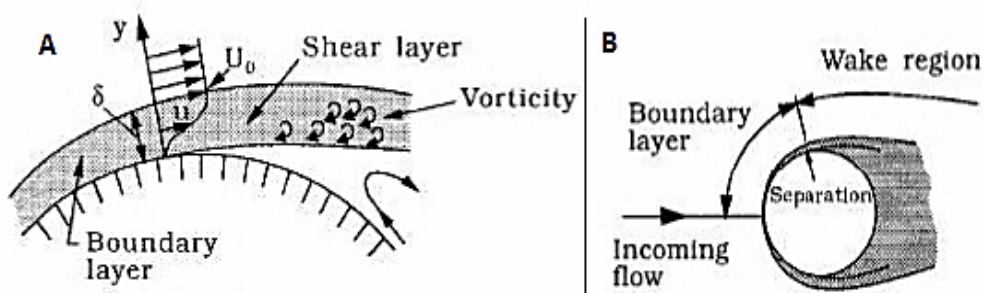
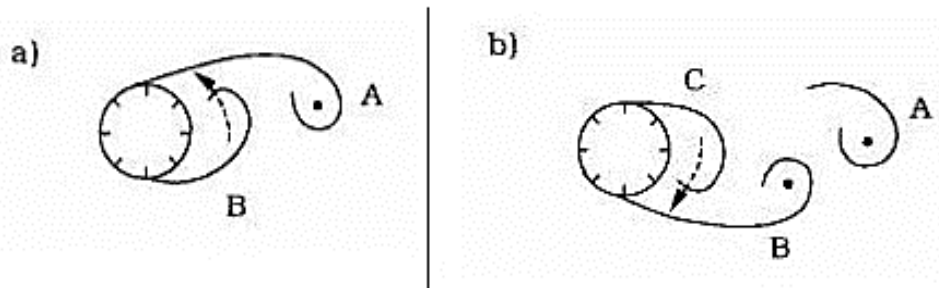


Figure 6 Boundary layer separation (Sumer & Fredsøe, 2006)

Due to friction in viscous flow, the particles close to the cylinder will lose their energy, i.e. the kinetic energy of the water particles in the boundary layer is not enough to overcome the downstream pressure field and this leads to flow separation from the cylinder as shown in the Figure 6A.

Form Figure 6, the boundary layer formed along the cylinder contains vorticity. The vorticity is fed into the shear layer which is formed in downstream of the separation point and causes the shear layer to roll up into a vortex with a sign similar to incoming vorticity. Likewise, we can observe one more vortex rotating in opposite direction i.e., on the other side of the cylinder as shown in Figure 7.



**Figure 7 (a): Prior to shedding of Vortex A, B is being drawn across the wake. (b): Prior to shedding B, Vortex C is being drawn across the wake (Sumer & Fredsøe, 2006)**

As mentioned earlier, the pair formed by these two vortices is actually unstable when exposed to small disturbances for  $Re > 40$ . As a result, one vortex will grow larger than the other when  $Re > 40$ . The larger vortex (Vortex A in Figure 7(a)) apparently becomes strong enough to draw the opposing vortex (Vortex B in Figure 7(b)) across the wake as shown in Figure 7. From Figure 7(b), the vorticity of the Vortex A is in clockwise direction, whereas that in Vortex B it is in anti-clockwise direction. The approach of vorticity of Vortex B will cut off further supply of vorticity to Vortex A from its boundary layer. This is the point where Vortex A is shed. Being a free vortex, Vortex A in Figure 7(b) is then transported downstream by the flow.

Following the shedding of Vortex A, a new vortex will be formed at the same side of the cylinder namely Vortex C (Figure 7(b)). Vortex B will now play the same role as Vortex A, namely it grow in size and strength so that it will draw Vortex C across the wake (Figure 7(b)). This will lead to the shedding of Vortex B. This process will continue each time a new vortex is shed at one side of cylinder where the shedding will continue to occur in an alternative manner between the sides of the cylinder(Sumer & Fredsøe, 2006).

### 2.3.3 Vortex-Shedding Frequency

The Strouhal number is used to define the vortex shedding frequency of a fixed cylinder

$$f_v = \frac{S_t \times U}{D} \quad (8)$$

The still water frequency

$$f_0 = \frac{1}{2\pi} \sqrt{\frac{k}{m+m_{a0}}} \quad (9)$$

Where  $m_{a0}$  is the added mass in still water.

The oscillating frequency

$$f_{osc} = \frac{1}{2\pi} \sqrt{\frac{k}{m+m_a}} \quad (10)$$

Where  $m_a$  is the frequency dependent added mass.

And the shedding process is defined by Reynolds number. Both these two parameters depends on diameter of the cylinder and the flow velocity.

Vortex shedding frequency depends on different aspects. The main aspects are as follows:

- Effect of roughness
- Effect of incoming turbulence
- Effect of cross-sectional shape
- Effect of wall proximity
- Effect of shear in incoming flow.

## 2.4 VIV of a Elastically Mounted Cylinder

The vortex induced vibrations are vibrations which are caused by the vortex shedding from both sides of the cylinder due to fluid motion. The shedding frequency is related to a full periodic cycle for the shedding process. By this forces will develop during the process and these are defined in IL and CF directions, referring that the direction of incoming fluid flow is undisturbed (Figure 8).

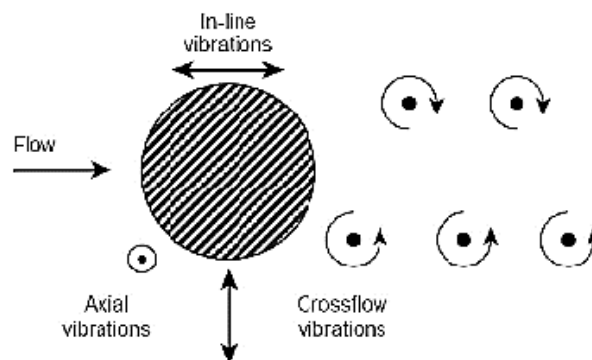


**Figure 8 Motion of cylinder due to vortex shedding (Le Cunff et al., 2002)**

The shedding frequency will increase as the velocity of current increases. A flexible structure with identical eigen frequencies in IL and CF directions will have IL responses at lower current velocity than CF. Figure 9 shows the observed trajectories at mid-span of a free spanning pipeline with increasing flow velocity, represented by reduced velocity. From Figure 9, one can

observe that IL motions starts at lower reduced velocity, but the CF motions have the largest amplitude ratios.

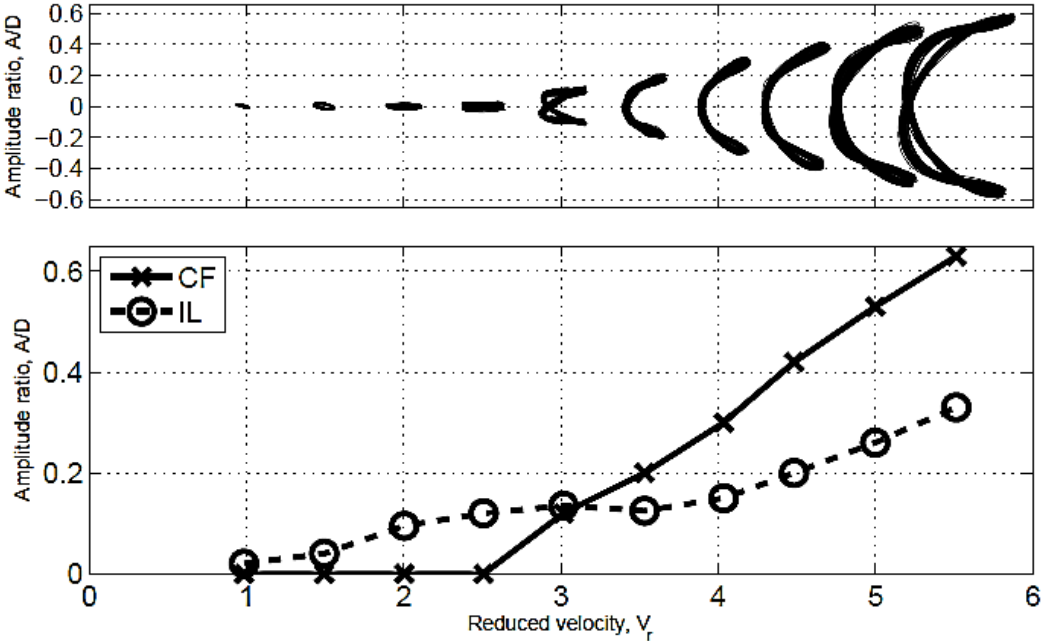


**Figure 9** The lower figure shows maximum response amplitude in IL and CF direction, while the upper figure shows the corresponding response trajectory at mid-span (Aronsen, 2007).

VIV is normally termed as a self-limiting process meaning that if the amplitude exceeds a certain level, the shedding process will no more transfer energy from fluid flow to the structure, but energy will transfer in reverse direction which leads to damping of the structure. The maximum oscillation amplitude is typically about 1.0D for subcritical Reynolds number region of a body which is free to oscillate in both IL and CF directions to the flow.

### 2.5 Lock-in

From Figure 10, if the vortex shedding frequency of cylinder matches with one of the natural frequencies of the body, it can causes resonance and the body vibrates at large amplitude, then it is said that body is in ‘Lock-in’. Lock-in is critical and it is not obvious that when body can become “lock-in” and it can occur in a range of frequencies. The range of frequencies strongly dependent on mass ratio  $m^*$ .

It is observed that the oscillation frequency is not equal to the eigen frequency in the still water since the added mass will vary depending on the flow and the oscillation conditions. In this case, the oscillation frequency will become a compromise in between the still water eigen frequency and the vortex shedding frequency. For lower and higher velocities than the critical lock-in velocity, the shedding frequency follows the Strouhal number relationship.

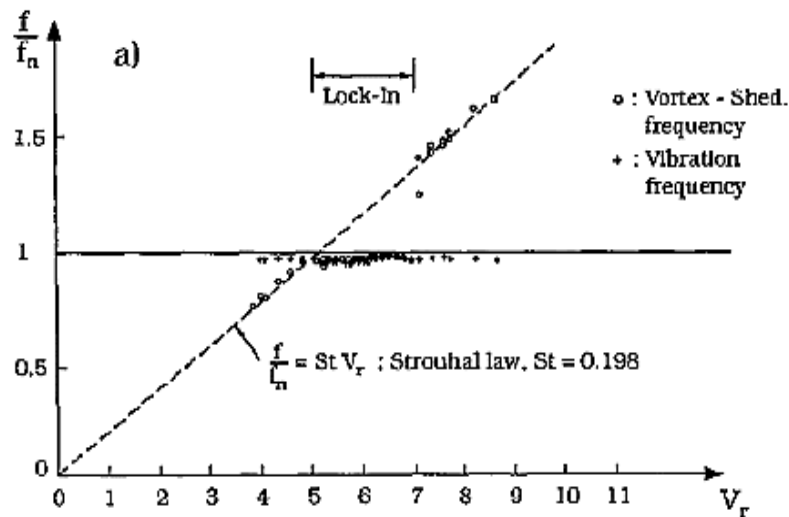


Figure 10 Lock in (Sumr & fredsøe, 1997)

## 2.6 Experimental Methods for Investigation of VIV

The aim of VIV experiments is to improve the understanding of the phenomenon of the VIV in order to be able to predict the response under various conditions. The response has been found to be a function of several parameters, and experimental methods are designed to investigate the effect of these parameters. The research methods for VIV includes experimental and numerical methods. In this section, a brief introduction is given to few methods using rigid cylinders. Flexible cylinder model tests are also commonly used to study VIV. Displacement, strain and response frequencies are measured. However, there are no direct force measurements along the cylinder. This is further discussed in Chapter 4 Description of the Shell Experiment.

### 2.6.1 Rigid Cylinder Free Oscillation Tests

The free oscillation test is performed to illustrate VIV by elastically supported rigid cylinder in constant current. When current acts on the cylinder, it will force the cylinder to vibrate.

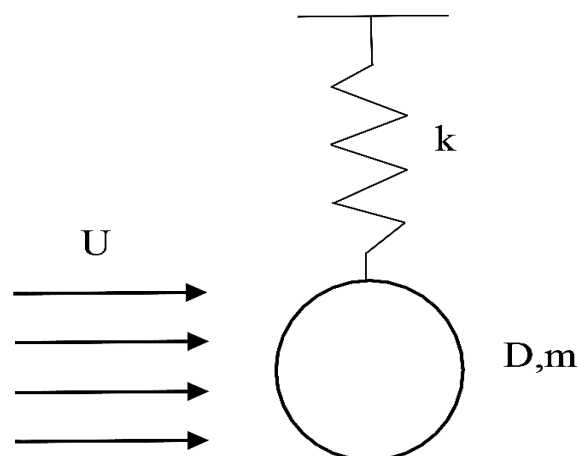


Figure 11 Free oscillation test set-up (Larsen, 2011)

Typical VIV displacement amplitude ratio  $A/D$  from free oscillation test is presented against reduced velocity and mass ratio in Figure 12. Since the influence of added mass variation on the eigen frequency will depend on the dry mass of the cylinder, a light and a heavy cylinder will respond differently to the incoming current velocity. The added mass can adjust the light cylinder's eigen frequency to a larger extent than the heavy cylinder's with the same dimensions. Therefore, the light cylinder can vibrate at wide reduced velocity range than the heavy one.

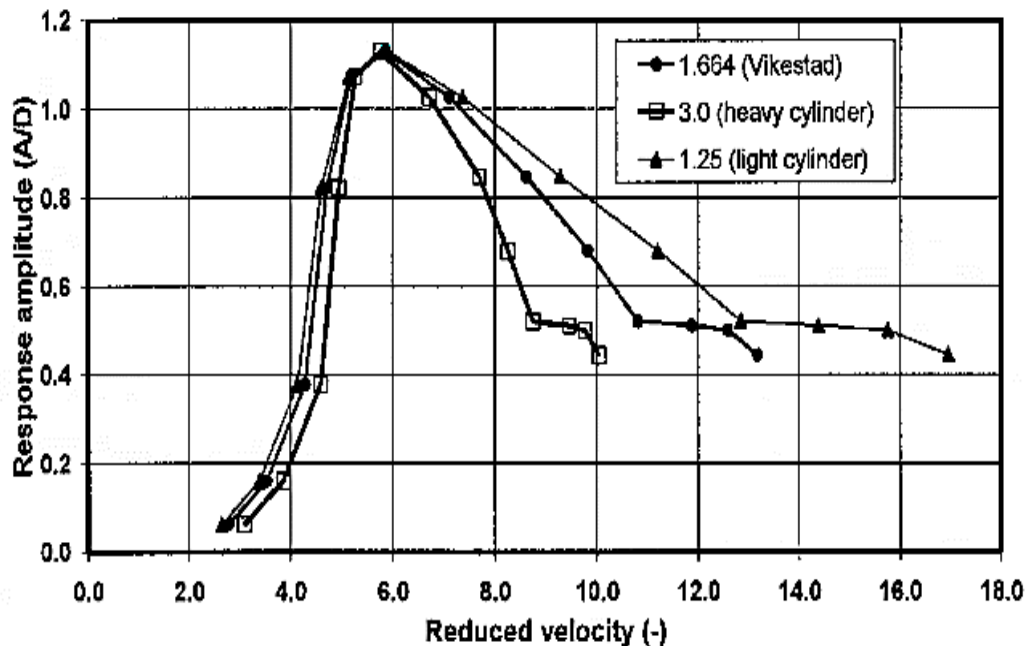


Figure 12 Response amplitudes for three cylinders with different weights (Larsen, 2011)

From free oscillation tests of rigid cylinders, it is possible to obtain information about parameters like:

- In-line amplitudes and frequencies
- Cross-flow amplitudes and frequencies
- Drag coefficient for an oscillating cylinder

When the tests are performed, it is possible to find the forces on the cylinder in terms of added mass as a function of the reduced velocity. The dynamic IL and CF force coefficients cannot be found from free oscillation tests because they are zero during the free oscillation. In order to obtain complete set of coefficients, forced oscillation test are performed on a cylinder.

### 2.6.2 Rigid Cylinder Forced Oscillation Tests

In forced oscillation experiment, the rigid cylinder section is given a prescribed motions. The prescribed motion given to the test cylinder should follow specified oscillation pattern. These motions may be harmonic in IL and CF directions or may be combination of these two directions. Example of CF and IL motions are given as

$$x = x_0 \sin(4\pi\omega_{osc}t - \epsilon) \quad (11)$$

$$y = y_0 \sin(2\pi\omega_{osc}t) \quad (12)$$

Where

$x$  and  $y$  are motions in IL and CF directions respectively

$x_0$  and  $y_0$  are amplitudes in IL and CF directions respectively

$\omega_{osc}$  is oscillating frequency

$t$  and  $\epsilon$  are time and phase angle between IL and CF respectively.

When the structure is oscillating with above described equations, the path of the cross-section will be an eight-figured motion as illustrated in Figure 13. These hydrodynamic forces can then be measured by processing the data from the test and one can identify the force components that are in phase with forced motion velocities and accelerations in IL and CF direction. From this, it is possible to find added mass, lift, drag and dynamic force coefficients of the cylinder.

Figure 13 shows an example of what happens when there is a phase angle between IL and CF motions.

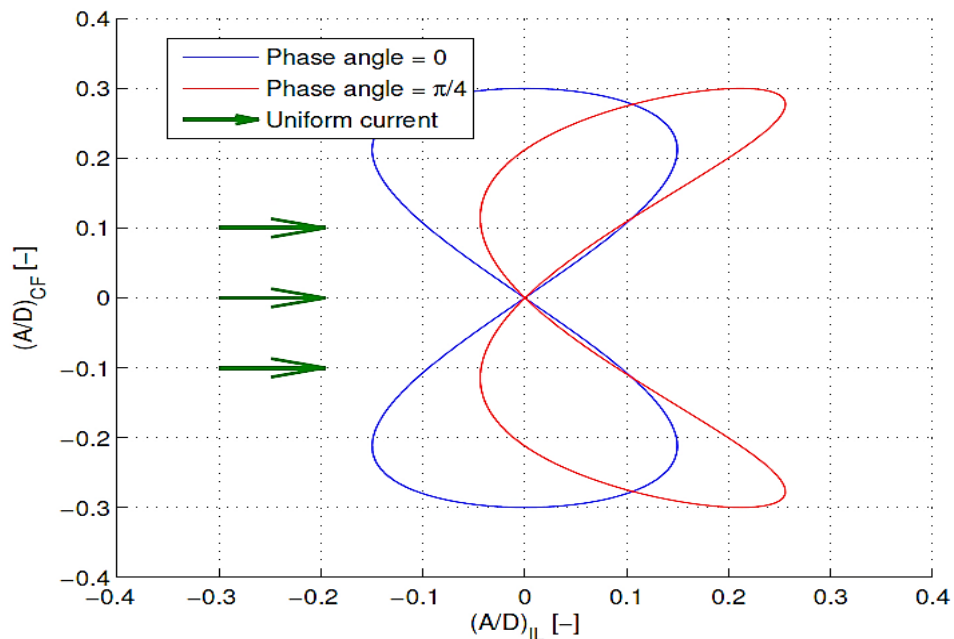


**Figure 13** An example of CF + IL trajectory (Larsen)

Results from the forced oscillation tests are usually presented as contour plots for coefficients in a non-dimensional frequency/amplitude plane shown in Figure 14.

Figure 14 illustrates the CF added mass coefficients for pure oscillation forced oscillation test done by (Gopalkrishnan, 1993). These coefficients are often used in empirical methods to calculate the response in CF direction. IL motions are known to influence the CF response, however, it is still reasonable to use the CF coefficients since the CF response is less sensitive to the response in its orthogonal direction than IL.

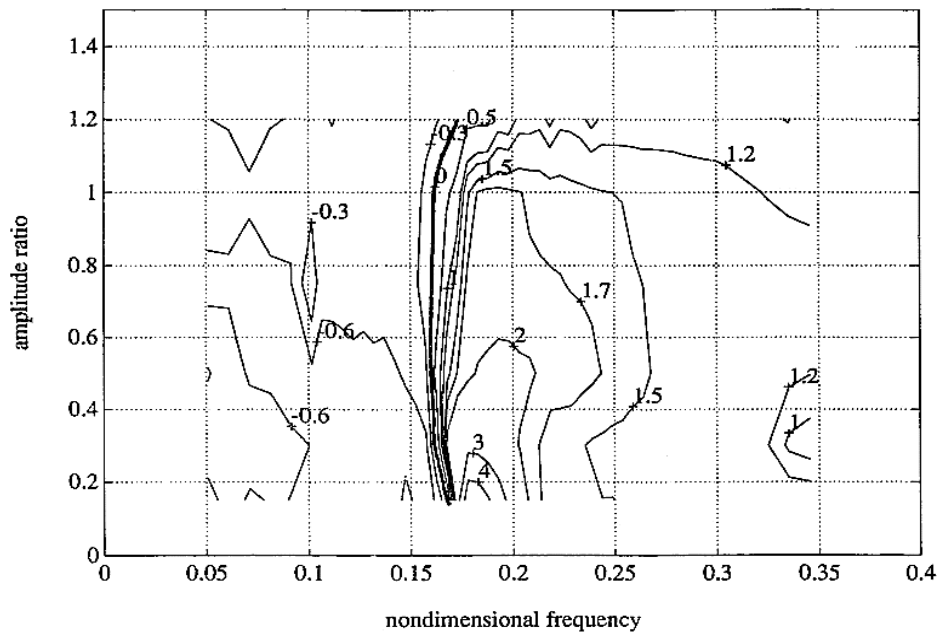


Figure 14 Contours of the CF added mass coefficient (Gopalkrishnan, 1993).

## 2.7 Methods to Predict VIV

Computer programs to predict VIV are based on two different principles:

1. Combination of structural response (usually by Finite Element Method) and fluid motions (Computational Fluid Dynamics). The Navier-stokes theory is used to describe the physics of the fluid and it is solved by FEM. The results are in detailed description of pressure and velocities in the fluid flow, based on this the resulting force acting on the cylinder can be calculated. This principle takes long time for computing.
2. Use of empirical model for hydrodynamic forces in combination of conventional model for the structure (usually it is based on FEM). This method is the basis for standard engineering tools for predicting VIV. The simulation run time is three to five times shorter than the earlier method, since the time consuming in CFD was saved by using only empirical methods.

With the advancement in computer technology, the numerical methods are expected to be faster and accurate. However, to attain this it needs time. The design analysis of VIV will be continuous based on the empirical models in future.

VIVANA is a program based on empirical methods and frequency analysis. This is developed by MARINTEK. Detailed description of VIVANA can be found in Chapter 3.

# Chapter 3 VIVANA Software

## 3.1 Introduction

### 3.1.1 Program Structure

The purpose of VIVANA is to calculate the response of slender marine structures such as risers, free span pipelines and cables excited by vortex shedding when subjected to ocean currents. This response is often referred to as Vortex-Induced Vibrations. This response depends upon the length of the structures, cross-section variations and current profiles, based on this properties the riser may experience single or multi-frequency response. Thus both response types can be analysed.

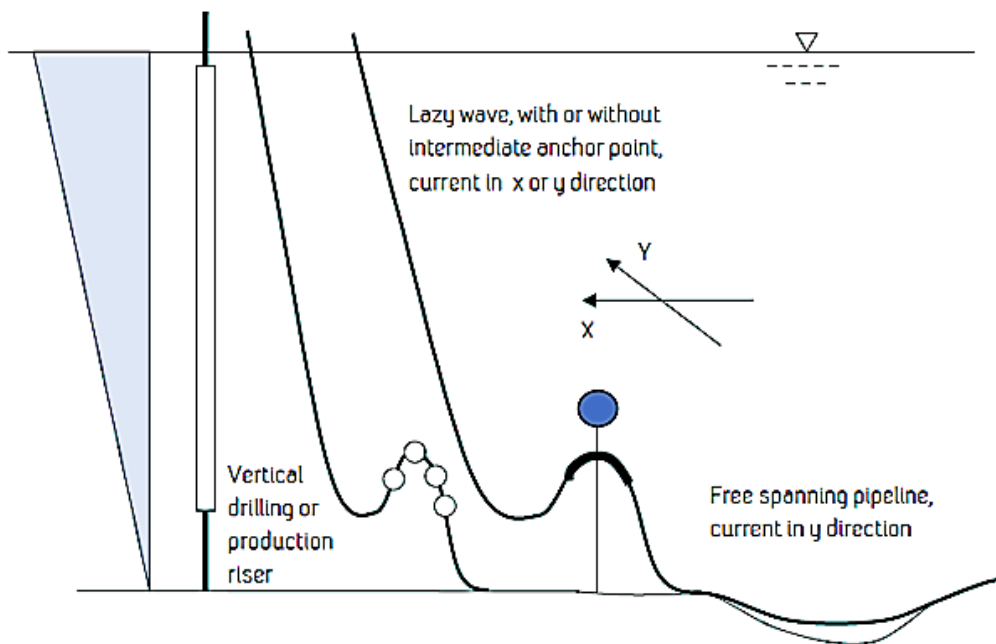


**Figure 15** Examples of slender structures that can be analysed by VIVANA (Passano et al., 2015)

VIVANA is linked to RIFLEX (Ormberg & Passano, 2015) (shown in Figure 16) which is developed by MARINTEK and tailor- made for static and dynamic analysis of slender marine structures. The two RIFLEX modules INPMOD and STAMOD are always a part of a VIVANA program system, while other RIFLEX modules are not needed. RIFLEX can handle a large variety of slender marine structures such as tensioned and flexible risers, anchor lines, umbilical's, tendons, pipeline during installation and free spanning pipelines. Such structures may hence also be analysed by VIVANA (Passano et al., 2015).

A complete VIV analysis consists of (Passano et al., 2015):

- An initial RIFLEX analysis using the INPMOD and STAMOD modules.
- The VIVEIG module computes normal modes and eigen frequencies.
- Some initial key parameters are calculated in INIVIV.
- The VIVRES module carries out the dynamic response analysis according to the method described herein. Cross-flow (CF) and/or in-line (IL) response can be calculated.
- The VIVFAT module calculates fatigue damage based on the results from VIVRES
- Finally VIV magnified drag coefficients are calculated in VIVDRG.

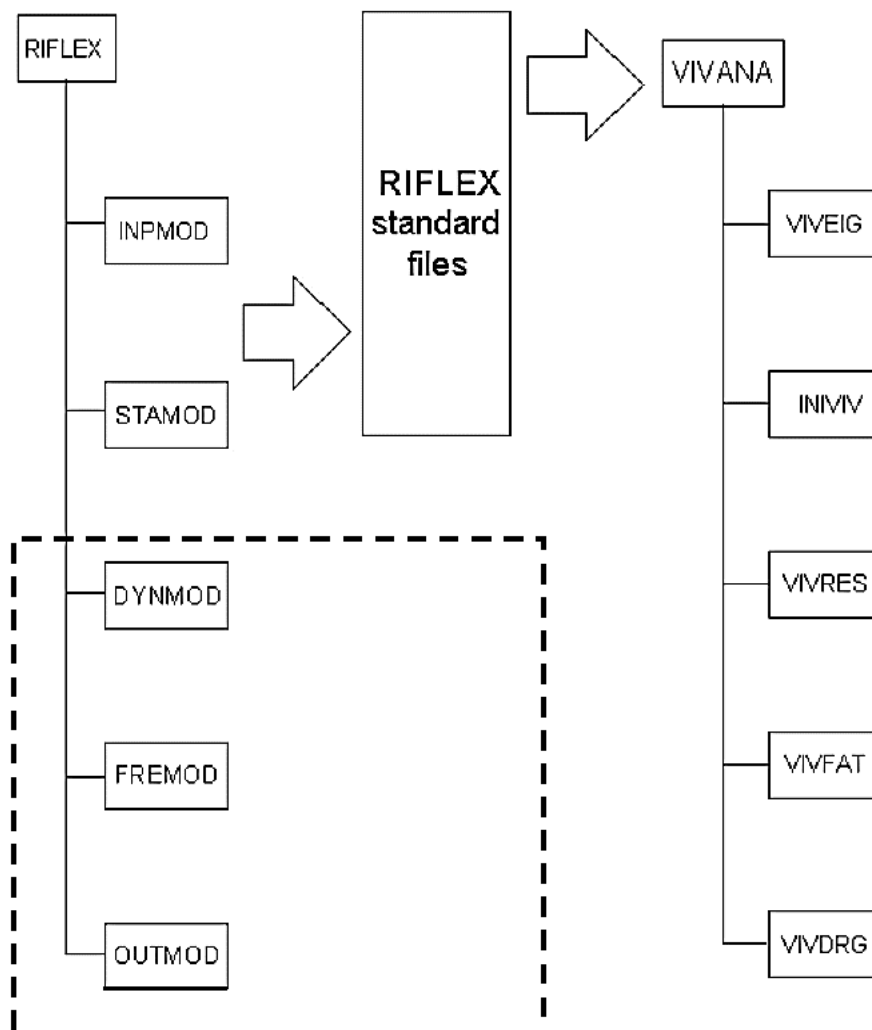


**Figure 16** The overall structure of VIVANA (Passano et al., 2015).

### 3.1.2 Analysis Options

Three analysis options are offered:

1. Cross-Flow response only  
This option is based on hydrodynamic coefficients found from the experiments.
2. Pure in line (IL) response only  
This option is applied based on hydrodynamic coefficients found from forced IL motion tests. This type of response takes place for current velocities lower than the on-set of CF vibrations, means that the reduced velocity related to the fundamental eigen frequency is lower than 2.5. This type of response is not of interest to marine risers, but it gives significant contribution to fatigue of free spanning pipelines and conductors.
3. Combined CF and IL response  
The response is calculated in two steps. Step 1 is the analysis of CF response and applies the same method and hydrodynamic coefficients as option 1. In step 2, the IL response is calculated and it is assumed to take place at two times of CF frequency. Analysis method is same as for pure IL response (option 2), but hydrodynamic coefficients are different. Normally, we can see larger IL response in combined CF and IL response than for pure IL response only.

## 3.2 Method Overview

A brief outline of the analysis procedure of VIVANA is given in the following:

### **Step 1. Static analysis**

The static shape of the structure needs to be found. This procedure will depend on the actual case and how it is modelled in RIFLEX(Ormberg & Passano, 2015). Once the static conditions are established, the normal flow velocity  $U_N$  along the structure is found from the shape of the structure and current profile.

### **Step 2. Eigenvalue analysis, still water**

The eigen frequencies and mode shapes of the structure must be found. Added mass is initially applied as for a non-vibrating structure in still water according to the data given by the user. The results will be given in terms of eigen vectors  $\phi_i$  and associated eigen frequencies  $\omega_i$ . A sufficient number of eigen values will be found so that all possibly active frequencies can be found when considering the maximum shedding frequencies along the structure.

### **Step 3. Identification of possible excitation frequencies**

Added mass under VIV conditions will become different from the still water values, which depends on the response frequency. Hence, iterations must be performed to carry out each eigen frequency that is considered as candidate for being excited by vortex shedding. This iteration is always required for both pure IL and CF response. For IL in combined CF and IL response, it is assumed that the IL frequency is two times of the CL.

#### **Step 4. Dedication of excitation zones**

Each response frequency will be associated to an excitation zone where vortex shedding may excite the structure at the actual frequency. The zone is defined by an interval for the local non-dimensional frequency. In VIVANA two different methods are used to define excitation zones:

- Time sharing method
- Space sharing method.

#### **Step 5. Calculation of cross-flow responses**

The frequency response method is used to calculate the dynamic response at the response frequencies found in Step 3 within the excitation zones defined as in Step 4. The response analysis applies an iteration that converges when the response is in accordance with the non-linear models for excitation and damping forces. In VIVANA, two different iteration strategies are used:

- Newton Raphson iteration
- Fixed point iteration.

#### **Step 6. Calculation of in-line response**

The IL response is calculated in the same way as for CF, but all data for hydrodynamic coefficients are different. The complete solution for a general VIV case will hence consist of two complex response vectors, one at the double frequency of the other.

#### **Step 7. Calculation of fatigue damage**

Fatigue damage is calculated on the basis of user defined SN curves and the calculated response. The Miner-Palmgren rule for damage accumulation is applied. Rain-flow cycle counting is used if the “simultaneously active frequencies” option is assumed, while an analytical solution can be used for the time sharing cases.

### **3.3 Time Sharing and Space Sharing**

The characteristics of VIV response for long, slender marine structures subjected to a non-uniform current are complicated and difficult to model. It is observed that the response will be a mixture of different modes and frequencies. This response will change its characteristics with varying current profile, influence of tension and bending stiffness, order of dominating modes, Reynolds number, mass ratio and probably other parameters as well. To date, there is no model that can take all of these parameters and their effects into account and replicate the response that has been observed. The approach that has been used, is to find the excitation zone for a particular frequency that is initiated and calculate the response of it independent of other active frequencies. The key aspect is to define this excitation zone. There are two different approaches to define this. They are as follows:

#### **3.3.1 Time Sharing**

The competing frequencies will dominate in a period of time. The analysis must find the duration of each competing frequency. The response takes place at a selected set of eigen

frequencies, but only one frequency will be active in a specified time period as shown in Figure 17. The excitation zones are allowed to overlap, but the frequencies compete to capture time windows (Wergeland & Larsen, 2015).

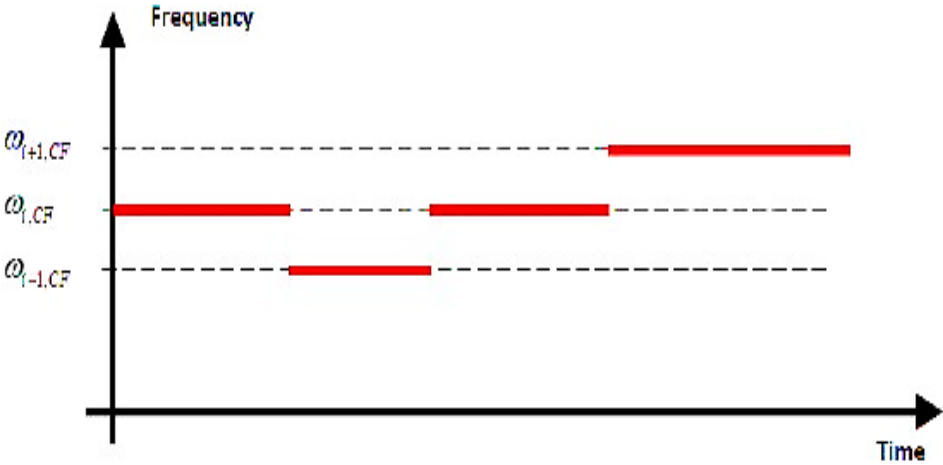


Figure 17 Illustration of time sharing process (Passano et al., 2015)

### 3.3.2 Space Sharing

The response takes place at selected set of eigen frequencies which act simultaneously. Every frequency will have a designated length when they are excited which is caused by the vortex shedding, which means the structure length will be shared among the response frequencies in defined zones. No overlap exists between these zones as shown in Figure 18.

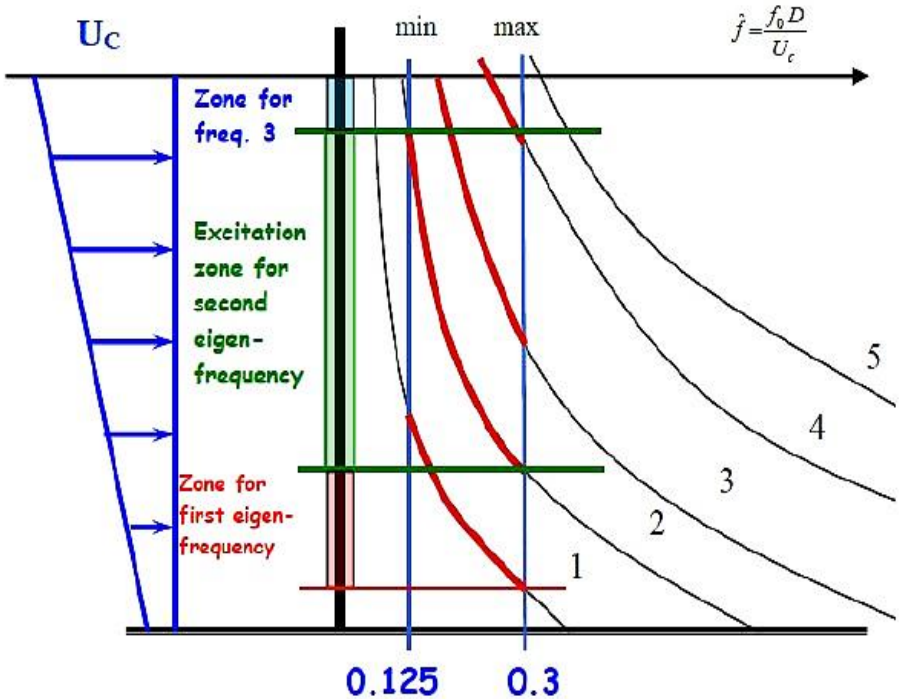


Figure 18 Space sharing process (Passano et al., 2015)

### 3.4 Frequency Response Method

The frequency response method is used to calculate the dynamic response at the dominant frequency identified in the previous steps (section 3.2). This method implies a linear relationship between static and dynamic response, this limitation will not be a problem since VIV amplitudes are small relative to the global dimensions of the structure, which means that the structural behaviour is linear.

Another assumption is that, vibrations takes place at discrete frequencies. In case of discrete frequencies the response may be calculated by using elements and the frequency response method.

#### Structural theory

By using FEM, the equation of motion of a structure undergoing VIV can be written as

$$M\ddot{r} + C\dot{r} + Kr = R \quad (13)$$

where  $M$ ,  $C$  and  $K$  are structural mass matrix, structural damping matrix and structural stiffness matrix respectively.  $\ddot{r}$ ,  $\dot{r}$  and  $r$  are acceleration, velocity and displacement respectively.

The external load  $R$  in this case will be harmonic with frequency  $\omega$ , but all loads at all degrees of freedom are not necessary in phase. It is convenient to describe this type of load patterns by a complex load vector  $X$  with harmonic time variation.

$$R = Xe^{i\omega t} \quad (14)$$

The response vector  $r$  will also be given a complex vector  $x$  and a harmonic time variation. Hence we have,

$$r = xe^{i\omega t} \quad (15)$$

By introducing hydrodynamic mass matrix  $M_H$  and damping matrix  $C_S$  in the dynamic equation, we have

$$-\omega^2(M_S + M_H)x + i\omega(C_S + C_H)x + Kx = X_L \quad (16)$$

Where  $M_S$ ,  $C_S$  and  $X_L$  are structural mass matrix, structural damping matrix and excitation force vector respectively. Non-zero terms are present within an excitation zones. The excitation force must always be in phase with the local response velocity.

The response vector  $x$  is complex. The vector describes a harmonic response at all nodes, but the responses may have different phases. This means that the response will not necessarily appear as a standing wave, but may have contributions from travelling waves. From a mathematical point of view,  $x$  is equivalent to a complex mode found from the damped eigenvalue problem.

Since the load vector  $X$  depends on the response vector  $x$ , the dynamic equilibrium function must be solved by iteration. The aim of this iteration is to identify a load vector that gives a consistent response vector in the sense that both amplitudes and phases are correct at all positions, and also consistent with the local flow conditions.

When the VIV response analysis is completed, we are left with N complex response vectors  $x_1, x_2 \dots \dots x_n$ . These are used in combination with the element stiffness matrices and cross-section properties to derive the time series of stresses. Hence, a multi-frequency response at discrete time increments is obtained.

The response is solved in frequency domain. A more detailed description of VIVANA can be found in (Passano, Larsen et al., 2015).

### 3.5 Hydrodynamic Coefficients

The analysis model is based on empirical coefficients of lift force, added mass and damping. The procedure for identifying all the coefficients applies the non-dimensional frequency as a controlling parameter (see equation 4).

#### 3.5.1 Added Mass Coefficient

The added mass coefficients in pure IL and CF are based on the experiments with the rigid cylinder given a harmonic motion (The trajectory of the cylinder is based on observed trajectories for cross sections of a flexible beam). The frequency of oscillation and response amplitude are systematically varied and these results are presented on contour plots. In general, it shows that added mass is dependent on both the frequency of oscillation and response amplitude. However in VIVANA, it is assumed that the response amplitude is less important than frequency.

Figure 19 shows the contour plots for added mass coefficients in CF oscillations. This defines the combinations of frequencies and amplitudes that have equal value of added mass coefficient. In both IL and CF analysis,  $A/D = 0.5$  is chosen as shown in Figure 19 (red line), this makes added mass as simple function of frequency.

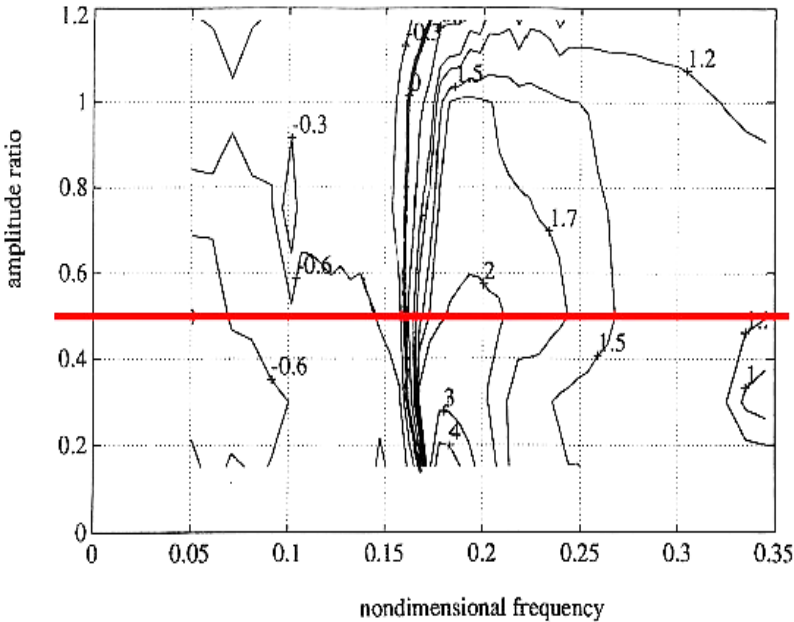
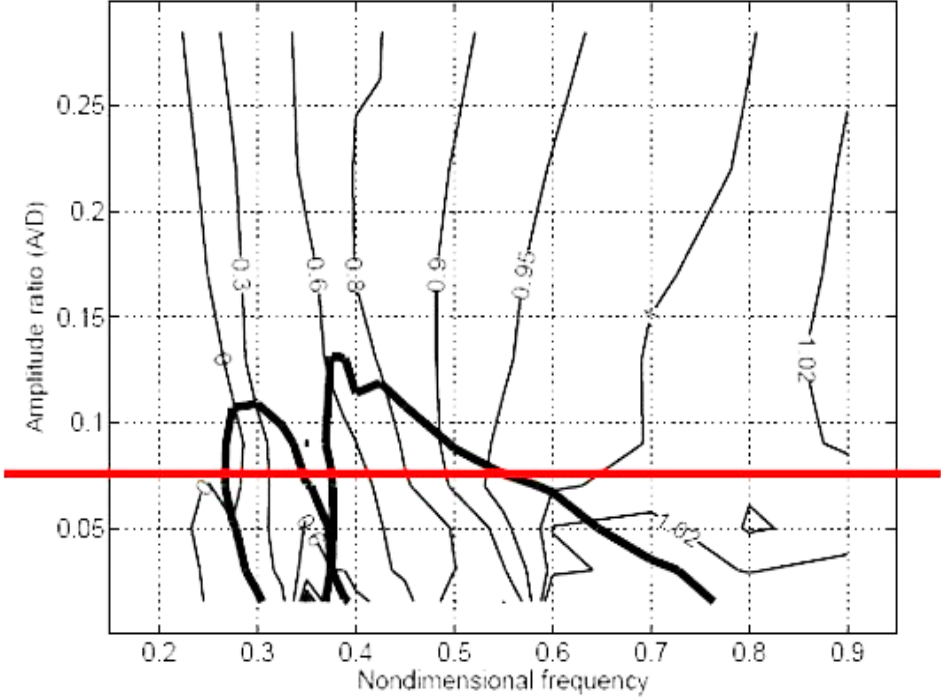


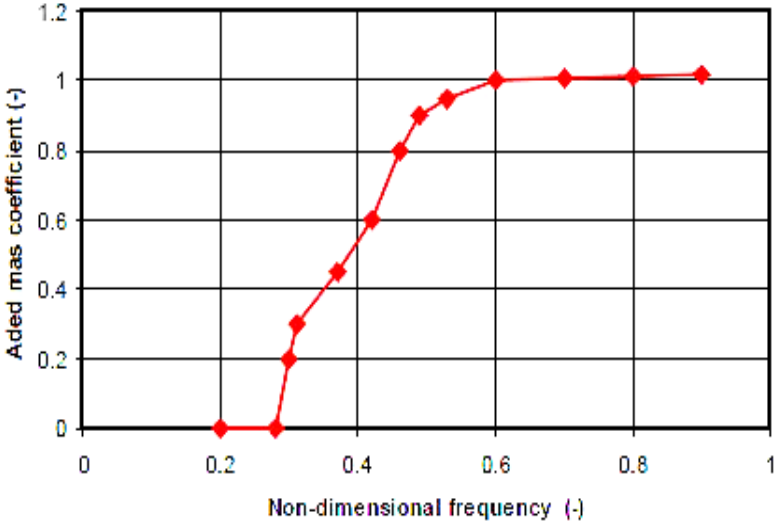
Figure 19 Contour plot of the CF added mass coefficients based on forced harmonic motions (Gopalkrishnan, 1993)

Figure 20 shows the added mass contour lines for IL oscillations presented by (Aronsen, 2007). The IL added mass is more sensitive to frequency variations than the amplitude variations, this gives to use the simplified added mass model as shown in the below figure. This added mass contour plot is assumed to be defined by the non-dimensional frequency and the actual is curve is found in the plot for a non-dimensional amplitude of 0.075 (red line in Figure 20).



**Figure 20 Contour plot of the CF added mass coefficients based on forced harmonic motions (Passano et al., 2015)**

By assuming that added mass coefficient is independent of the amplitude and it is given as a simple function of the frequency as shown in Figure 21 and Figure 22. This function is used in VIVANA model.



**Figure 21 The VIVANA model for added mass as a function of frequency for IL response (Passano et al., 2015)**

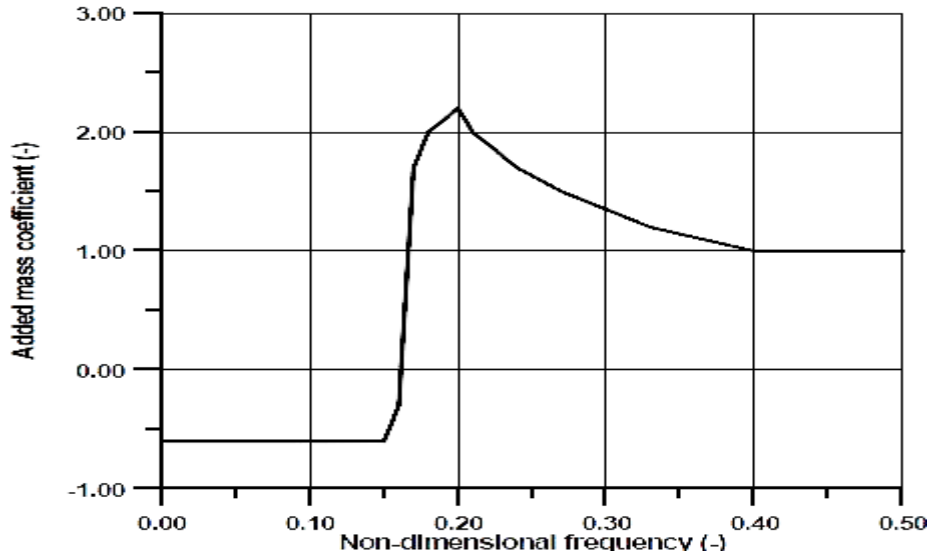


Figure 22 The VIVANA model for added mass as a function of frequency for CF VIV (Passano et al., 2015)

### 3.5.2 Excitation Coefficients

The excitation force in IL and CF directions at a given point on the structure is defined as a component of the hydrodynamic force that is in phase with the response velocity at the point on the structure and for IL and CF respectively. The excitation force on an element with unit length is given by

$$F_{e,IL/CF} = \frac{1}{2} \rho C_{e,IL/CF} D_H U_N^2 \quad (17)$$

Instead of defining the excitation coefficients as a two-parameter function as frequency and response amplitude as shown in Figure 23, VIVANA's built in model uses a set of parameters that applies coefficient as a function of response amplitude.

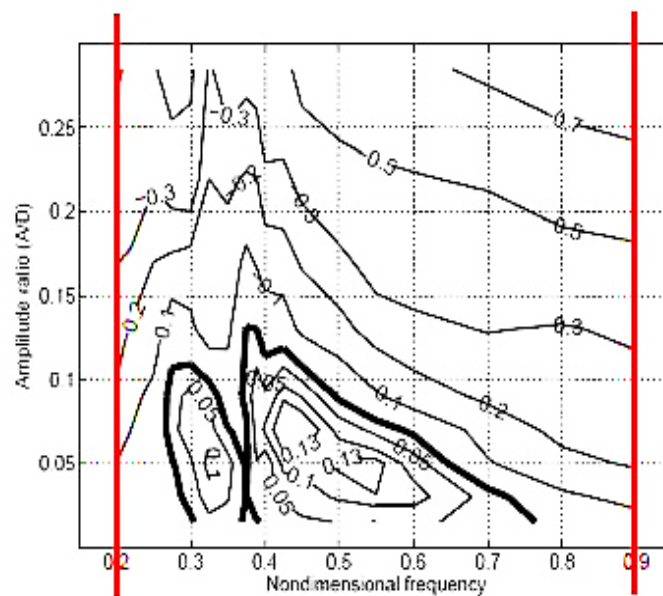


Figure 23 Contour plot curves for the IL excitation coefficient (Gopalkrishnan, 1993).

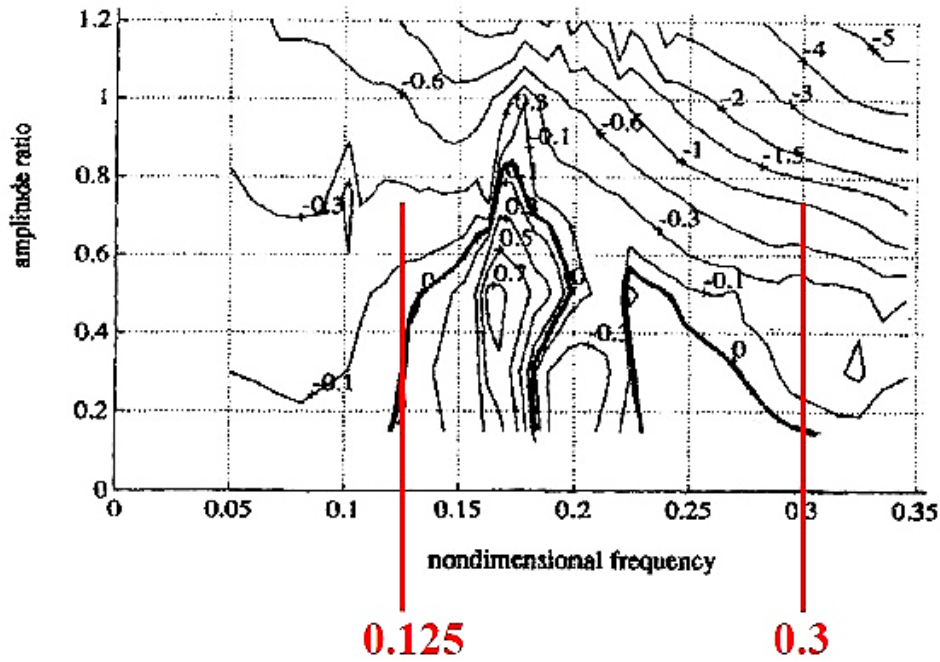


Figure 24 Contour plot curves for CF excitation coefficient (Gopalkrishnan, 1993)

From above two figures, the positive excitation coefficient which can give excitation to marine slender structures is in interval of 0.2 - 0.9 and 0.125 - 0.3 for pure IL response and CF respectively.

For a given non-dimensional frequency Figures 25 and 26 and shows how the IL and CF excitation coefficient is defined as a function of non-dimensional response amplitude respectively. The curves are assumed to have maximum value at B, meaning that AB and BC can be given as two second order polynomial when the three points A, B and C are defined. As discussed above, VIV is self-limiting process, which is easy to understand by realizing that  $C_e$  becomes negative if the amplitude exceeds certain value. Excitation force  $F_e$ , will hence change from excitation force to damping force. The response amplitude for a circular cylinder is limited to  $\frac{A}{D} < 1.2$ . This is valid only for circular sections only. The self-limiting vortex shedding process may not be valid for non-circular sections and they may experience galloping.

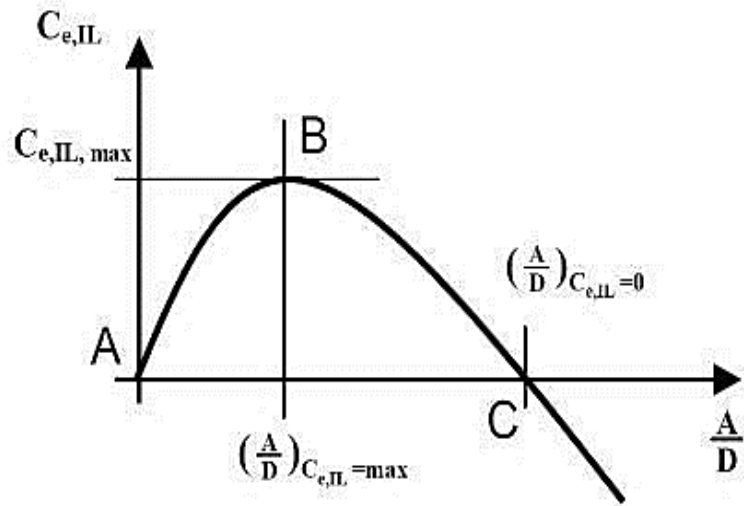


Figure 25 Three point excitation coefficient curve for pure IL response (Passano et al., 2015)

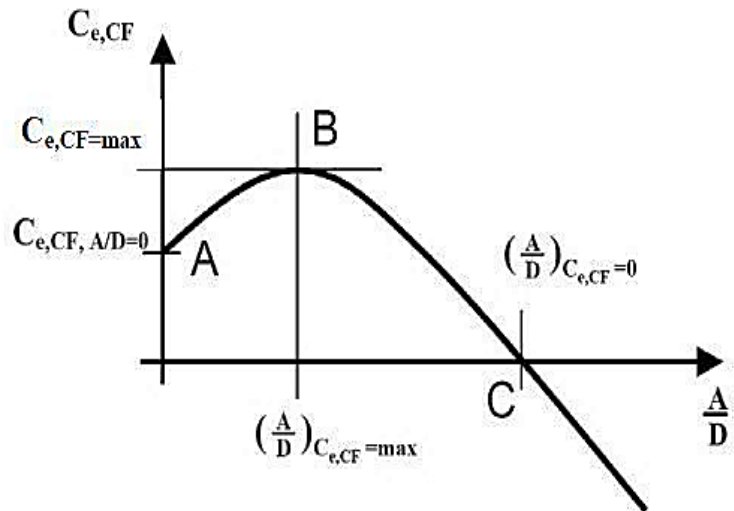


Figure 26 Three point excitation coefficient curve for CF response (Passano et al., 2015)

# Chapter 4 Description of the Shell Experiment

Shell Oil Company conducted riser VIV tests with staggered buoyancy elements at MARINTEK offshore ocean. The goal of this test was to investigate VIV responses of riser model with staggered buoyancy elements for different velocities in uniform flow. The knowledge is utilized in this thesis to accomplish a more detailed and organized investigation. The purpose of this chapter is to give a detailed description of the Shell riser VIV tests. Results presented in this chapter are taken from Rao et al., 2015 and Jhingran et al., 2011). It is known that VIV responses are strongly influenced by buoyancy element dimensions, arrangement and other parameters Wu et al., 2016. In present study, the Shell test is used. However, the method is applicable to other test data as well.

## 4.1 Experimental Setup

For clear understanding of VIV, the Shell Oil Company performed a testing program on hydrodynamic effects of a riser models that are subjected to VIV with five different configurations of buoyant regions on SLWR at MARINTEK Ocean Laboratory. The model riser with staggered buoyancy segments is shown in Figure 27.

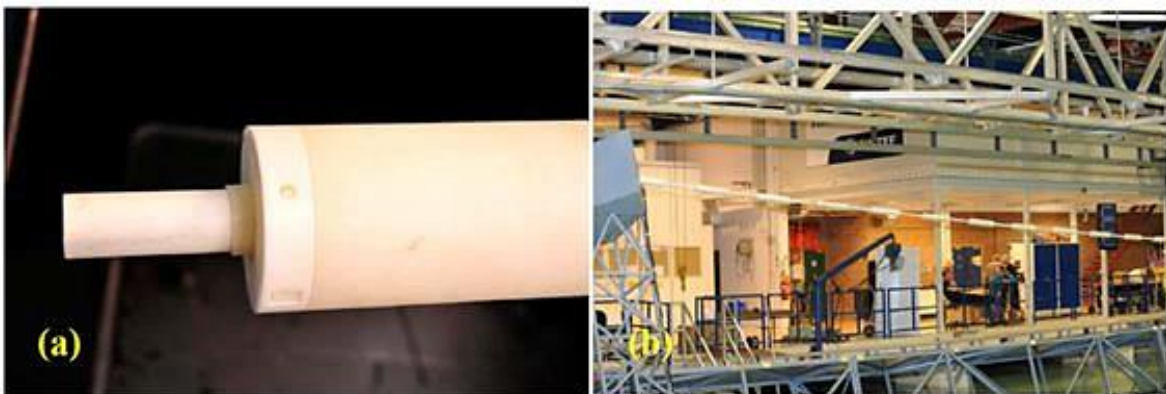


**Figure 27 (a) the riser and buoyancy mode (b) the riser during experiments (Jhingran et al., 2012).**

The presence of the buoyancy sections on a riser may decrease the fatigue damage rate due to decrease in vortex shedding frequency as it is associated with larger diameter. With same flow speed, a bare riser will vibrate at a higher frequency than a riser with fully covered buoyancy modules of larger diameter. When a flexible riser with both bare and buoyancy regions are excited by the same flow, two different frequencies are excited and a competition exists between lift forces of these two excited frequencies. The point of this test was to analyse “under

which buoyancy configuration, would be the VIV excitation on the buoyant section dominate the response?"

### 4.2 Experiment Description

The Ocean Laboratory is 10.0 m depth with 50.0 m wide and has a length of 80.0 m. The area of basin is fitted with an adjustable floor of 48.0 m by 42.0 m. By this adjustable floor, the depth can be adjustable from 0.0 m to 8.7 m. A new testing rig was fabricated for this experiment by using the previous knowledge of testing a riser from MARINTEK with 40.5 m long horizontal truss, which was suspended from crane system/gondola as shown in Figure 28. At lower end of each pendulum, which were suspended from each end of horizontal truss beam, clump weights were attached to two vertical pendulums where the riser ends are attached to clump weights via universal joints.

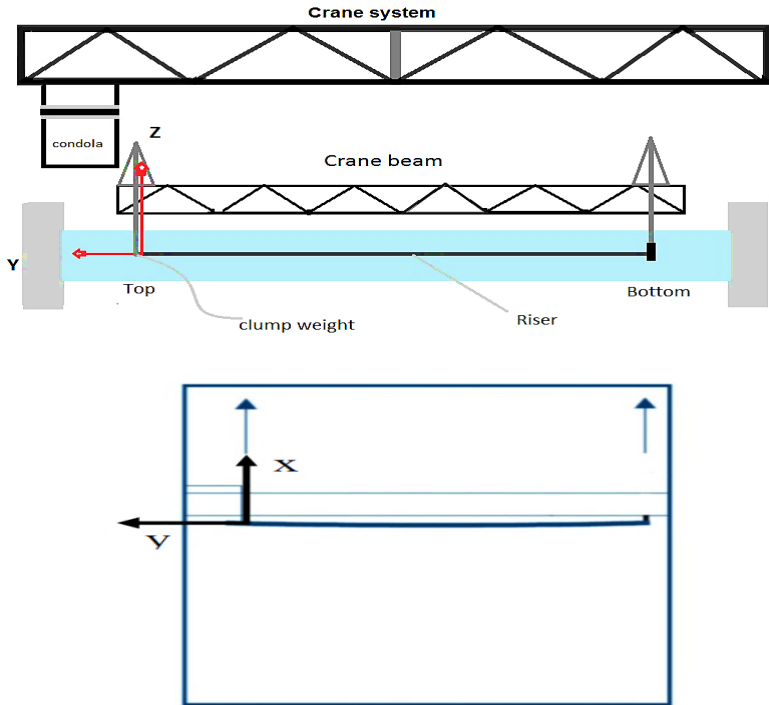


Figure 28 Test setup and coordinate system; upper: front view; lower: top view (Jhingran et al., 2012).

#### 4.2.1 Riser Model Configuration

The bare riser model used in this experiment was 38.0 m long and 30.0 mm outer diameter ( $OD_C$ ) with a buoyancy element of 40.86 cm long with 80.0 mm in outer diameter ( $OD_B$ ) (see Figure 29). For measuring the bending stress and accelerations in IL and CF directions, dense instruments were fitted in the inner core along the riser. The buoyancy modules were fabricated with polyurethane into half cylinders, which were clamped to 30.0 mm bare riser model and locked with clips to secure in place. To accommodate accelerometers in the inner core of the pipe, cavities were left in buoyancy halves. The two cylinder halves of buoyancy modules were fabricated with a central groove to accommodate the bare riser model as shown in Figure 30.

In staggered buoyancy test, the length of individual buoyancy element was represented with  $L_B$  and the length of bare riser between two adjacent buoyancy sections is defined as  $L_C$ . Figure 29 represents the schematic of a riser with buoyancy elements. These lengths were measured as multiples of length of a buoyancy module i.e.  $L_C = 2$  means the gap between two adjacent buoyancy sections is equal to length of two buoyancy segments. The various configurations bare risers with buoyancy sections are represented in Table 1.

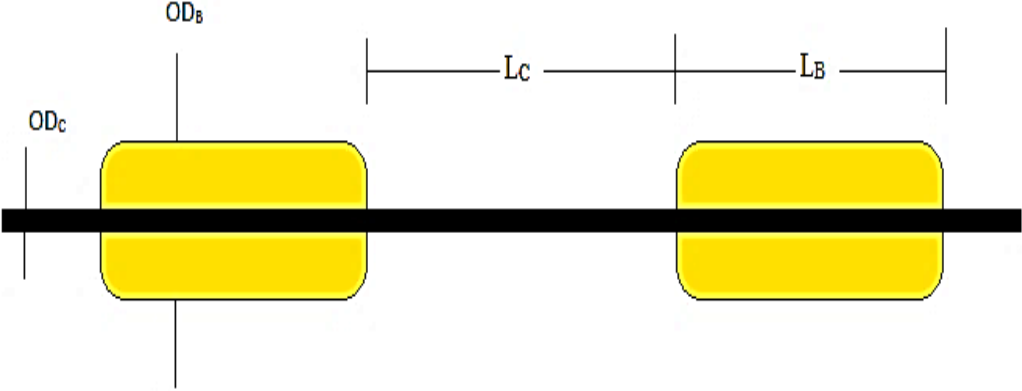


Figure 29 Definition of gap lengths and buoyancy segment lengths (Jhingran et al., 2012)

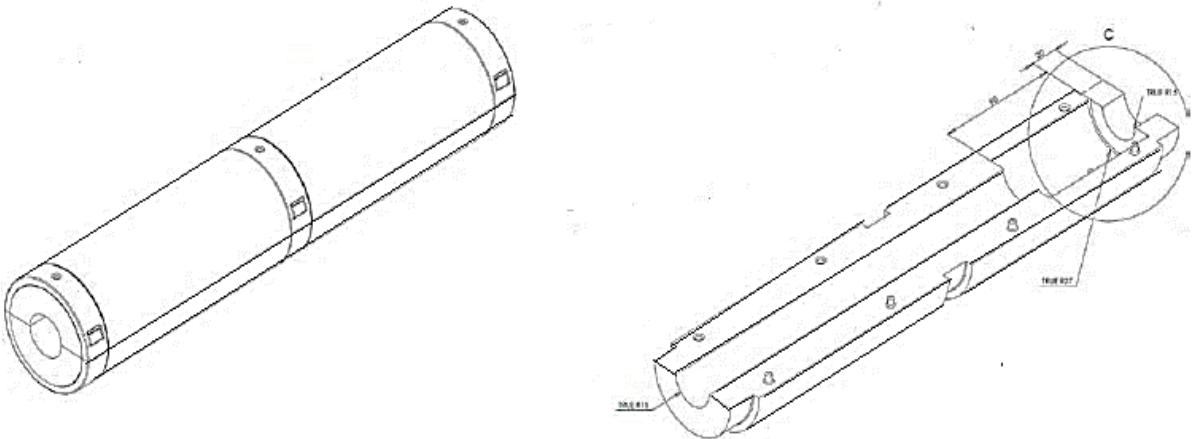


Figure 30 The buoyancy modules as half cylinders with central groove to accommodate the riser (Jhingran et al., 2012).

Where  $\frac{L_C}{L_B} = \frac{\text{Length of gap as number of buoyancy modules}}{\text{Length of buyoancy section as number of buyoancy modules}}$ , this ratio shows not only the length of gap segments and buoyancy length but also shows the percentage of buoyancy coverage over the riser.

To study the effect of buoyancy modules on VIV, the configuration of buoyancy elements are populated with five different configurations as shown Table 1 and their pictorial representation is shown in Figure 31.

**Table 1 Configurations of buoyancy modules (Jhingran et al., 2012)**

Configuration condition number	Test configuration
1	$L_C/L_B = 2/2$
2	$L_C/L_B = 1/1$
3	$L_C/L_B = 3/2$
4	$L_C/L_B = 3/1$
5	$L_C/L_B = 5/2$

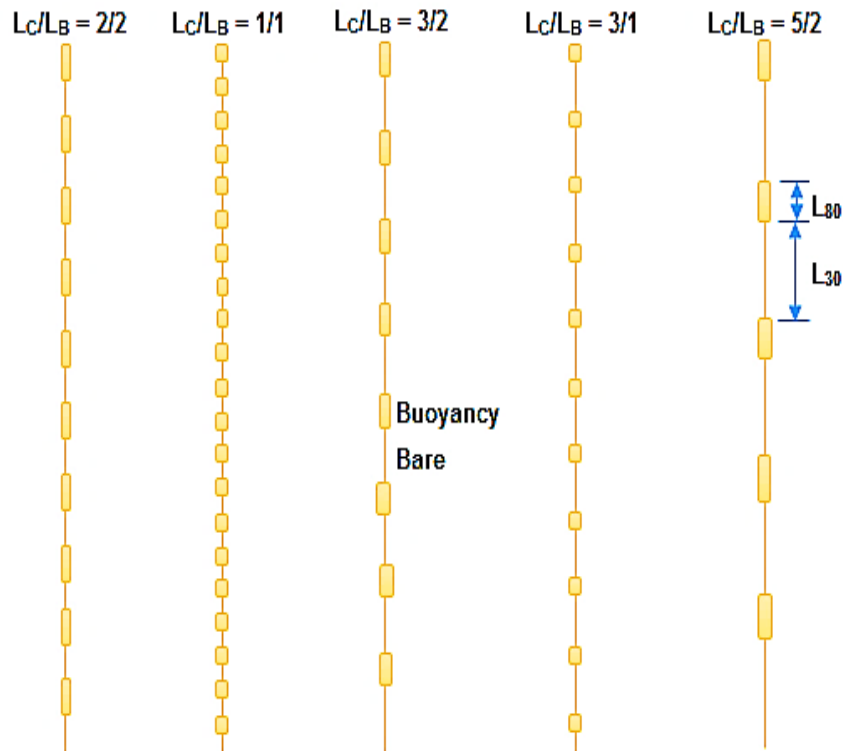


**Figure 31 Staggered buoyancy configurations over the riser (Rao et al., 2015)**

**For example:**

If we consider for configuration condition number 1:  $L_C/L_B = 2/2$  which represents  $L_C = L_B = 2/2 = 2 \times 0.4086$  m. This ratio has the advantage of representing either the length of bare segments and buoyancy modules or ratio of length of bare or gap length to the buoyancy region over the riser. The aspect ratio of the buoyancy element for this configuration is  $L_C/D_B = 2 \times 0.4086 / 0.08 \approx 10$ .

Figure 31 shows five different configurations of riser with staggered buoyancy modules. For all tests, the ratio of diameter of buoyancy element to the diameter of bare riser was 2.67. This non-integer part ratio prevented the vortex frequency of bare riser from being the multiple of vortex shedding frequency of buoyancy elements. This is an important consideration because if the vortex shedding frequency of the buoyancy elements is equal to the vortex frequency of the bare riser then it may strengthen the total response of VIV of the SLWR. For example, if

the ratio of diameter of buoyancy element to the diameter of bare riser is 3, then the third harmonic frequency from the bare riser will match with first harmonic frequency of the buoyancy part which results in greater fatigue damage of the riser.

The below table shows the properties of a pipe model used for Shell experiment:

**Table 2 Pipe model properties (Rao et al., 2015)**

<b>Parameters</b>	<b>Bare pipe</b>	<b>Buoyancy element</b>
Total length between pinned ends (m)	38.00	38.00
Outer diameter (mm)	30.00	80.00
Outer/inner diameter of fiber glass rod/pipe (mm)	27/21	27/21
The length of one buoyancy element (mm)	--	0.4086
Bending stiffness, EI (Nm <sup>2</sup> )	572.3	572.3
Young's modulus, E (N/m <sup>2</sup> )	$3.46 \times 10^{10}$	$3.46 \times 10^{10}$
Mass in air (kg/m)	1.088	5.708
Weight in water (kg/m)	0.579	0.937
Mass ratio	1.54	1.14

#### 4.2.2 Test Arrangement

The test consisted of 45 runs at varying towing velocities with varying buoyancy configurations. Each buoyant configuration consisted of 9 runs at varying towing velocities. The riser was exposed to uniform velocity with a maximum current speed of 1.2 m/s with  $Re \approx 96,000$  for buoyancy segment diameter of 80 mm. The tension applied to the pipe was constant for each test but varied with buoyant configuration and flow speed from test to test. Range of mean tension was 5900 N to 7800 N. In order to measure all the parameters needed to calculate the hydrodynamic coefficients, 30 strain gauges and 20 accelerometers were densely spaced along the length of riser in cross-flow (CF) and in-line (IL) directions of flow. In addition to strain gauges and accelerometers, two tri-axial transducers with rate of 1200 were sampled on both ends of the riser.

#### 4.3 Test Results

The test data has been extensively studied by Rao et al., 2015 and Jhingran et al., 2016. The interaction of bare riser and buoyancy elements and its influence on the riser responses (frequency, displacement and fatigue damage) have been investigated.

##### 4.3.1 Response Frequency

Due to the buoyancy region on SLWR, it consists of a staggered configuration with two different diameters, lift forces on the buoyancy sections will compete with the lift forces from the bare riser at different vortex shedding frequencies. For a staggered buoyancy riser, the bare region of the riser is power-in-region with higher excitation frequency while the buoyancy region is power-in-region with lower excitation frequency. The structural system is no longer linear because damping and amplitude influence each other. There are two excitation forces due

to presence of two excitation frequencies, one from excitation of bare region and other is from excitation of buoyancy region. The non-linear interaction exists between the responses of cylinder at two excitation frequencies only when its wave number and frequency meet the dispersion relation. For staggered buoyancy riser, the dispersion relation is not recognizable due to non-uniform distribution of mass.

Figures 32 and 33 presents the excitation frequencies associated with bare and buoyancy segments respectively from the Shell experiment.

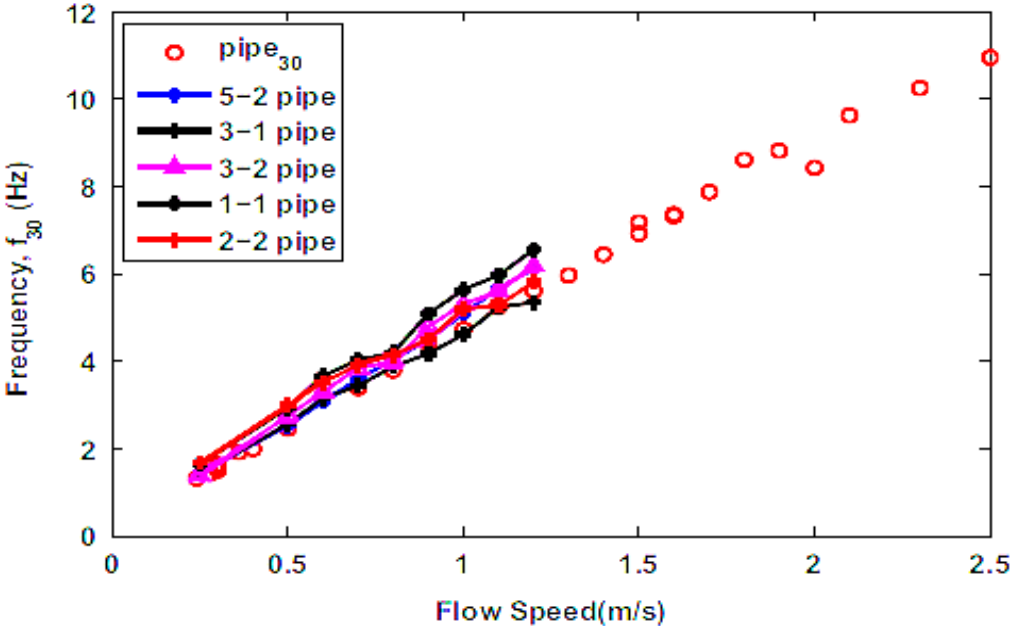


Figure 32 Frequency associated with bare section plotted against flow speed (Rao et al., 2015)

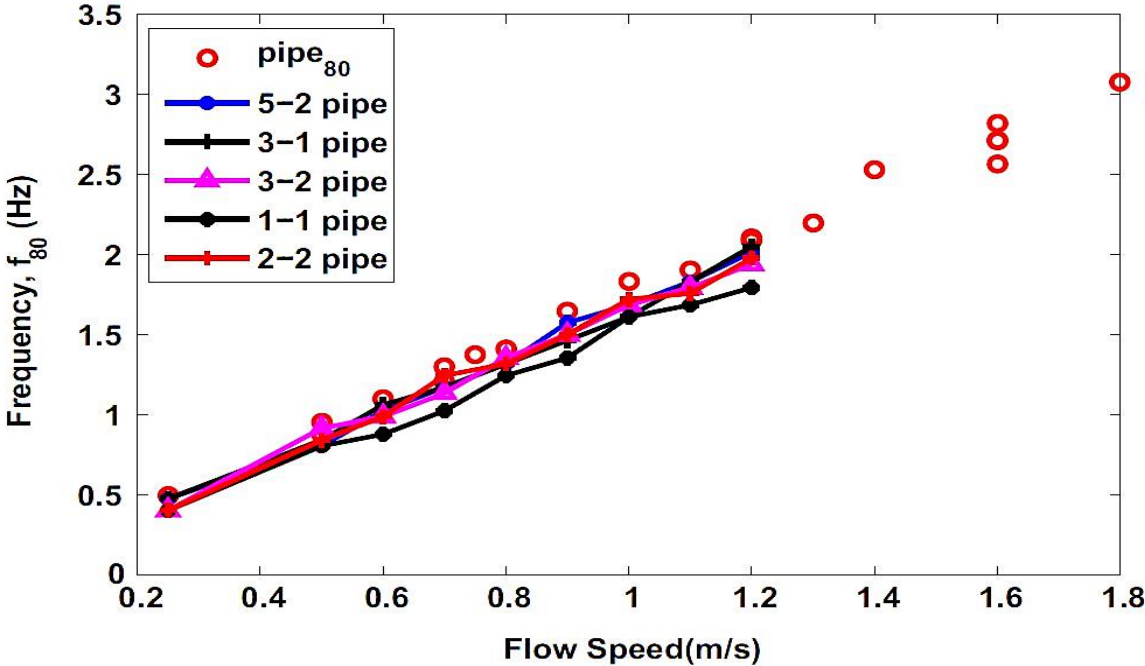


Figure 33 Frequency associated with buoyancy section against flow speed (Rao et al., 2015)

The excitation frequency is linearly related to the flow speed. The vortex shedding frequency is controlled by two different diameters ( $D_{30}$ : diameter of bare riser and  $D_{80}$ : diameter of buoyancy element). Table 3 presents the observed Strouhal number for bare riser and riser with staggered buoyancy elements.

**Table 3 The summary of  $S_t$  for bare riser and staggered buoyancy riser (Rao et al., 2015)**

Type of the pipe	$S_t$ for $D= 30$ mm	$S_t$ for $D= 80$ mm
Pipe <sub>30</sub> /pipe <sub>80</sub>	0.136	0.130
5-2 pipe	0.153	0.136
3-1 pipe	0.125	0.129
3-2 pipe	0.148	0.125
1-1 pipe	0.155	0.125
2-2 pipe	0.143	0.132

Note that this Strouhal number is different from that is used to define the shedding frequency of a fixed cylinder, which is about 0.2 in sub-critical Reynolds number range ( $10^3 - 10^5$ ) for a bare cylinder. The non-dimensional frequency for bare riser ( $D_{30}$ ) is in the range of 0.125 – 0.155 for different configurations. It can also be seen that the non-dimensional frequency for the buoyancy section ( $D_{80}$ ) in general lower than the bare riser. This is probably because the buoyancy section has the shorter length over diameter ration ( $\frac{L_B}{D_B} = 5$  and 10), which may be lead to more significant 3D effect. Hence, the corresponding non-dimensional frequency is smaller.

### 4.3.2 Maximum Fatigue Damage

The maximum fatigue damage for different configurations is summarized in Figure 34 for different configurations.

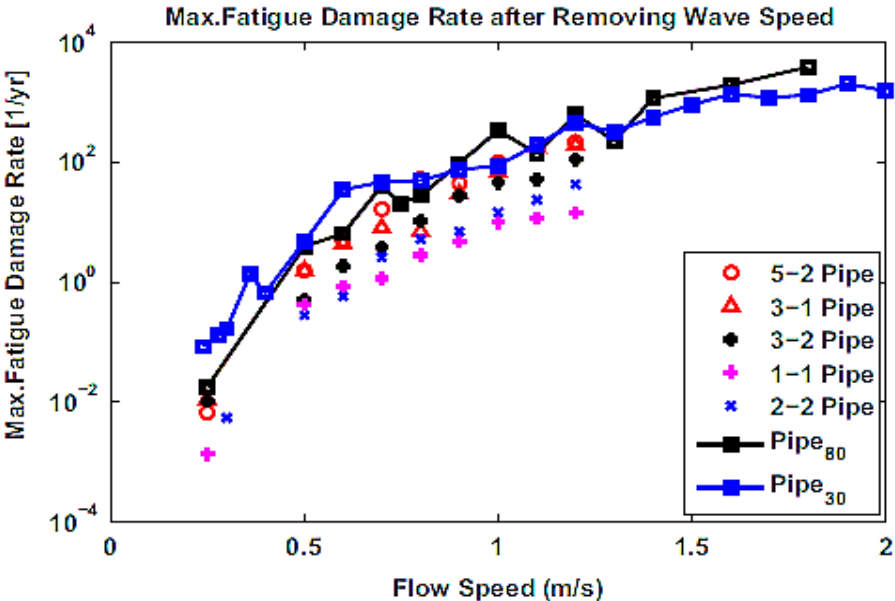


**Figure 34 Max. fatigue damage rate plotted against flow velocity (Rao et al., 2015)**

The fatigue damage rate of the staggered buoyancy riser configurations is in the range of 10 – 100 (1/yrs.) at 1.2 m/s for different configurations. The fatigue damage rate for two bare riser configurations with diameter of 30 mm and 80 mm are also presented in the figure. The constant diameter riser have higher fatigue damage rate than the riser with staggered buoyancy elements. The configuration with 1-1 has the lowest damage rate and is preferred configuration based on these tests. It was also shown in the same study that the fatigue damage contribution of the non-linear interaction frequency in the most cases are below 8% and 3 out of 45 cases are close to 20% (Rao, Vandiver et al., 2015).

### 4.3.3 Response Amplitude

In this test, the response amplitude was estimated by two methods: first was to use real modes obtained from a Finite Element Method (FEM) model of the riser and the second was to use sinusoidal functions. Figure 35 shows the reconstructed with sinusoidal and real mode shapes for 2-2 configuration at 1.0 m/s. In Figure 35, the blue line represents the reconstructed displacement accomplished with sinusoidal mode shapes and the red line represents the reconstructed response with real mode shapes. The figure shows that the riser is responding two modes due to bare and buoyancy element excitation. The figures left and right shows the comparison between the reconstructed displacement with real and sinusoidal mode shapes at higher and lower excitation frequencies respectively. The dominant response mode to excitation on buoyancy module was 3<sup>rd</sup> mode and for bare riser section is 11<sup>th</sup> mode.

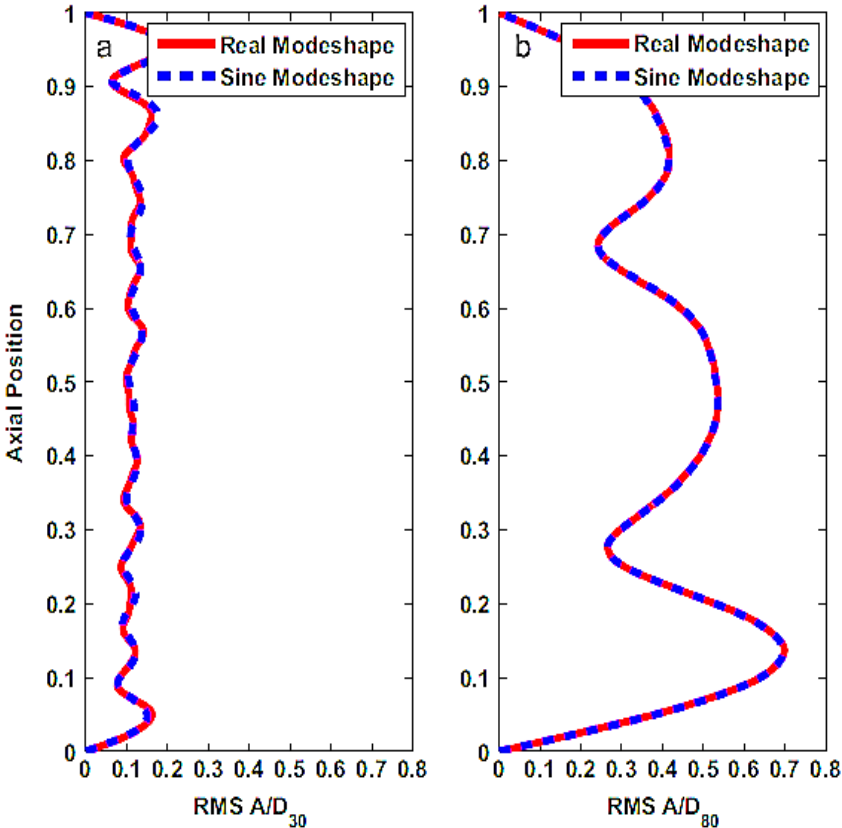


Figure 35 Reconstructed CF displacements for configuration 2-2 at U = 1.0 m/s (Rao et al., 2015)

# Chapter 5 VIVANA Simulation with Default Parameters

The source of input data for VIVANA is based on the Shell experiment conducted in the Ocean Basin at MARINTEK. The VIVANA analysis was conducted with 40 cases at varying buoyancy configurations and varying towing velocities. Each buoyant configuration consisted of 8 cases at varying towing velocities with uniform flow. The maximum flow of current is up to 1.2 m/s with  $Re \sim 96,000$  for  $OD_B = 80$  mm. The tension in the pipe for each run was approximately constant for each test but varied with uniform flow speed and configuration of buoyancy modules from test to test. The mean tensions ranged from 6000 N to 8000 N.

Figure 36 shows the riser model in VIVANA. This riser model is constructed based on the data from the Shell oil company experiment at MARINTEK Ocean basin. The properties of the riser model is as shown in Table 2.

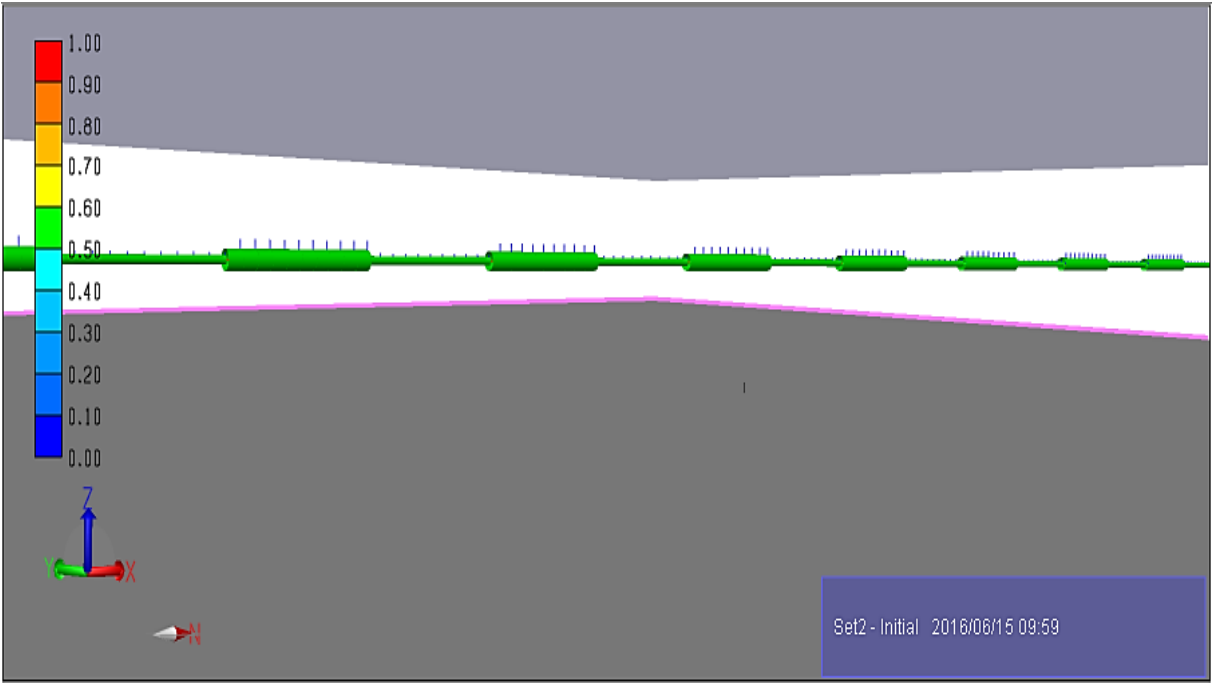


Figure 36 Riser with staggered buoyancy elements model in VIVANA

## 5.1 Presentation of Results and Comparison with Experiment results

In this section, the prediction results from VIVANA using default set of excitation parameters are presented and are compared with results from the Shell experiment at MARINTEK.

### 5.1.1 Response Frequency

The predicted response frequency is presented as a function of flow speed in Figure 37. In the graph below, each  $L_C/L_B$  value is associated with two curves; top set of curves represents the frequency of bare riser section while bottom set of curves represents frequency of buoyancy section for different buoyancy configurations. From the Figure, it is clear that for a particular  $L_C/L_B$  value, there exists a dual nature of VIV response in bare and buoyant sections.

While comparing with the measurement data (Figure 32 & Figure 33), the response frequencies are over-predicted. It means that a higher response mode is predicted. This will lead to higher stress and fatigue damage if the displacement amplitude remains the same. The equivalent  $S_r$  number can be estimated from the predicted frequencies and it is in the range of 0.16 – 0.18.

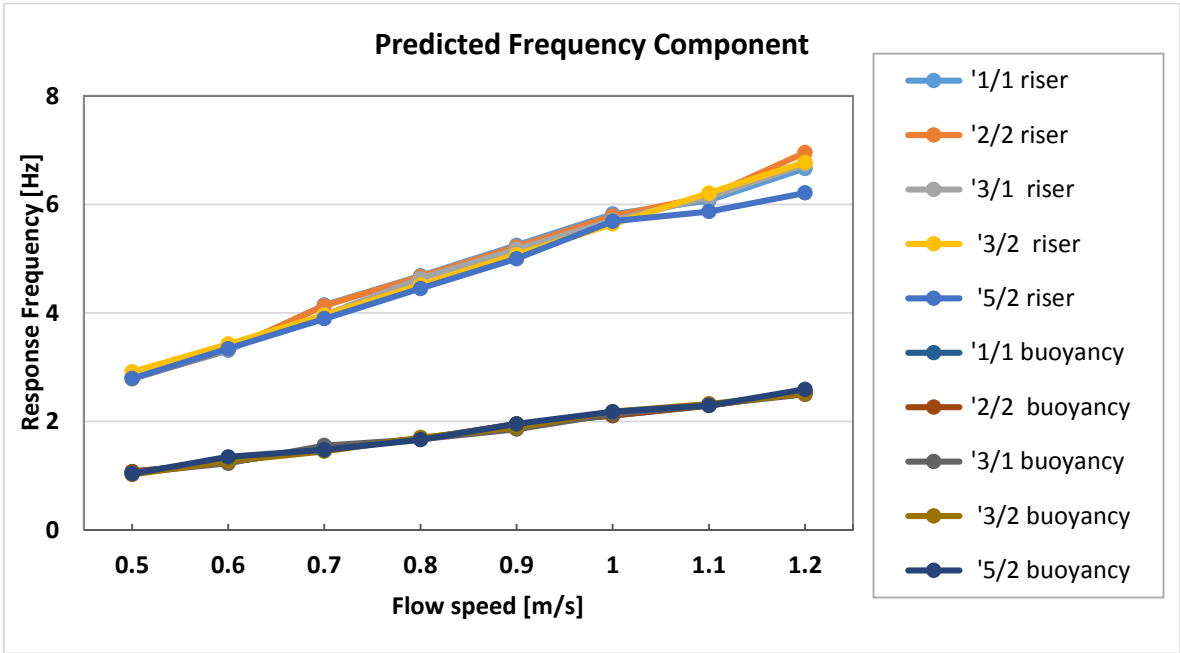
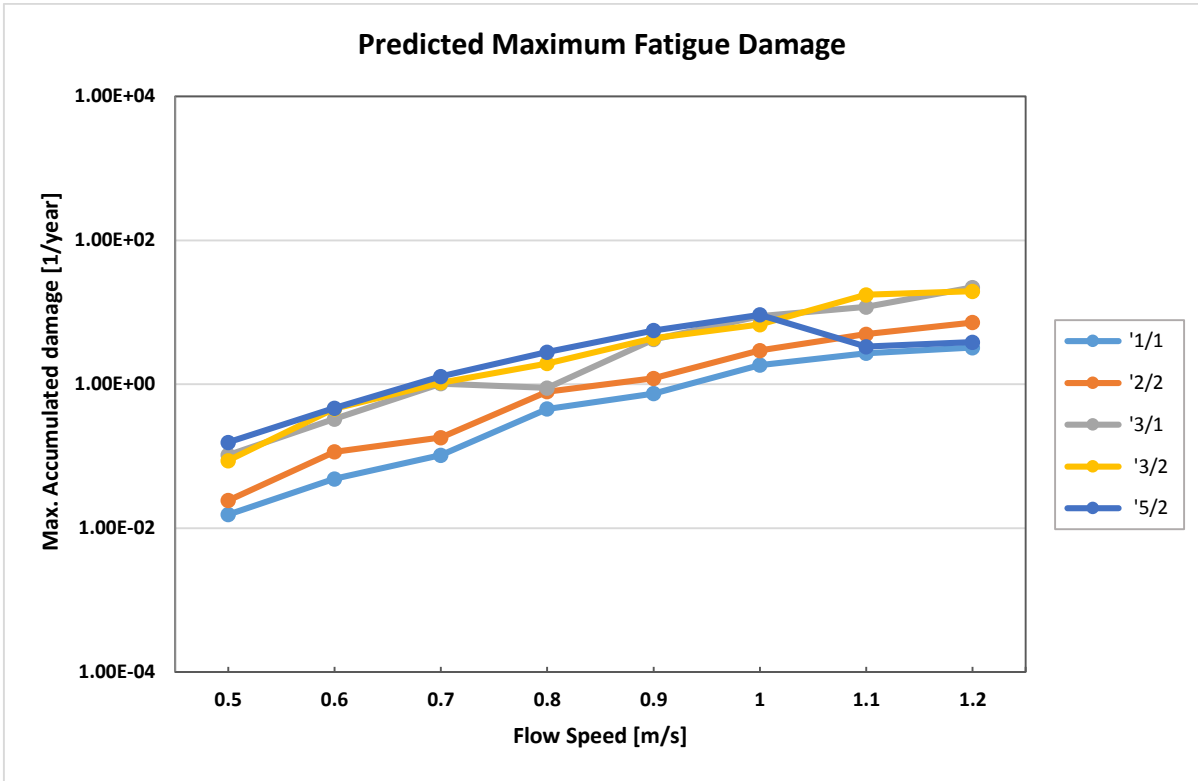


Figure 37 Predicted frequency components with default set of parameters (Wu et al., 2016)

### 5.1.2 Maximum Fatigue Damage

In general practice, S-N curves are used to estimate the fatigue damage rate of the risers. The S-N curve used is  $N \cdot S^m = C$ , with slope  $m = 3$ ,  $N$  being number of cycles,  $S$  is stress range and  $C$  is a parameter based on the type of material. Figure 38 shows the maximum fatigue rate versus flow velocity for different bare to buoyancy configurations ( $L_C/L_B$ ). For the configuration with  $L_C/L_B = 1/1$  has the lowest fatigue damage whereas highest is for  $L_C/L_B = 5/2$ .



**Figure 38 Predicted fatigue damage with default set of parameters (Wu et al., 2016)**

The predicted maximum fatigue damage at  $U=1.2$  m/s is in the range of 3 -22 (1/yrs.) for different configurations. The fatigue damage prediction follows the same trend as what was observed from the experiment. The fatigue damage is under-predicted, even though the response frequencies are over-predicted.

### 5.1.3 Response Amplitude

The predicted A/D for 2-2 configuration at  $U=1.0$  m/s is presented in Figure 39. It shows that the riser is responding at two response frequencies/modes due to bare riser and buoyancy element excitation. The predicted shedding frequency of the buoyancy element is about 2.1 Hz and the 5<sup>th</sup> mode of the riser system is excited. While the shedding frequency of the bare riser section is 5.8 Hz, which corresponds to the 14<sup>th</sup> mode.

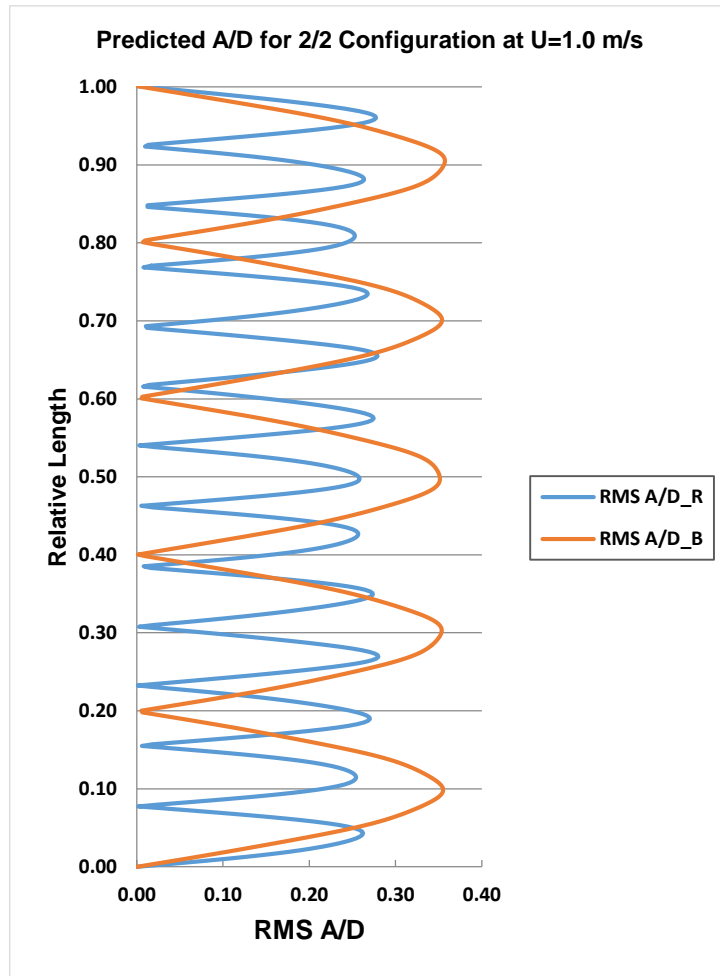


**Figure 39 Predicted CF amplitude with default set of parameters for 2-2 configuration at 1.0 m/s (Wu et al., 2016)**

The snapshots of the displacement are shown in Figure 40.

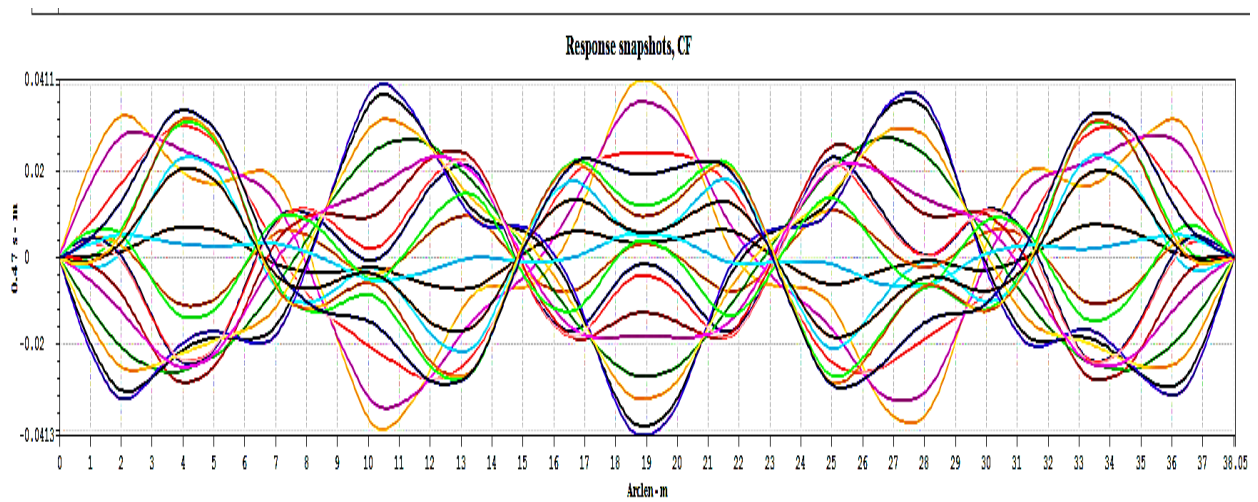


**Figure 40 Snapshots of CF displacement with default set of parameters for 2-2 configuration at 1.0 m/s (Wu et al., 2016)**

## **5.2 Uncertainties**

The main uncertainties in VIVANA for this thesis is the input data and the results from the Shell experiment.

### **5.2.1 Uncertainties in the Extraction of the Test Results**

Input data for generating riser model in VIVANA is not fully available from the experiment and this made to assume some data based on the available information from Rao et al., 2015 and Jhingran et al., 2012. The results from the Shell experiment presented in the form of graphs for response frequency and maximum accumulated damage do not provide any numerical values. Uncertainty may be associated while extracting information from those graphs. There is no available output data for response amplitude and mode numbers for configurations at different flow speeds except for 2/2 configuration at  $U=1.0$  m/s flow speed. This is the main limitation while comparing the results from VIVANA analysis to the Shell experiment results in order to obtain an optimal set of excitation parameters based on different flow speed conditions. This allowed to select an optimal set of parameters based only on one flow condition i.e. for 2/2 configuration at 1.0 m/s flow speed. In addition, these tests were carried out in the uniform flows, which means that the VIV responses are limited to a small range of the non-dimensional frequency.

### **5.2.2 Uncertainties in the Default Force Coefficient Parameters**

The default hydrodynamic force coefficient parameters are generalized based on rigid cylinder test. It has limitations to describe the responses of a flexible cylinder where the IL responses can have significant influences on CF ones. There is also lack of model to account for the interaction between bare riser section and the buoyancy element. It is observed that the response frequency is over-predicted when using the default parameters.

# Chapter 6 Modification of Hydrodynamic Coefficients

## 6.1 Default Excitation Coefficient Database in VIVANA

From Figure 41, larger Strouhal values are seen for the smooth cylinder at certain Re.  $S_t$  of 0.47 is not realistic for offshore riser due to the presence of turbulence. The effect of turbulence on  $A/D$  and  $C_e$  is not considered in this thesis and considered of less importance than a Strouhal number.

The Figure 41 shows the default Strouhal number curve as a function of Re used in VIVANA.

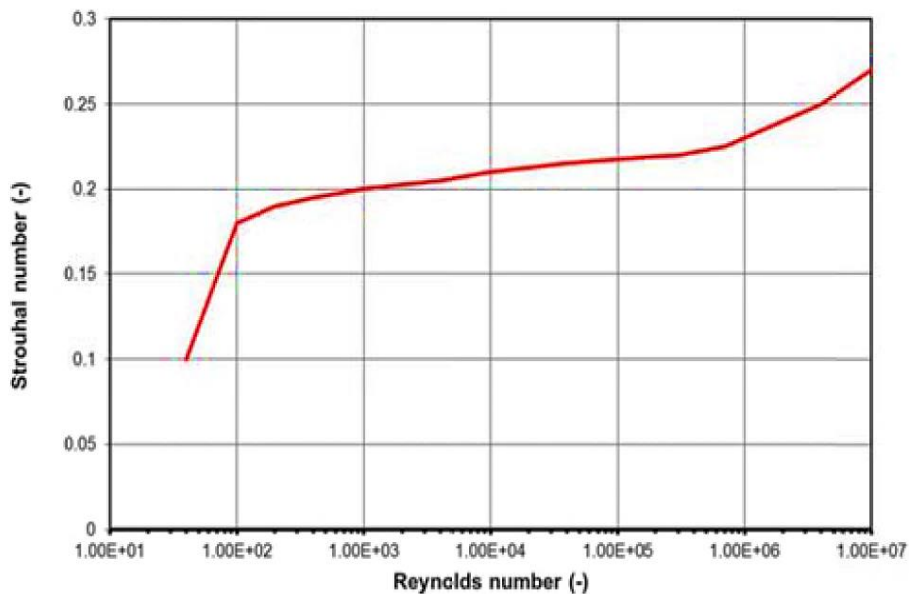


Figure 41 Strouhal number as a function of Reynolds number (Larsen C M et al., 2009)

The built-in set of excitation parameters in VIVANA is defined as a function of response amplitude ratio for a given non-dimensional frequency as shown in Figure 25 and Figure 26. The curves in those figures are explained as follows:

- Point A defines the excitation coefficient value when the amplitude is zero,  $C_{e,CF,A/D=0}$
- Point B defines the maximum excitation coefficient  $C_{e,CF=\max}$  to the corresponding amplitude ratio  $A/D_{C_{e,CF=\max}}$
- Point C defines the  $A/D$  values when the excitation coefficient is zero.

Both the amplitude ratio and excitation coefficient are significantly based on Reynolds number and surface roughness ratio. In the present thesis, the effect of Re and surface roughness ratio on two parameters is explicitly not considered. In order to use VIV tools such as VIVANA, the hydrodynamics coefficients should be modified according to the actual flow conditions that took place in the Shell experiment at MARINTEK.

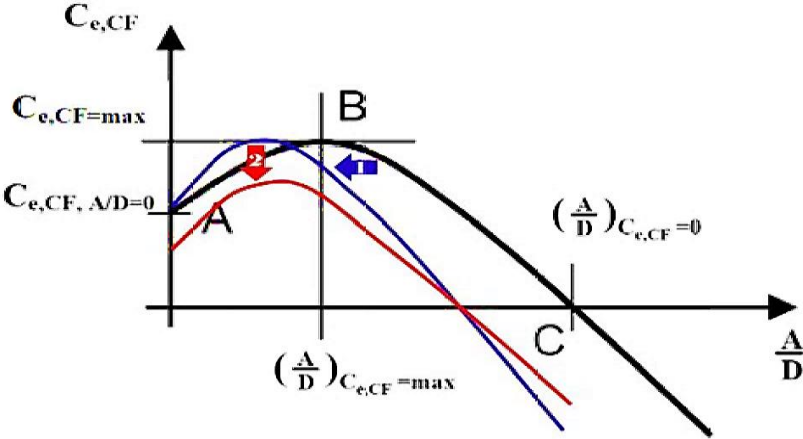


Figure 42 Black curve: default CF excitation coefficient curve at particular non-dimensional frequency in VIVANA, Blue curve: after amplitude modification, red curve: after excitation coefficient modification (Yin et al., 2015).

### 6.1.1 Change in Range of Non-dimensional Frequency

In VIVANA, the default value of non-dimensional frequency for corresponding peak values of response amplitude ratio and excitation force coefficient is 0.172. In the present analysis, this value is ranged from 0.13 – 0.20 with an interval of 0.02 for different amplitude ratio and excitation coefficient modification factors as stated in below sections.

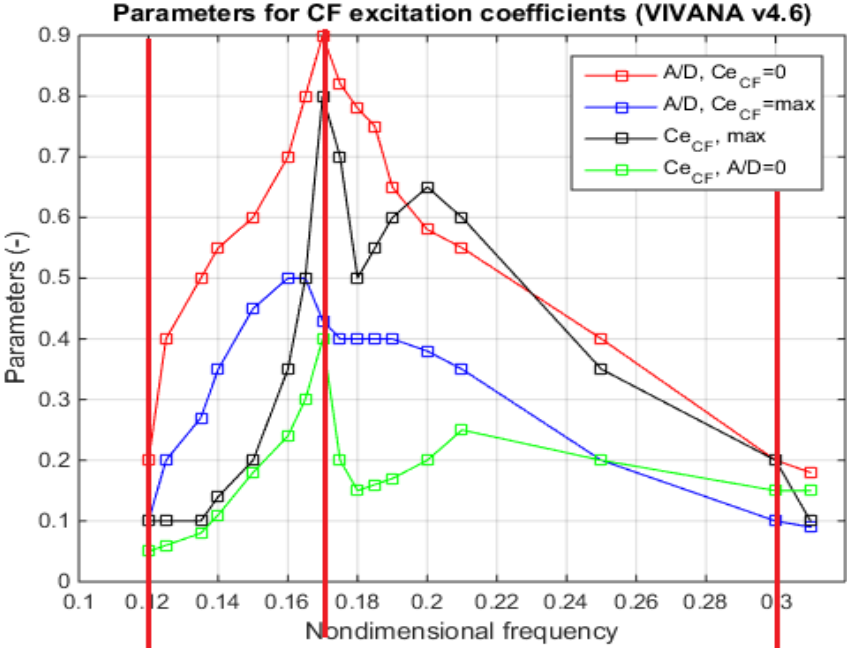


Figure 43 Parameterization of the excitation coefficient curves.

The default Ce curves VIVANA contains 26 rows of different  $\hat{f}_{CF}$  points as shown in Table 4. These 26 points are simplified by reducing to 3 points (red lines) as shown in Figure 43, represents the peak Ce curve. The lower and upper ranges of non-dimensional frequency ranges are same as the default set of parameters in VIVANA (Table 4) and they remain constant for every test case, only the middle row of excitation parameters as shown in Table 5 is changed based on the modification factors of amplitude ratio and excitation coefficient. The values between specified points will be linearly interpreted in VIVANA.

**Table 4 Default set of parameters from VIVANA (Passano et al., 2015)**

$\hat{f}_{CF}$	$\left(\frac{A}{D}\right)_{C_{e,CF}=0}$	$\left(\frac{A}{D}\right)_{C_{e,CF}=\max}$	$C_{e,CF=\max}$	$C_{e,CF,\frac{A}{D}=0}$
0.12	0.149	0.1	0.1	0
0.125	0.266	0.2	0.1	0
0.127	0.4	0.214	0.1	0.016
0.13	0.451	0.235	0.1	0.04
0.135	0.505	0.27	0.1	0.08
0.14	0.53	0.35	0.14	0.11
0.15	0.588	0.45	0.2	0.18
0.16	0.658	0.5	0.35	0.24
0.165	0.746	0.5	0.5	0.3
0.168	0.89	0.46	0.78	0.35
0.172	0.9	0.43	0.8	0.4
0.175	0.837	0.4	0.7	0.2
0.18	0.761	0.4	0.4	0.1
0.185	0.706	0.4	0.3	0
0.19	0.666	0.4	0.2	0
0.2	0.615	0.38	0.1	0
0.21	0.592	0.35	0.1	0
0.22	0.575	0.313	0.1	0
0.23	0.539	0.275	0.1	0
0.24	0.504	0.238	0.1	0
0.25	0.42	0.2	0.1	0
0.27	0.312	0.16	0.1	0
0.28	0.247	0.14	0.1	0
0.29	0.186	0.12	0.1	0
0.3	0.16	0.1	0.1	0
0.31	0.136	0.09	0.1	0

By parameterization of Ce curves as shown in Figure 43, only three rows of excitation parameters are selected and they are termed as one set of excitation parameters throughout the remaining part of this thesis.

**Table 5 Default set of parameters (Passano et al., 2015)**

$\hat{f}_{CF}$	$\left(\frac{A}{D}\right)_{C_e,CF=0}$	$\left(\frac{A}{D}\right)_{C_e,CF=\max}$	$C_{e,CF=\max}$	$C_{e,CF,\frac{A}{D}=0}$	Modification factor	
					$\gamma_{A/D}$	$\gamma_{C_e}$
120	0.149	0.100	0.100	0.000	-	-
172	0.900	0.430	0.800	0.400	1.0	1.0
00	0.160	0.100	0.100	0.000	-	-

The lower and upper range of non-dimensional frequency are 0.120 and 0.30 respectively and they remain constant for every test with their respective amplitude ratios and excitation coefficients as shown in Table 5. The non-dimensional frequency corresponding to second row (i.e. at  $\hat{f}_{CF}$  of 0.172) in Table 5 is changed for every set and its excitation coefficients are multiplied with modification factors to generate new sets of excitation parameters.

### 6.1.2 Amplitude Ratio Modification

In order to obtain the similar range of results from VIVANA simulation when compared with the Shell experiment, the amplitude ratio should be modified according to existing experimental results. The amplitude modification factor is defined as

$$\gamma_{A/D} = \frac{A/D_{C_e,CF=0,\max}}{(A/D_{C_e,CF=0,\max})_{\text{def}}} \quad (18)$$

where

$(A/D_{C_e,CF=0,\max})_{\text{def}}$  is the default maximum amplitude ratio from VIVANA theory manual.

$A/D_{C_e,CF=0,\max}$  is the modified maximum response amplitude ratio.

$\gamma_{A/D}$  is the amplitude modification factor.

#### **For example:**

In VIVANA, the default peak value of  $(A/D_{C_e,CF=0})_{\text{def}}$  is 0.9 at a non-dimensional frequency of 0.172 and the amplitude ratio modification factor is ranged between 0.5 – 1.5.

When  $\gamma_{A/D} = 0.8$ , then we have

$$A/D_{C_e,CF=0} = (A/D_{C_e,CF=0})_{\text{def}} \times \gamma_{A/D} = 0.9 \times 0.8 = 0.72 \quad (19)$$

The blue line in the Figure 42 shows the modified excitation coefficient curve after applying a modification factor less than 1. It is clear that the response amplitude ratio values at points B and C become smaller than the original curve (black line), but the excitation coefficient values at points A and B remain same.

### 6.1.3 Excitation Coefficient Modification

The excitation coefficient modification factor is defined as:

$$\gamma_{C_e} = \frac{C_{e_{A/D=\max}}}{(C_{e_{A/D=\max}})_{\text{def}}} \quad (20)$$

Where

$(C_{e_{A/D=\max}})_{\text{def}}$  is the default excitation coefficient data set

$C_{e_{A/D=\max}}$  is the modified excitation coefficient data set

$\gamma_{C_e}$  is the excitation coefficient modification factor.

#### **For example:**

The default peak value of  $(C_{e_{A/D=\max}})_{\text{def}}$  is 0.8 at a non-dimensional frequency of 0.172 and by choosing  $\gamma_{C_e}$  as 0.8, then we have

$$C_{e_{A/D=\max}} = (C_{e_{A/D=\max}})_{\text{def}} \times \gamma_{C_e} = 0.8 \times 0.8 = 0.64 \quad (21)$$

Figure 42 shows the modification process. By applying amplitude ratio modification factor (step 1) at each non-dimensional frequency, the blue excitation coefficient curve is obtained. Based on step 1, the final excitation coefficient curve (red curve) is obtained after applying excitation coefficient modification factor (step 2).

## 6.2 Procedure to Obtain an Optimal Set of Parameters

In this section, the procedure to obtain an optimal set of parameters is explained. In order to obtain an optimal set of parameters, different sets of excitation parameters are generated by using modification factors and these sets are used to run the simulation. The results are compared with the experimental results in terms of response frequency, mode and maximum accumulated fatigue damage and the best approximation is selected as the optimal set of parameters based on the specified criteria.

### 6.2.1 Generating New Set of Excitation Parameters

Besides to the default set of excitation parameters, amplitude ratio and excitation coefficient modification factors are used to generate the new set of parameters to obtain an optimal set based on response frequency, mode and fatigue damage comparison. In this thesis, these modification factors range is chosen without considering the effect of Reynolds number and surface roughness ratio.

For generating new sets of excitation parameters, one default set of excitation parameters is selected from VIVANA theory manual for a non-dimensional frequency of 0.172 as shown in Table 6. These are the peak values for this non-dimensional frequency. Modification factors are used to multiply these excitation parameters to generate new sets of excitation parameters.

**Table 6 Default set of excitation coefficient parameters (Passano et al., 2015)**

$\hat{f}_{CF}$	$\left(\frac{A}{D}\right)_{C_{e,CF}=0}$	$\left(\frac{A}{D}\right)_{C_{e,CF}=\max}$	$C_{e,CF}=\max$	$C_{e,CF,\frac{A}{D}=0}$
0.172	0.9	0.43	0.8	0.4

The range of amplitude ratio modification factor in this thesis is considered as 0.7 – 1.2 with an interval of 0.05. This range is selected based on criteria that A/D should not exceed 1.2 as damping will occur.

The range of excitation force coefficient modification factor is 0.8 – 1.75 with an interval of 0.05. Different new sets of parameters are generated by considering the range of non-dimensional frequency and modification factors. An example of generating a new set of parameters is defined in Table 7 (for more sets see appendix). Figure 44 presents the computation loop in VIVANA to achieve an optimal set of parameters for a specific flow speed. For every iteration, the results are compared with the experimental results and an optimal set of excitation parameters are selected.

**Table 7 New sets of excitation parameters for different modification factors for a riser with staggered buoyancy elements.**

S-Test No.	$\hat{f}_{CF}$	$\left(\frac{A}{D}\right)_{C_{e,CF}=0}$	$\left(\frac{A}{D}\right)_{C_{e,CF}=\max}$	$C_{e,CF}=\max$	$C_{e,CF,\frac{A}{D}=0}$	Modification factor	
						$\gamma_{A/D}$	$\gamma_{Ce}$
1	0.13	0.63	0.301	0.64	0.32	0.70	0.8
2	0.13	0.675	0.3225	0.64	0.32	0.75	0.8
3	0.13	0.72	0.344	0.64	0.32	0.80	0.8
4	0.13	0.765	0.3655	0.64	0.32	0.85	0.8
5	0.13	0.81	0.387	0.64	0.32	0.90	0.8
6	0.13	0.855	0.4085	0.64	0.32	0.95	0.8
7	0.13	0.90	0.430	0.64	0.32	1.00	0.8
8	0.13	0.945	0.4515	0.64	0.32	1.05	0.8
9	0.13	0.99	0.473	0.64	0.32	1.10	0.8
10	0.13	1.035	0.4945	0.64	0.32	1.15	0.8
11	0.13	1.08	0.516	0.64	0.32	1.20	0.8

S-Test represents the sets of parameters used for Riser with Staggered Buoyancy Elements.

## Computational loop to achieve the optimal set of excitation parameters for a specific flow speed

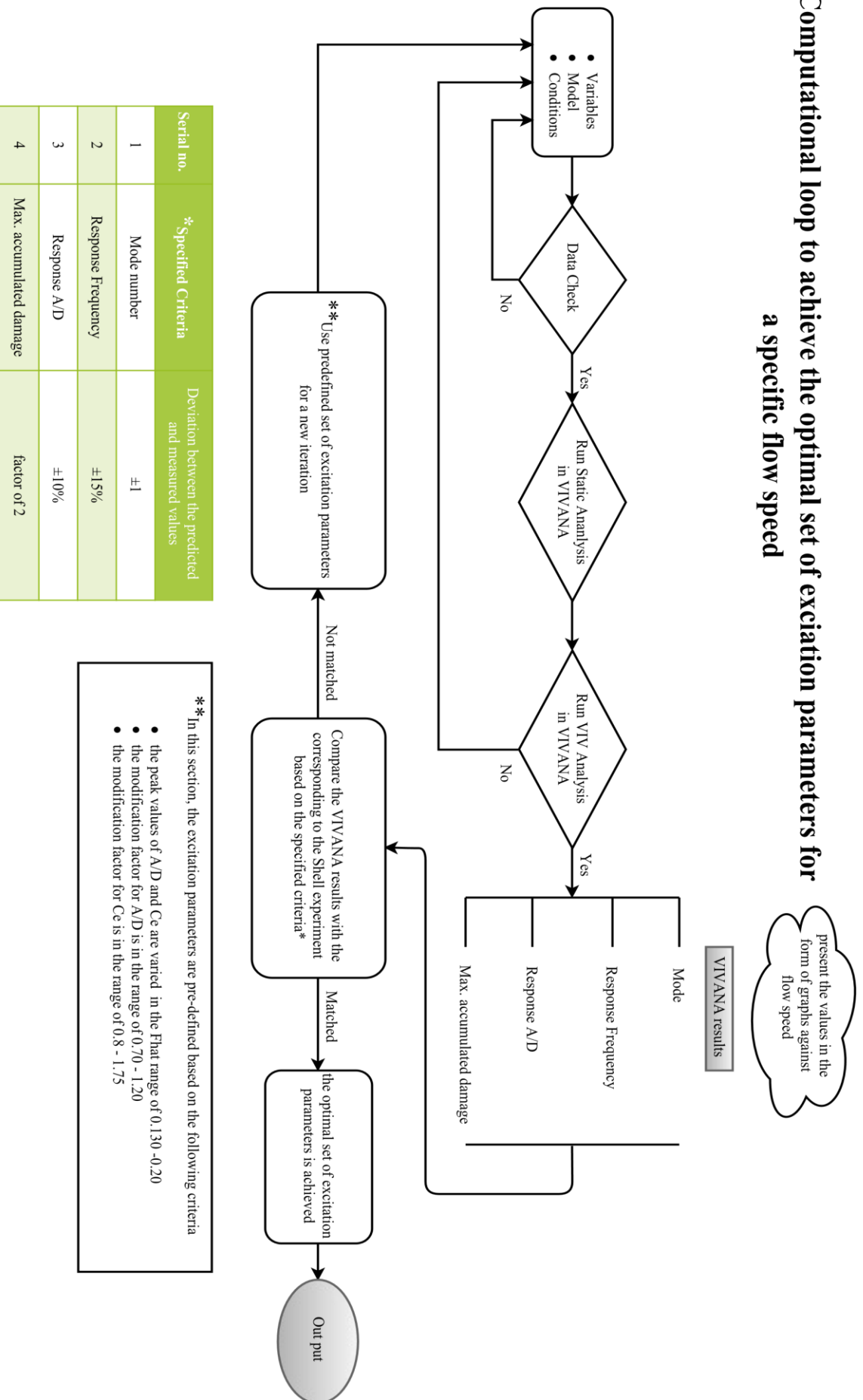


Figure 44 Algorithm showing how to obtain an optimal set of excitation coefficient parameters

### 6.3 Testing the Algorithm of VIVANA for Bare Riser

In this section, the verification and validation of an algorithm of VIVANA program are briefly explained. This program relies on hydrodynamic force coefficient database generated from forced motion test with a rigid bare cylinder section. In order to verify VIVANA, its algorithm is tested by running simulations for a bare riser at 1.0 m/s flow speed with default excitation coefficient parameters from VIVANA and the user defined excitation coefficient parameters. These results are compared in terms of response frequency, mode number and maximum accumulated damage and it is verified whether it is possible to produce best fit (best set of parameters) to default curve based on specified criteria.

For this verification, new sets of excitation coefficient parameters are generated in a similar way as mention above but with different range modification factors. The non-dimensional frequency for this section is ranged between 0.130 – 0.190 with an interval of 0.02, whereas the modification factors for A/D and Ce are ranged between 0.5 – 1.2 with an interval of 0.1. Table 7 shows the new sets of excitation parameters with amplitude modification factor from 0.5 – 1.2 and excitation coefficient modification factor of 0.8.

**Table 8 New sets of excitation parameters for different modification factors for a bare riser.**

Test No.	$\hat{f}_{CF}$	$\left(\frac{A}{D}\right)_{C_{e,CF}=0}$	$\left(\frac{A}{D}\right)_{C_{e,CF}=\max}$	$C_{e,CF=\max}$	$C_{e,CF\frac{A}{D}=0}$	Modification factor	
						$\gamma_{A/D}$	$\gamma_{Ce}$
2193	0.166	0.45	0.215	0.64	0.32	0.5	0.8
2194	0.166	0.54	0.258	0.64	0.32	0.6	0.8
2195	0.166	0.63	0.301	0.64	0.32	0.7	0.8
2196	0.166	0.72	0.344	0.64	0.32	0.8	0.8
2197	0.166	0.81	0.387	0.64	0.32	0.9	0.8
2198	0.166	0.90	0.430	0.64	0.32	1	0.8
2199	0.166	0.99	0.473	0.64	0.32	1.1	0.8
2200	0.166	1.08	0.516	0.64	0.32	1.2	0.8

Test represents the sets of parameters used for bare riser for testing the algorithm.

#### **VIVANA analysis:**

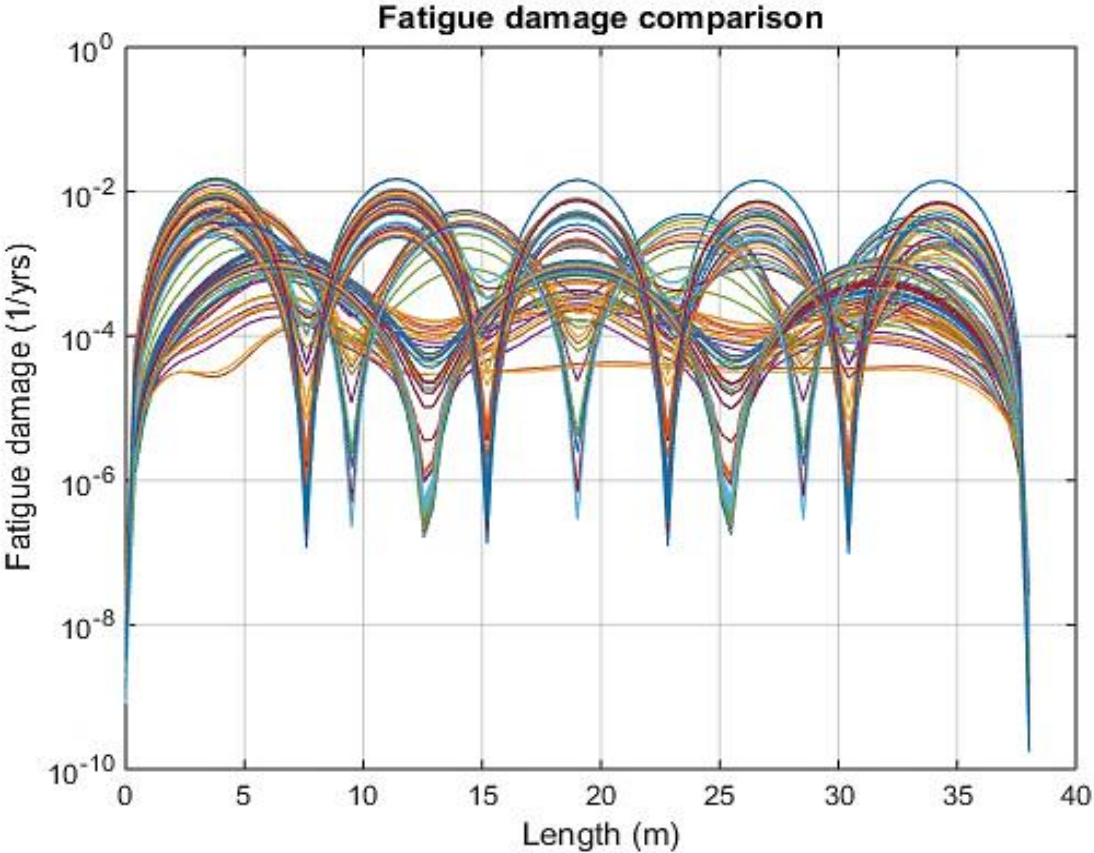
- VIVANA version 4.0.8 has been used
- Pure CF VIV analysis
- Current direction: perpendicular to SLWR plane (global XZ) (see Figure 36)
- SN curve: one slope D curve from DNV-RP-C203 with slope = 3. The curve is defined by  $\log N = \log C - m \log S$
- Excitation coefficients
  - a. Default data from VIVANA
  - b. User defined data based on modification factors
- Flow speed 1.0 m/s
- Properties of bare riser model are as in Table 9

Table 9 represents the input data used for generating the bare riser model in VIVANA.

**Table 9 Bare riser model properties.**

Parameters	Bare pipe
Total length between pinned ends (m)	38.00
Outer diameter (mm)	30.00
Bending stiffness, EI (Nm <sup>2</sup> )	572.3
Young's modulus, E (N/m <sup>2</sup> )	3.46×10 <sup>10</sup>
Mass in air (kg/m)	1.088
Weight in water (kg/m)	0.579
Mass ratio	1.54
Added mass coefficient	1.0

Based on the range of non-dimensional frequency and modification factors range, 3720 different sets of excitation parameters are generated and these sets are used to check whether it is possible to generate a set which gives the best fit to the default curve (default set of parameters in VIVANA). By using 3720 test cases, Figure 45 is generated and every test case is verified and compared with default test case in terms of response frequency, mode number and maximum accumulated fatigue damage.



**Figure 45 Fatigue damage comparison for different sets of excitation coefficient parameters**

By comparing the response values from the above figure, the best fit to default curve is selected based on specified criteria as mentioned in the below Table 10.

**Table 10 Specified criteria for selecting the best set of parameters.**

Specified Criteria	Deviation between the predicted test case and default test case in
Mode	$\pm 0$
Response Frequency	$\pm 10\%$
Max. Fatigue damage	Factor of 2

The set which gave the good prediction to the default set of excitation parameters in VIVANA is shown in Table 11. And its corresponding fatigue damage comparison and mode number, response frequency are shown in Figure 46 and Table 12 respectively.

**Table 11 Set of parameters which gave good prediction to the default parameters.**

Test No.	$\hat{f}_{CF}$	$\left(\frac{A}{D}\right)_{C_e,CF=0}$	$\left(\frac{A}{D}\right)_{C_e,CF=\max}$	$C_{eCF=\max}$	$C_{eCF, \frac{A}{D}=0}$	Modification factor	
						$\gamma_{A/D}$	$\gamma_{C_e}$
2197	0.12	0.149	0.1	0.1	0	-	-
	0.166	0.81	0.387	0.64	0.32	0.9	0.8
	0.300	0.160	0.100	0.100	0.000	-	-

Test = number of test cases for bare riser for testing the algorithm.

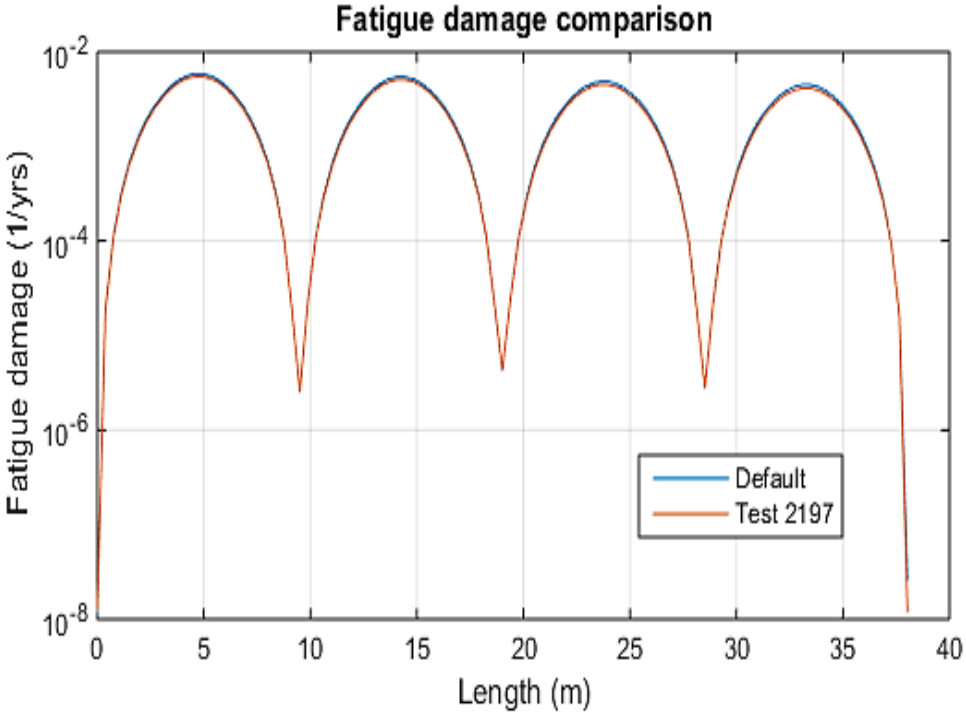


**Figure 46 Comparison of accumulated fatigue damage between Test no. 2197 and default case.**

**Table 12 Response values for the default set of parameters and Test no. 2197.**

Test no.	Max. Fatigue damage $\times 10^{-3}$	Bare riser response	
		Mode no.	Frequency
default curve	5.8639	4	2.778
2197	5.4830	4	2.778

For Test no. 2197, the mode number and response frequency are identical to the default test case with mode number as 4 and response frequency as 2.778 Hz. But the maximum accumulated fatigue damage for Test no. 2197 is 6.5% less than the default test case which is acceptable based on the specified criteria. This is because of change in the peak non-dimensional frequency as it is shifted towards the left side when compared with the default contour plot for excitation coefficient curves (see Figure 47 ) and change in the amplitude ratios and excitation coefficients.

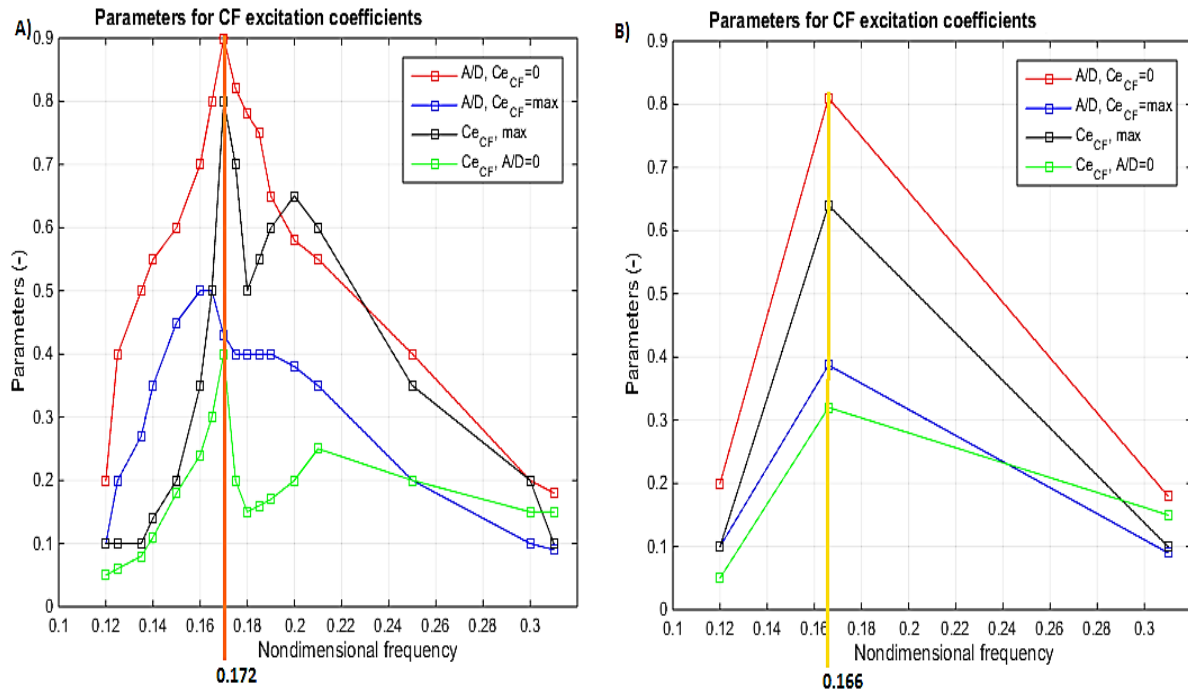


**Figure 47 Comparison between the contour curves of A) default set of parameters and B) set of parameters for Test no. 2197.**

## 6.4 Testing the Algorithm of VIVANA for a Riser with Staggered Buoyancy Elements

In this section, the verification and validation of an algorithm of VIVANA program are briefly explained for riser with staggered buoyancy elements for 2/2 configuration at 1.0 m/s flow speed. In order to verify VIVANA, its algorithm is tested by running simulations for a buoyancy riser with default excitation coefficient parameters of VIVANA and the user defined excitation coefficient parameters. These results are compared in terms of response frequency, mode number and maximum accumulated damage and it is verified whether it is possible to produce best fit (best set of parameters) to default curve based on specified criteria.

For generating new sets of excitation coefficient parameters, the procedure presented in section 6.3 is used with same range of non-dimensional frequency and modification factors for both amplitude ration and excitation coefficients.

**Table 13 New sets of excitation parameters for different modification factors for a bare riser.**

Test** No.	$\hat{f}_{CF}$	$\left(\frac{A}{D}\right)_{C_{e,CF}=0}$	$\left(\frac{A}{D}\right)_{C_{e,CF}=\max}$	$C_{eCF=\max}$	$C_{eCF, \frac{A}{D}=0}$	Modification factor	
						$\gamma_{A/D}$	$\gamma_{Ce}$
2425	0.170	0.45	0.215	0.72	0.36	0.5	0.9
2426	0.170	0.54	0.258	0.72	0.36	0.6	0.9
2427	0.170	0.63	0.301	0.72	0.36	0.7	0.9
2428	0.170	0.72	0.344	0.72	0.36	0.8	0.9
2429	0.170	0.81	0.387	0.72	0.36	0.9	0.9
2430	0.170	0.90	0.430	0.72	0.36	1	0.9
2431	0.170	0.99	0.473	0.72	0.36	1.1	0.9
2432	0.170	1.08	0.516	0.72	0.36	1.2	0.9

Test\*\* represents the sets of parameters used for riser with staggered buoyancy elements testing the algorithm.

### **VIVANA analysis:**

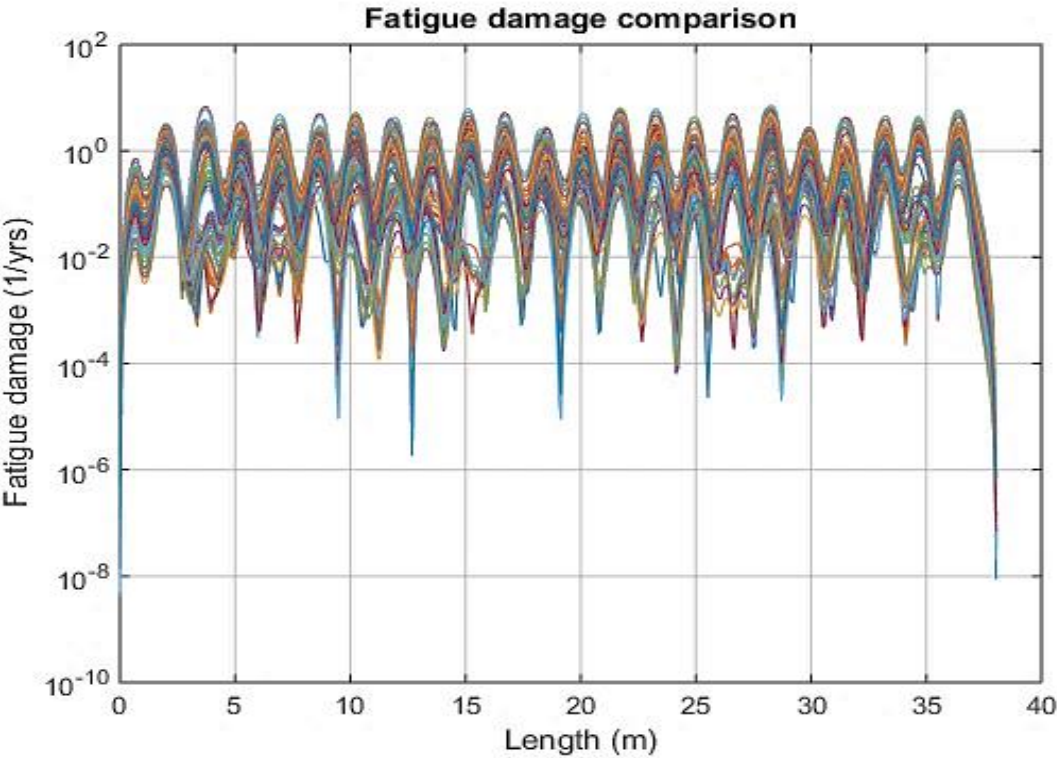
- VIVANA version 4.0.8 has been used
- Pure CF VIV analysis
- Current direction: perpendicular to global XZ (see Figure 36)
- SN curve: one slope D curve from DNV-RP-C203 with slope = 3. The curve is defined by  $\log N = \log C - m \log S$
- Excitation coefficients
  - a. Default data from VIVANA
  - b. User defined data based on modification factors
- Flow speed 1.0 m/s
- Properties of riser with staggered buoyancy elements are as in Table 14
- Added mass coefficient is 1.0

Table 14 represents the input data used for generating the riser with staggered buoyancy elements model in VIVANA.

**Table 14 Properties of the Riser with staggered buoyancy elements for VIVANA analysis.**

Parameters	Bare pipe	Buoyancy element
Total length between pinned ends (m)	38.00	38.00
Outer diameter (mm)	30.00	80.00
Outer/inner diameter of fiberglass rod/pipe (mm)	27/21	27/21
The length of one buoyancy element (mm)	--	0.4086
Bending stiffness, EI (Nm <sup>2</sup> )	572.3	572.3
Young's modulus, E (N/m <sup>2</sup> )	3.46×10 <sup>10</sup>	3.46×10 <sup>10</sup>
Mass in air (kg/m)	1.088	5.708
Weight in water (kg/m)	0.579	0.937
Mass ratio	1.54	1.14

Based on the range of non-dimensional frequency and modification factors range, 3720 different sets of excitation parameters are generated and these sets are used to check whether it is possible to generate a set which gives the best fit to the default curve (default set of parameters in VIVANA). By using 3720 test cases, Figure 48 is generated from VIVANA analysis and every test case is verified and compared with default test case in terms of response frequency, mode number and maximum accumulated fatigue damage.



**Figure 48 Fatigue damage comparison for different sets of excitation coefficient parameters**

By comparing the response values from the above figure, the best fit to default curve is chosen based on specified criteria as mentioned in the below Table 15.

**Table 15 Specified criteria for selecting the best set of parameters.**

Specified Criteria	Deviation between the predicted test case and default test case in %
Mode	±0
Response Frequency	±5
Max. Fatigue damage	±10

The set which gives the good prediction to the default set of excitation parameters in VIVANA is shown in Table 16. And its corresponding fatigue damage comparison and mode number, response frequency are shown in Figure 49 and Table 17 respectively.

**Table 16 Set of parameters which gave good prediction to the default parameters.**

Test** No.	$\hat{f}_{CF}$	$\left(\frac{A}{D}\right)_{C_{e,CF}=0}$	$\left(\frac{A}{D}\right)_{C_{e,CF}=\max}$	$C_{eCF=\max}$	$C_{eCF, \frac{A}{D}=0}$	Modification factor	
						$Y_{A/D}$	$Y_{Ce}$
	0.12	0.149	0.1	0.1	0	-	-
2430	0.17	0.99	0.473	0.72	0.36	1.0	0.9
	0.300	0.160	0.100	0.100	0.000	-	-

Test\*\* = number of test cases for riser with staggered buoyancy elements for testing algorithm.

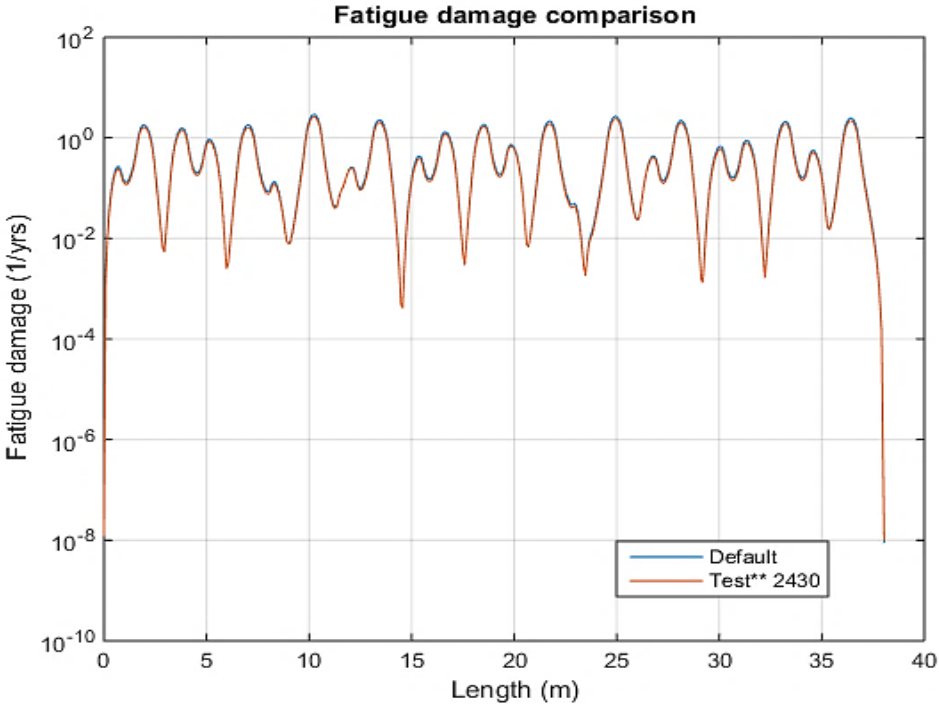


**Figure 49 Comparison of max. accumulated fatigue damage between Test no. 2430 and default case.**

**Table 17 Response values for the default set of parameters and Test no. 2197.**

Test** no.	Max. Fatigue damage	Responses			
		Buoyancy		Bare	
		Mode no.	Frequency	Mode no.	Frequency
default	2.9407	5	2.1905	14	5.7855
2430	2.6486	5	2.1905	14	5.7855

For Test no. 2430, the mode number and response frequency are identical to the default set of parameters. But the maximum accumulated fatigue damage for Test no. 2430 is 9.9% less than the default set of parameters which is acceptable based on the specified criteria. This is due to shift in the peak non-dimensional frequency as shown in the Figure 50.

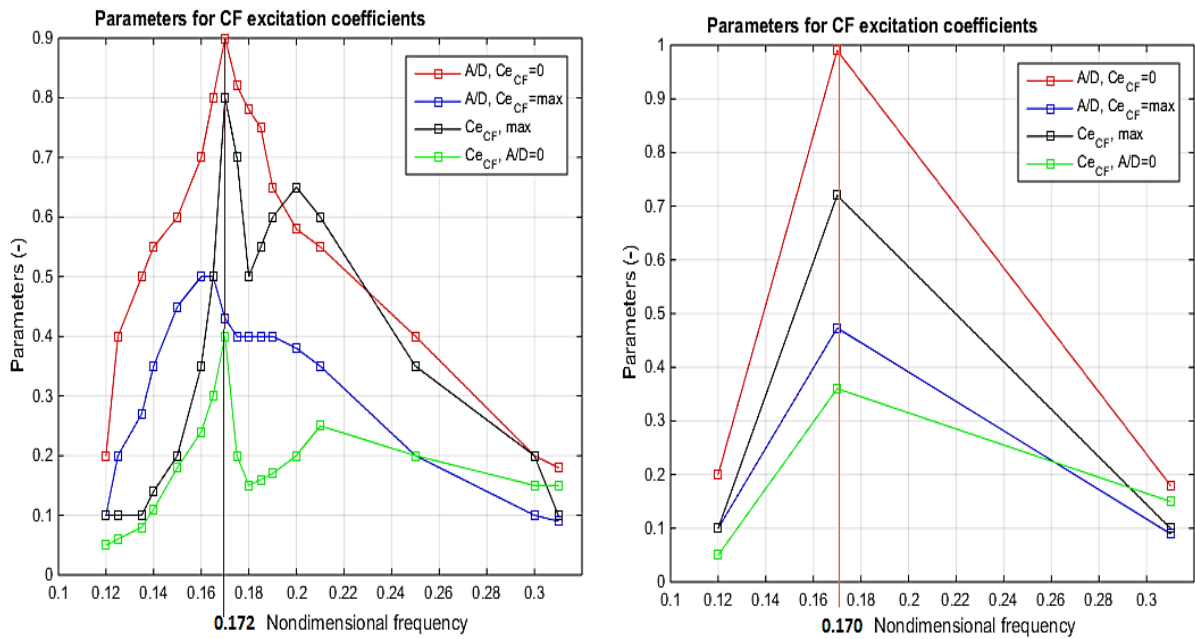


**Figure 50 Comparison between contour curves of default set of parameters (left plot) and set of parameters for S-Test no. 2430 (right plot)**

# Chapter 7 Prediction of an Optimal Set of Excitation Parameters

This chapter describes how and on what basis the optimal set of parameters is obtained.

## 7.1 Experimental Results

Buoyancy riser with 2/2 configuration at 1.0 m/s flow speed is considered to predict an optimal set of excitation parameters. For generating new sets of parameters, the concept presented in section 6.1.2 is applied in this chapter. In this section, the results are compared with the experimental results from Rao et al., 2015 in terms mode number, response frequency and maximum accumulated damage. The results for experiment are presented in section 4.3. For simplicity, buoyancy riser with 2/2 a single flow speed at 1.0 m/s is considered and results are extracted from experimental graphs. These extracted values are presented in the below Table 18. Uncertainty may be associated with these values since these are extracted from the graphs.

**Table 18** Extracted values from experiment for 2/2 configuration at 1.0 m/s (Figure 34 )

Flow speed m/s	Max. Fatigue damage [1/year]	Bare part		Buoyancy part	
		Mode no.	Response Frequency [Hz]	Mode no.	Response Frequency [Hz]
1.0	14.527	11	5.154	3	1.7063

## 7.2 VIVANA Analysis Results

By considering the range of non-dimensional frequency and modification factors, 18040 test cases have been generated. By running the simulation for these test cases at 1.0 m/s, different test cases give similar behaviour when compared with the experimental values as shown in the above table. Figure 51 shows the behaviour of the staggered buoyancy riser for different test cases.

### VIVANA analysis:

- VIVANA version 4.0.8 has been used
- Pure CF VIV analysis
- Current direction: perpendicular to SLWR plane (global XZ) (see Figure 36)
- SN curve: one slope D curve from DNV-RP-C203 with slope = 3. The curve is defined by  $\log N = \log C - m \log S$

- Excitation coefficients
  - User defined data sets based on range of non-dimensional frequency and modification factors
- Flow speed 1.0 m/s
- Properties of the riser with staggered buoyancy elements are as presented in Table 14
- Added mass coefficient 1.0

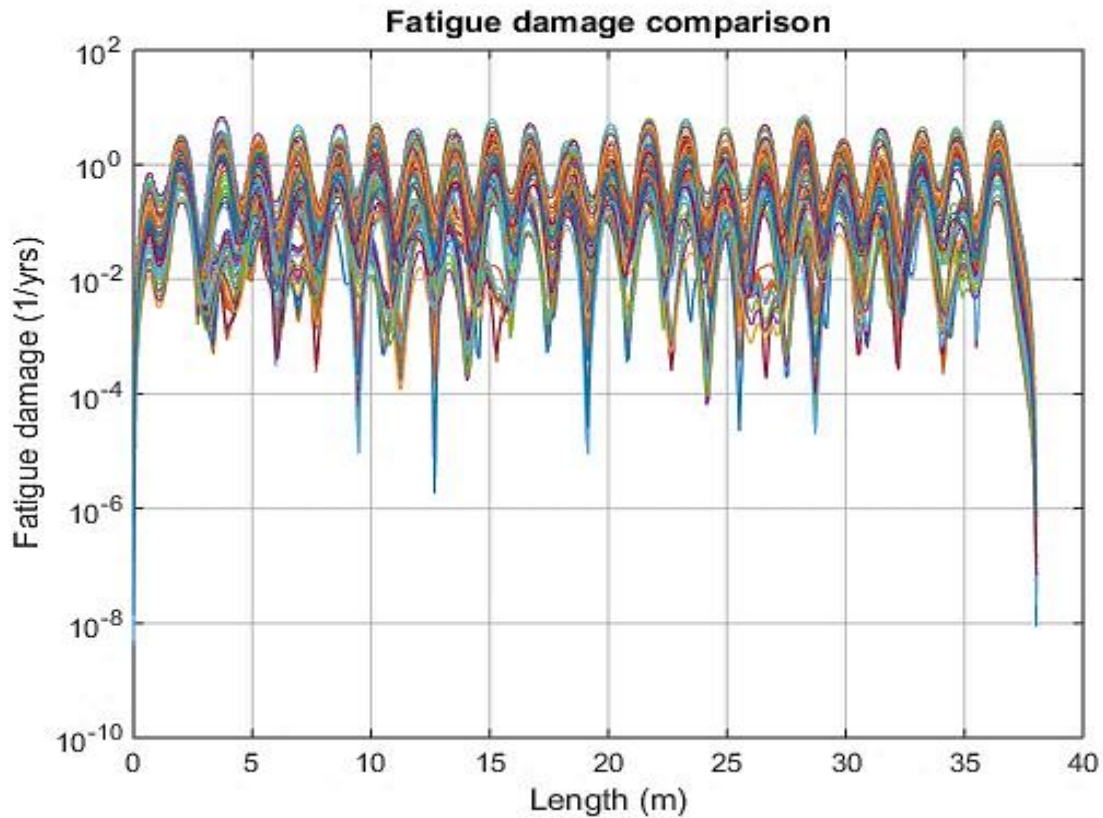


**Figure 51 Fatigue damage comparison for different sets of excitation coefficient parameters**

By interpolating the results for 9156 test cases and comparing these responses with the experimental results for 2/2 configuration at 1.0 m/s flow speed, four test cases gave good approximation as shown in the below Figure 52. Table 19 presents four test cases with excitation coefficients and their modification factors.

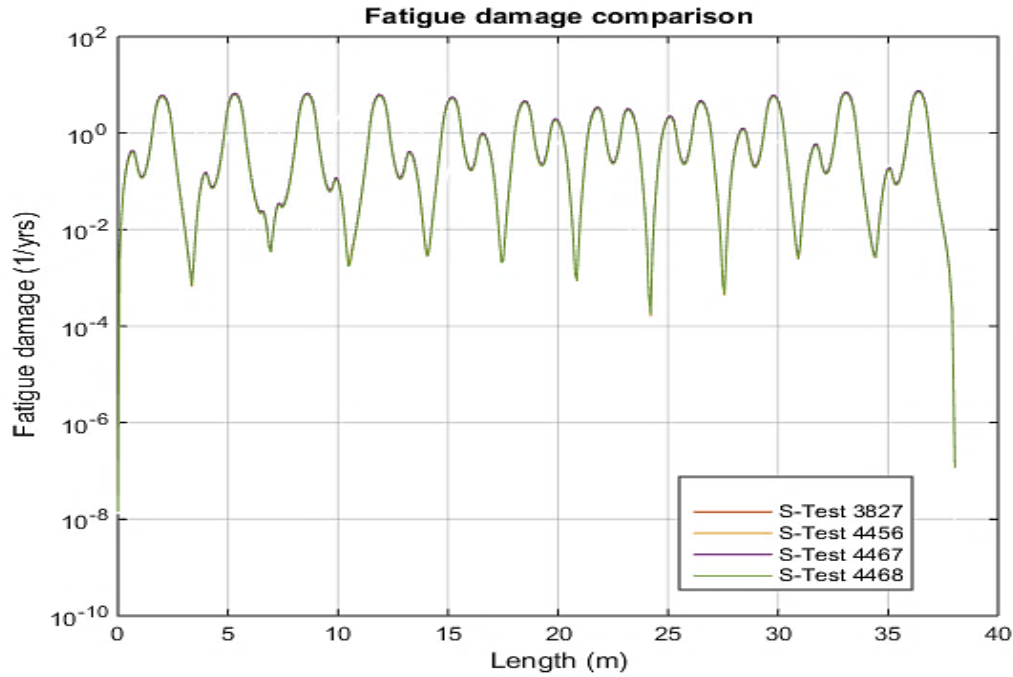


Figure 52 Fatigue damage for test cases that showed similar behaviour.

Table 19 Test cases that showed similar behaviour with the experiment.

S-Test No.	$\hat{f}_{CF}$	$\left(\frac{A}{D}\right)_{C_{e,CF}=0}$	$\left(\frac{A}{D}\right)_{C_{e,CF}=\max}$	$C_{e,CF=\max}$	$C_{e,CF, \frac{A}{D}=0}$	Modification factor	
						$\gamma_{A/D}$	$\gamma_{Ce}$
3827	0.146	1.035	0.4945	1.40	0.70	1.15	1.75
4456	0.148	1.035	0.4945	1.360	0.680	1.15	1.70
4467	0.148	1.035	0.4945	1.40	0.70	1.15	1.75
4468	0.148	1.08	0.5160	1.40	0.70	1.20	1.75

Table 20 shows the specified criteria for selecting the optimal set of parameters. The deviation of mode number for VIVANA analysis from the experiment is chosen as  $\pm 1$ , for frequency it is  $\pm 10\%$ , for response amplitude  $\pm 10\%$  and for maximum accumulated fatigue damage it is chosen as a factor of 2 which means that the fatigue damage for VIVANA analysis is half of the fatigue damage from the Shell experiment.

Table 20 Specified criteria for selecting an optimal set of parameters

Specified Criteria	Deviation between the predicted results and experimental results
Mode	$\pm 1$
Response Frequency	$\pm 15\%$
Response A/D	$\pm 10\%$
Max. Fatigue damage	Factor of 2

From the above sets of excitation parameters, Table 21 shows an optimal set of excitation parameters based on specified criteria as stated in the below Table 20.

**Table 21 Optimal set of parameters with their modification factors.**

S-Test No.	$\hat{f}_{CF}$	$\left(\frac{A}{D}\right)_{C_{e,CF}=0}$	$\left(\frac{A}{D}\right)_{C_{e,CF}=\max}$	$C_{eCF=\max}$	$C_{eCF\frac{A}{D}=0}$	Modification factor	
						$\gamma_{A/D}$	$\gamma_{C_e}$
3827	0.120	0.1490	0.1000	0.100	0.000	-	-
	0.146	1.035	0.4945	1.400	0.700	1.15	1.75
	0.300	0.1600	0.100	0.100	0.000	-	-

Figure 53 shows the fatigue damage curve along the length of the riser for S-Test no. 3827 and its corresponding mode number and response frequency are presented in Table 22.

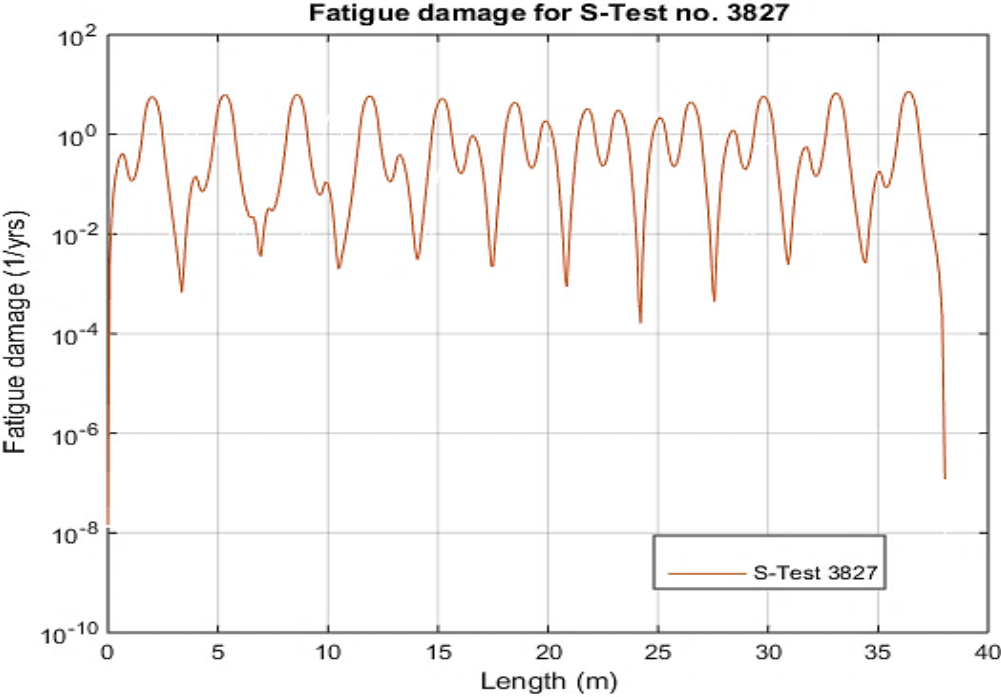


**Figure 53 Fatigue damage comparison for S-Test no. 3827.**

**Table 22 Results from VIVANA for S-Test no. 3827**

S-Test no.	Flow speed [m/s]	VIVANA simulation				Fatigue damage [1/year]
		Bare part		Buoyancy part		
		Mode no.	Frequency	Mode no.	Frequency	VIVANA
3827	1.0	12	5.1467	3	2.0019	7.2597

**Response Amplitude:**

The predicted response frequency is presented as a function of flow speed in Figure 54. When comparing with the measure A/D (Figure 35), it is shown that by using the optimal set of parameters, the prediction of response amplitude for bare part is over-predicted and for buoyancy part it is under-predicted. This is because of using single set of excitation parameters for both bare and buoyancy parts of the riser.

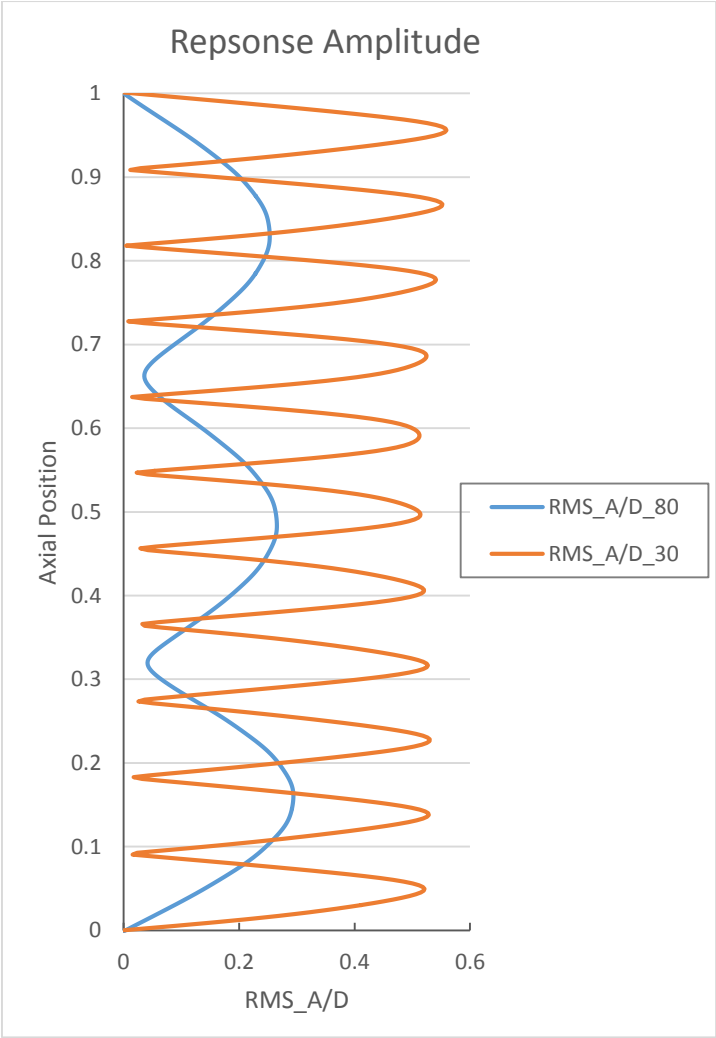


**Figure 54 Predicted CF A/D with optimal set of parameters for 2/2 configuration at 1.0 m/s**

By using the optimal set of excitation parameters as shown in Table 21 for 2/2 configuration at different flow speeds, Table 23 presents the comparison between the experimental results and the VIVANA analysis results. The response frequency for both bare and buoyancy parts of the riser for experiment and VIVANA analysis are similar for all flow speeds. But the fatigue damage is different for both the results and it is within a range of factor of 2.

**Table 23 Comparison between experimental results and VIVANA analysis for different flow speeds for 2/2 configuration with an optimal set of excitation parameters.**

Flow speed [m/s]	Bare part				Buoyancy part				Fatigue damage [1/year]	
	Measured results		Predicted results		Measured results		Predicted results		Measured results	Predicted results
	M*	F*	M*	F*	M*	F*	M*	F*		
0.5	-	2.993	6	2.450	-	0.859	2	1.016	0.2791	0.083
0.6	-	3.488	7	2.992	-	0.963	2	1.205	0.5932	0.271
0.7	-	3.904	9	3.508	-	1.249	2	1.366	2.668	0.733
0.8	-	4.451	10	4.038	-	1.327	2	1.514	5.207	1.635
0.9	-	4.997	11	4.585	-	1.483	3	1.812	7.272	3.413
1.0	11	5.154	12	5.147	3	1.718	3	2.002	14.593	7.260
1.1	-	6.377	12	5.725	-	1.796	3	2.168	23.423	11.846
1.2	-	5.882	13	5.809	-	1.952	3	2.318	43.825	18.140

M\* = Mode number, F\* = Response frequency.

The below two figures (Figure 55 and Figure 56) shows the comparison between measured data (Rao, Vandiver et al., 2015), prediction data for optimal set of parameters and for default set of parameters in terms of response frequency and maximum accumulated fatigue damage. This figure presents the data for the above mentioned optimal set of excitation parameters (Table 21) for 2/2 configuration for different velocities ranging 0.5 m/s to 1.2 m/s. The fatigue damage prediction follows the same trend as what was observed from the measured data. The fatigue damage was under-predicted even though the response frequencies are approximately identical to the measured data.

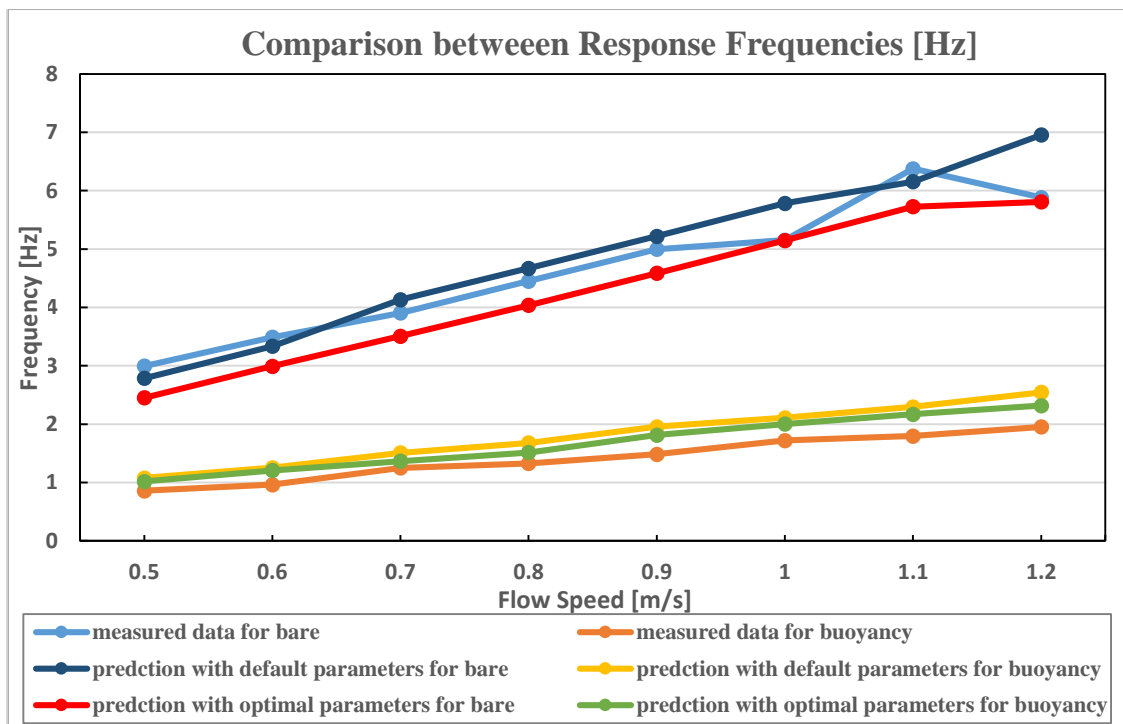


**Figure 55 Comparison between measured response frequency and predicted response frequency**

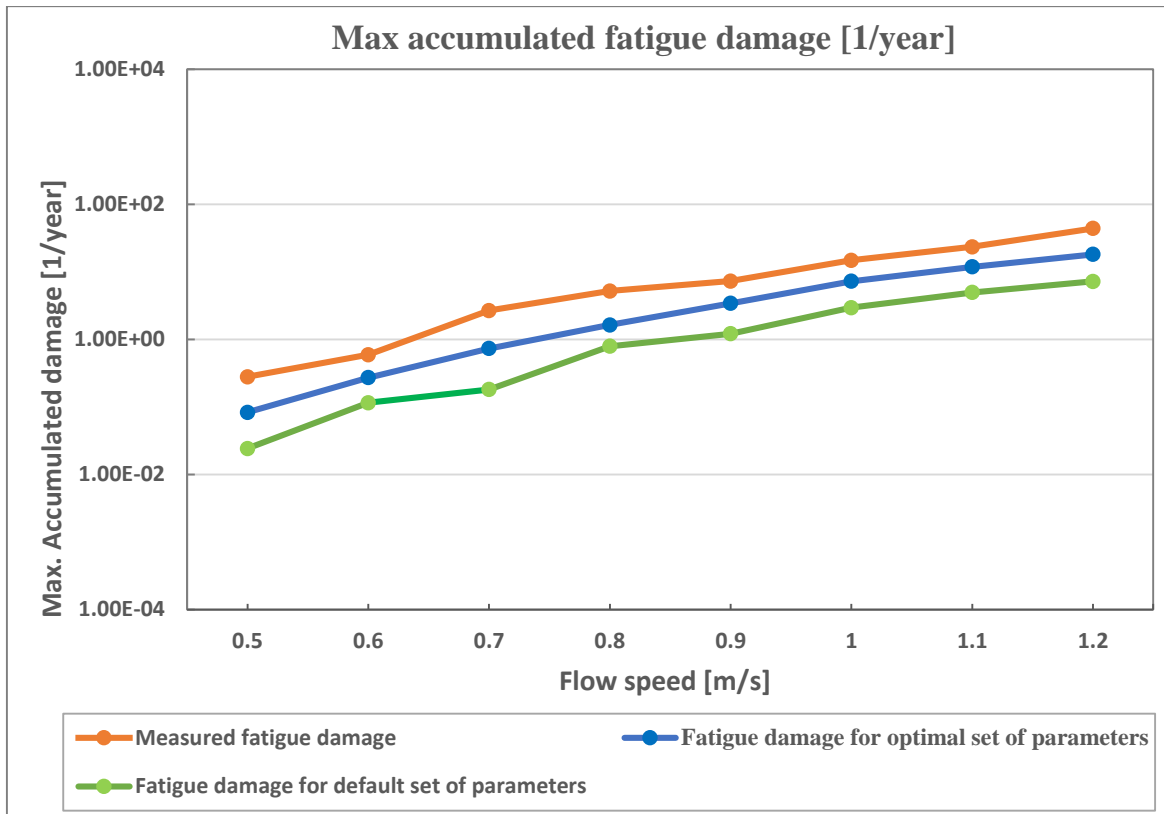


Figure 56 Comparison between measured fatigue damage, fatigue damage for optimal set of parameters and for default set of parameters.

Figure 57 shows the contour plot for the optimal set of parameters by using values in Table 21.

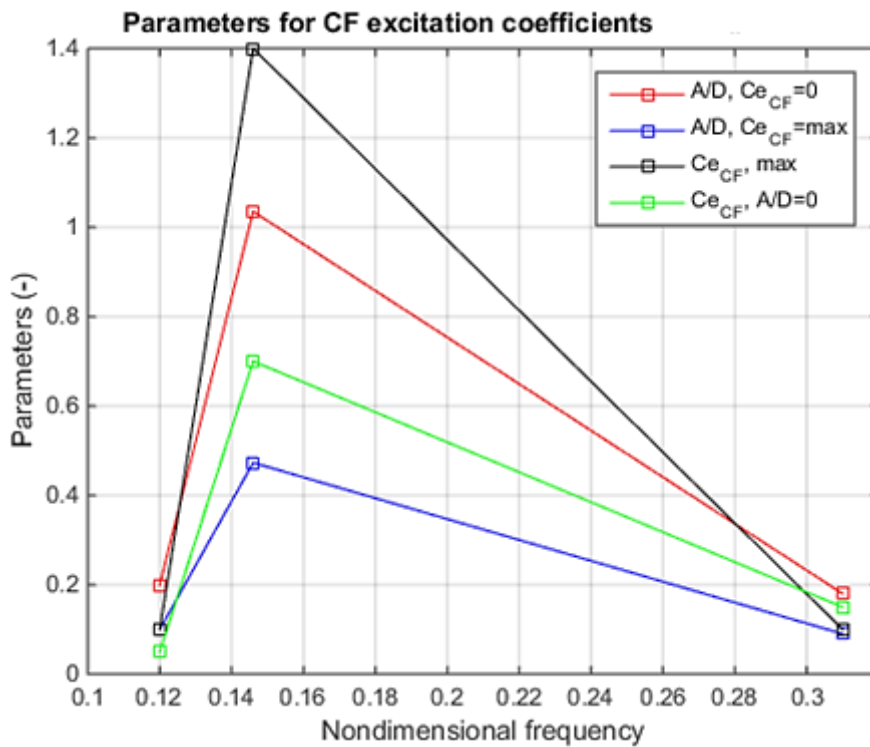


Figure 57 Contour plot for optimal set of parameters.

### 7.3 Discussion and Conclusion

In sections 7.1 and 7.2 an overview of mode number, excited frequencies and fatigue damage of a riser with staggered buoyancy elements for both experiment and user defined optimal set of parameters as in Table 17 and Table 20 are shown respectively.

The prediction is compared with experiment and original prediction with default set of excitation parameters in Table 24. It can be seen from the table that the response frequency is better predicted using optimal set of excitation parameters. They are also lower than the values using default set of excitation parameters because the highest  $\left(\frac{A}{D}\right)_{c_e=0}$  values shift to lower  $\hat{f} \approx 0.146$ . The predicted response displacement for bare riser is over-predicted and for buoyancy part it is under-predicted as shown in Figure 54 for the optimal set of parameters. CF fatigue damage is much lower than the test results, for e.g. we can say at a factor of 2. The uncertainty in fatigue damage is because, in Shell experiment the measured fatigue damage contains higher order frequency components. The measured fatigue damage values are not directly available and the extraction from the literature may also leads to uncertainty. In addition to these, other factors that might influence the prediction are as follows:

**a) Reynolds effect**

Reynolds number may influence on the VIV responses such as mode number, frequency, response amplitude and fatigue damage (Swithenbank et al., 2008). The hydrodynamic force/coefficient will be influenced at different Re. the Reynolds number effect is not explicitly modelled in the force coefficient database in present study.

**b) IL/CF interaction**

The inverse force estimation method has been used to extract hydrodynamic forces and coefficients along s bare flexible cylinder from a limited number of acceleration and strain measurements (Wu et al., 2009) and (Wu, Lie, et al., 2016). The maximum value of the estimated excitation coefficient is significantly higher than in the present VIVANA default curves as shown in the Figure 43. The coefficient contours are centred on two peaks at non-dimensional frequencies  $\hat{f} \approx 0.15$  and 0.2. The primary excitation zone is around  $\hat{f} \approx 0.15$ . This database may not be valid for riser with staggered buoyancy elements. However, it shows some of the same characteristics of the optimal set of parameters obtained from present study from staggered buoyancy element tests.

**c) Bare riser/buoyancy element interaction**

It is expected that the different buoyancy element configurations will lead to different hydrodynamic force/coefficients due to the differences in the interaction effect. One configuration has been analyzed in present study. Further study of other configurations are needed.

**d) Uniform flow**

The model was subjected to uniform flows, which means the response occurs around a narrow range of non-dimensional frequency. In our case, the response is around  $\hat{f} \approx 0.13 - 0.14$ .

An optimal set of parameters is selected based on one test case. This set of parameters is applied to predict the rest of the cases with the same configurations. The prediction shows consistent trend compared to the measurements. It indicates that this set of parameters are robust. However, more test cases could be analysed and a refined selection procedure will be needed.

The predicted response amplitude for an optimal set of excitation parameters is not matching with the measured data, this is mainly because of using single set of excitation parameters for both bare and buoyancy parts of the riser. It is expected to get better agreement with the measured data by using the two different sets of excitation parameters each for bare and buoyancy parts.

**Table 24 Comparison between experimental and VIVANA analysis results**

<b>Comparison</b>	<b>Mode and <math>F_R</math></b>	<b>Mode and <math>F_B</math></b>	<b>Max. RMS A/D<sub>R</sub></b>	<b>Max. RMS A/D<sub>B</sub></b>	<b>Max. fatigue damage (1/yrs.)</b>
Measurement	~11 & 5.154(Hz)	3 1.718(Hz)	0.2	0.7	~14.593
Default parameter	14 & 5.8(Hz)	5 2.1(Hz)	0.25	0.35	3.0
Optimal set of parameters	12 & 5.147(Hz)	3 2.002(Hz)	0.553	0.293	7.260

$F_R$  = response frequency for bare part,  $F_B$  = response frequency for buoyancy part  
 Max. RMS A/D<sub>R</sub> is Maximum Root Mean Square Amplitude ratio for bare riser  
 Max. RMS A/D<sub>B</sub> is Maximum Root Mean Square Amplitude ratio for Buoyancy element.

# Chapter 8 Recommendations for Further Work

The contribution of present thesis is to develop an algorithm to extract valuable information from flexible cylinder test data and find an optimal set of parameters which improves the accuracy of VIV prediction.

According to what previously explained, the following topics are considered in the present thesis:

- Evaluate the VIV prediction using default parameters in VIVANA
- Develop an algorithm to find the optimal set of excitation parameters using data from flexible cylinder VIV tests
- Evaluate the prediction of an optimal set of excitation parameters

Optimal set of parameters are obtained for one of the tested staggered buoyancy configurations (2/2). Similar study should be carried out for other configurations as well. It is known that the VIV responses will be influenced by the arrangement of the buoyancy elements. The algorithm can also be applied to other VIV tests with/without suppression devices and obtain optimal force model.

The analysis method needs to be further developed. The focus in present study has been to find optimal excitation parameters. The obtained optimal excitation parameters have shown improvement in the prediction compared to the experimental results except for response amplitude. So it is recommended to use two different sets of excitation parameters for each bare and buoyancy parts to get better agreement with the experiment. The added mass and damping model may also be included in such algorithm in the future.

The developed algorithm can be also applied to flexible cylinder test data with suppression devices and improve the accuracy of the prediction.

Such analysis should be combined with other types of analysis techniques, e.g. inverse analysis, time-frequency analysis, so that the obtained parameters will be more robust and represent physics of a flexible cylinder subjected to VIV.

## References

- Aronsen, K. H. (2007). *An experimental investigation of in-line and combined in-line and cross-flow vortex induced vibrations*. (2007:253), Norwegian University of Science and Technology, Faculty for Engineering Science and Technology, Marine Technology, Trondheim.
- Blevins, R. D. (1994). *Flow-induced vibration* (2nd ed., Reprint ed. w/ updating and new preface. ed.). Malabar, Fla: Krieger.
- Dahl, J. M., Hover, F. S., Triantafyllou, M. S., & Oakley, O. H. (2010). Dual resonance in vortex-induced vibrations at subcritical and supercritical Reynolds numbers. *J. Fluid Mech.*, *643*, 395-424. doi:10.1017/S0022112009992060
- Gopalkrishnan, R. (1993). *Vortex-Induced Forces on Oscillating Bluff Cylinders*: Woods Hole Oceanographic Institution, M. A.
- Jhingran, V., Zhang, H., Lie, H., Henning, B., & J.Kim, V. (2012). *Buoyancy Spacing Implications for Fatigue Damage due to Vortex-Induced Vibrations on a Steel Lazy Wave Riser (SLWR)*. Paper presented at the Offshore Technology Conference, Houston, Texas, USA.
- Larsen, C. M, Lie H, Passano E, Yttervik R, Wu Jie, & G, B. (2009). *VIVANA Theory Manual*. Retrieved from Trondheim.:
- Larsen, C. M. Vortex Induced Vibration Introduction. (Department of Marine Technology, NTNU).
- Larsen, C. M. (2011). *VIV-A short incomplete introduction to fundamental concepts*. Retrieved from Trondheim, Norway:
- Le Cunff, C., Biolley, F., Fontaine, E., Etienne, S., & Facchinetti, M. (2002). Vortex-induced vibrations of risers: Theoretical, numerical and experimental investigation. *Oil Gas Sci. Technol.*, *57*(1), 59-69.
- Li., S., & Nguyen., C. (2010). *Dynamic Response of Deepwater Lazy-Wave Catenary Riser*. Paper presented at the Deep Offshore Technology International, Amsterdam, Netherlands.
- Miau, J., Tsai, H., Lin, Y., Tu, J., Fang, C., & Chen, M. (2011). Experiment on smooth, circular cylinders in cross-flow in the critical Reynolds number regime. *Experimental Methods and their Applications to Fluid Flow*, *51*(4), 949-967. doi:10.1007/s00348-011-1122-2
- Ormberg, H., & Passano, E. (2015). *Riflex User Manual, V3.0*. Norway.
- Passano, E., Larsen, C. M., Lie, H., & Wu, J. (2015). *VIVANA Theory Manual*. user manual. Norsk Marinteknisk Forskningsinstitutt AS. Norway.
- Rao, Z., Vandiver, J. K., & Jhingran, V. (2015). Vortex induced vibration excitation competition between bare and buoyant segments of flexible cylinders. *Ocean Engineering*, *94*, 186-198. doi:10.1016/j.oceaneng.2014.12.005
- Sumer, B. M., & Fredsøe, J. (2006). *Hydrodynamics around cylindrical structures* (Rev. ed. ed. Vol. vol. 26). New Jersey: World Scientific.
- Sumr, B. M., & fredsøe, J. (1997). *Hydrodynamics around cylindrical structures (Advanced series on ocean engineering, volume 12)*: World Scientific Publishing Co. Pte. Ltd.

- Swithenbank, S. B., Larsen, C. M., Vandiver, J. K., & Lie, H. (2008). Reynolds number dependence of flexible cylinder viv response data (Vol. 5, pp. 503-511).
- Wergeland, T. V., & Larsen, C. M. (2015). Vortex Induced Vibrations in Fish Farm Structural Elements: NTNU.
- Wu, J., Lekkala, M. R., & Ong, M. C. (2016). *PREDICTION OF RISER VIV WITH STAGGERED BUOYANCY ELEMENTS*. Paper presented at the International Conference on Ocean, Offshore and Arctic Engineering OMAE2016, Busan, Korea.
- Wu, J., Lie, H., Larsen, C. M., Liapis, S., & Baarholm, R. (2016). Vortex-induced vibration of a flexible cylinder: Interaction of the in-line and cross-flow responses. *Journal of Fluids and Structures*, 63, 238-258. doi:10.1016/j.jfluidstructs.2016.03.001
- Wu, J., Mainçon, P., Lie, H., & Larsen, C. M. (2009). VIV force identification using classical optimal control algorithm (Vol. 5, pp. 559-570).
- Yin, D., Wu, J., Lie, H., Baarholm, R. J., & Larsen, C. M. (2015). VIV prediction of Steel Catenary Riser - A reynolds number sensitivity study (Vol. 2015-, pp. 1018-1027).

# Appendix

## A.1 Input files

In this work, three types of input files have been used in VIVANA.

**sima\_inpmo**d.inp - input file containing necessary data about the riser structure.

**sima\_stamo**d.inp - input file needed for the STAMOD calculation.

**sima\_vivana**.inp - input file for VIVANA

These files are not attached in the text, however, they have been uploaded on an USB-disc given to the supervisor.

## A.2 Files from the VIVANA analysis

The analysis from the VIVANA consisted two files, one with the simulation results and the other with plots for the results.

**sima\_vivana.res** – file containing the results

**sima\_vivana.mpf** – file containing matrix plots for the simulation results

## A.3 MAT Lab files

During the semester many scripts have been used in MAT Lab in order to do necessary calculations. The most important scripts and the functions have been attached together with the thesis. This may give the reader a better understanding how the different functions and scripts are designed for this work. All scripts and functions have been uploaded to the USB-disc.

### A.3.1 MatLab script for running the simulation for different sets of excitation parameters at 1.0 m/s flow speed

```
1. close all
2. clear all
3.
4.     %% create new VIVANA input files and save them in separate
       folders
5.     % replace the string "__PropExcCoeff__" in the template
       file with
6.     % desired input data in data folder and
7.     % create new folders with these files
8.     % this file defines 7 set of different parameters and
       compare the
9.     % predicition with default parameters

10.    %% Path and file names
11.    workPath = 'C:\\Sintef\\temp\\VIVANA optimization\\test';
12.    sourcePath = 'C:\\Sintef\\temp\\VIVANA
       optimization\\test';
13.    templatePath = [sourcePath '\\ ' 'template1.0'];
       % path to the template input file
14.    DefaultPath = [sourcePath '\\ ' 'default1.0'];
       % path to the default input file
```

```

15.
16.     inpFileName = 'vertical_vivana.inp';
17.     % the template input file name
18.     inpmodfile = 'vertical_inpmod.inp';
19.     % the template input file name
20.     stamodfile = 'vertical_stamod.inp';
21.     % the template input file name
22.     caseid='vertical'
23.
24.     %% Define parameters
25.     ids=[{1030}]; % id of the
26.     new folder which contains the created input file
27.     CL0=[0.146 1.035 0.4945 1.4 0.7];
28.     % define new parameters for 7 runs
29.     %% Read template file
30.     inp = fileread([templatePath '\\' inpFileName]);
31.     % read the template input file
32.     inp = strjoin(strsplit(inp, '\r\n'), '\n');
33.     % Split read string at specified delimiter
34.
35.     %% Create input files
36.     for ind = 1:length(ids)
37.         % create new input files
38.         id = ids{ind};
39.         caseName = ['case' num2str(id)];
40.         % create new folder
41.         casePath = [workPath '\\' caseName];
42.         mkdir(casePath);
43.
44.         dataInpFileName = ['data' num2str(id) '.txt'];
45.         % file name
46.         dataInpFilePath = [sourcePath '\\data\\'
47. dataInpFileName]; % path to the file with new excitation
48. coefficient parameters
49.
50.         data=num2str(CL0(ind,:));
51.         % read new parameters defined in CL0
52.         data = strjoin(strsplit(data, '\r\n'), '\n');
53.
54.         caseInp = strrep(inp, '__PropExcCoeff__', data);
55.         % replace the contents PropExcCoeff in the original file
56.         with new contents
57.
58.         fid = fopen([casePath '\\' inpFileName], 'wt');
59.         % write in the file
60.         fprintf(fid, '%s', caseInp);
61.         fclose(fid);
62.
63.         copyfile([templatePath '\\' inpmodfile], casePath)
64.         % copy inpmod file
65.         copyfile([templatePath '\\' stamodfile], casePath)
66.         % copy stamod file
67.
68.     end
69.
70.     %% Perform VIVANA analysis

```

```

53.     % Default parameters
54.
55.     res_def=riflex('isv',DefaultPath, caseid);
56.     % Results saved in res
57.     % fat_def0=res_def.vivana(46).values(:,2)
58.     % Fatigue damage
59.
60.     % len=res_def.vivana(46).values(:,1);
61.     % length
62.
63.     indx=0
64.
65.     for i=1:length(res_def.vivana)
66.
67.         cmp=strcmp(res_def.vivana(i).name(1:7), ['Max acc'])
68.         % look for the text 'Max accumulated damage'
69.
70.         if cmp==1
71.
72.             indx=i
73.             % find the index to the matrix corresponding to 'Max
74.             accumulated damage'
75.
76.         else
77.
78.         end
79.
80.     end
81.
82.     fat_def=res_def.vivana(indx).values(:,2);
83.     % Fatigue damage
84.
85.     len=res_def.vivana(indx).values(:,1);
86.     % Riser length
87.
88.     % New parameters
89.
90.     for ind = 1:length(ids)
91.         id = ids{ind};
92.         caseName = ['case' num2str(id)];
93.         % create new folder
94.         casePath = [workPath '\\ ' caseName];
95.
96.         res(ind)=riflex('isv',casePath, caseid);
97.         % Run inpmod, stamod and vivana (include path to Myfunc
98.         before running this script!!!). Results saved in res
99.
100.        % fat(ind,:)=res(ind).vivana(46).values(:,2)
101.        % Fatigue damage
102.
103.        indx=0
104.
105.        cmp=0
106.
107.        for i=1:length(res(ind).vivana)

```

```

97.         cmp=strncmp(res(ind).vivana(i).name(1:7), ['Max
acc']) % look for the text 'Max accumulated damage'
98.
99.         if cmp==1
100.
101.             indx=i
% find the index to the matrix corresponding to 'Max
accumulated damage'
102.
103.             else
104.
105.             end
106.
107.         end
108.
109.         fat(ind,:)=res(ind).vivana(indx).values(:,2);
% Fatigue damage
110.
111.     end
112.
113.     %% Comparison
114.
115.     figure
116.     semilogy(len,fat_def,len,fat(1,:))
117.     xlabel('Length (m)')
118.     legend('Default','Test** 2430')
119.     ylabel('Fatigue damage (1/yrs)')
120.     grid on
121.     title('Fatigue damage comparison')

```

### A.3.2 MAT lab script for generating the contour plots for default set of excitation parameters

```

1. clear all
2. close all
3.
4.
5.
6. % Excitation region 0.125-0.31 VIVANA V4.6.1
7. %          fhat      ac10      c10 ac1max  clmax   a0c1      cla0
8.
9. cedata=[ .120      .200  0      .100      .100  0      .050
10.         .125      .400  0      .200      .100  0      .060
11.         .135      .500  0      .270      .100  0      .080
12.         .140      .550  0      .350      .140  0      .110
13.         .150      .600  0      .450      .200  0      .180
14.         .160      .700  0      .500      .350  0      .240
15.         .165      .800  0      .500      .500  0      .300
16.         .170      .900  0      .430      .800  0      .400
17.         .175      .820  0      .400      .700  0      .200
18.         .180      .780  0      .400      .500  0      .150
19.         .185      .750  0      .400      .550  0      .160
20.         .190      .650  0      .400      .600  0      .170
21.         .200      .580  0      .380      .650  0      .200
22.         .210      .550  0      .350      .600  0      .250
23.         .250      .400  0      .200      .350  0      .200
24.         .300      .200  0      .100      .200  0      .150
25.         .310      .180  0      .090      .100  0      .150];
26.
27.     f_new=cedata(:,1);
28.     Ceviv=cedata(:,7:-2:3);
29.     ADviv=cedata(:,6:-2:2);
30.
31.     ADnew=[0.0:0.1:1.5];
32.     for i=1:length(f_new)
33.
34.         % Curve 1
35.         A1 = (Ceviv(i,1)-Ceviv(i,2))/(ADviv(i,2)^2);
36.         B1 = -2*A1*ADviv(i,2);
37.         C1 = Ceviv(i,1);
38.
39.         % Curve 2
40.         A2 = -Ceviv(i,2)/(ADviv(i,2)^2-
41.         2*ADviv(i,2)*ADviv(i,3)+ADviv(i,3)^2);
42.         B2 = -2*A2*ADviv(i,2);
43.         C2 = -A2*ADviv(i,3)^2-B2*ADviv(i,3);
44.
45.         for j=1:length(ADnew)
46.             if ADnew(j)<ADviv(i,2)
47.                 Cenew(i,j)=A1*ADnew(j)^2+B1*ADnew(j)+C1;
48.             else
49.                 Cenew(i,j)=A2*ADnew(j)^2+B2*ADnew(j)+C2;
50.             end
51.         end
52.     end

```

```

53.     ifhat=[2 8 10];
54.     figure
55.     plot(ADnew,Cenew(ifhat,:))
56.     legend('fhat=0.125','fhat=0.17','fhat=0.18')
57.     grid on
58.     xlabel('A/D')
59.     ylabel('Ce')
60.     title('Excitation coefficient vs. A/D at three different
        fhat (VIVANA v4.6)')

61.
62.
63.     figure
64.     [X,Y]=meshgrid(f_new,ADnew);
65.     nv2=[-5 -4 -3 -2 -1 -0.5 0 0.5 1 1.4];
66.     [C,h] = contour(X,Y,Cenew',nv2);
67.     colormap jet
68.     % text(0,1.25,'b'),'FontSize',15)
69.     xlim([0.125 0.3])
70.     ylim([0.2 1.2])
71.     grid on
72.     xlabel('Nondimensional frequency')
73.     ylabel('A/D')
74.     title('Excitation coefficient contour generated from
        VIVANA v4.6')
75.     clabel(C,h);
76.
77.     % Save plots on file, plotXXXX.eps
78.     %
79.     % plotfile = ['Fig. 5-4 '];
80.     %
81.     % saveas(gcf, [plotfile, '.tiff']);
82.
83.     %           fhat    acl0    aclmax    clmax    cla0
84.     figure
85.     plot(cedata(:,1),cedata(:,2),'-
        rs',cedata(:,1),cedata(:,4),'-
        bs',cedata(:,1),cedata(:,5),'-
        ks',cedata(:,1),cedata(:,7),'-gs')
86.     legend('A/D, Ce_C_F=0','A/D, Ce_C_F=max','Ce_C_F,
        max','Ce_C_F, A/D=0')
87.     xlim([0.1 0.32])
88.     % ylim([0.2 1.4])
89.     grid on
90.     xlabel('Nondimensional frequency')
91.     ylabel('Parameters (-)')
92.     title('Parameters for CF excitation coefficients (VIVANA
        v4.6)')

```

### A.3.2 MAT lab script for generating the contour plots for different sets of excitation parameters

```

1. clear all
2. close all
3.
4.
5.
6. % Excitation region 0.125-0.31 VIVANA V4.6.1
7. %           fhat      ac10      c10 ac1max  c1max      a0c1      cla0
8.
9. cedata=[0.120      0.200  0      0.100      0.100  0      0.050
10.         0.146      1.035  0      0.473      1.400  0      0.700
11.         0.310      0.180  0      0.090      0.100  0      0.150];
12.
13.     f_new=cedata(:,1);
14.     Ceviv=cedata(:,7:-2:3);
15.     Adviv=cedata(:,6:-2:2);
16.
17.     % ADnew=[0.0:0.1:1.5];
18.     ADnew=[0.0:0.1:0.2];
19.     for i=1:length(f_new)
20.
21.         % Curve 1
22.         A1 = (Ceviv(i,1)-Ceviv(i,2))/(Adviv(i,2)^2);
23.         B1 = -2*A1*Adviv(i,2);
24.         C1 = Ceviv(i,1);
25.
26.         % Curve 2
27.         A2 = -Ceviv(i,2)/(Adviv(i,2)^2-
28.         2*Adviv(i,2)*Adviv(i,3)+Adviv(i,3)^2);
29.         B2 = -2*A2*Adviv(i,2);
30.         C2 = -A2*Adviv(i,3)^2-B2*Adviv(i,3);
31.
32.         for j=1:length(ADnew)
33.             if ADnew(j)<Adviv(i,2)
34.                 Cenew(i,j)=A1*ADnew(j)^2+B1*ADnew(j)+C1;
35.             else
36.                 Cenew(i,j)=A2*ADnew(j)^2+B2*ADnew(j)+C2;
37.             end
38.         end
39.     end
40.
41.     % ifhat=[2 8 10];
42.     ifhat=[1 2 3];
43.     figure
44.     plot(ADnew,Cenew(ifhat,:))
45.     legend('fhat=0.125','fhat=0.166','fhat=0.18')
46.     grid on
47.     xlabel('A/D')
48.     ylabel('Ce')
49.     title('Excitation coefficient vs. A/D at three different
50.           fhat (VIVANA v4.6)')
51.     figure

```

```

52.     [X,Y]=meshgrid(f_new,ADnew);
53.     nv2=[-5 -4 -3 -2 -1 -0.5 0 0.5 1 1.4];
54.     [C,h] = contour(X,Y,Cenew',nv2);
55.     colormap jet
56.     % text(0,1.25,'b'),'FontSize',15)
57.     xlim([0.125 0.3])
58.     ylim([0.1 1.2])
59.     grid on
60.     xlabel('Nondimensional frequency')
61.     ylabel('A/D')
62.     title('Excitation coefficient contour generated from
VIVANA v4.6')
63.     clabel(C,h);
64.
65.     % Save plots on file, plotXXXX.eps
66.     %
67.     % plotfile = ['Fig. 5-4 '];
68.     %
69.     % saveas(gcf, [plotfile, '.tiff']);
70.
71.     %           fhat      acl0      aclmax  clmax   cla0
72.     figure
73.     plot(cedata(:,1),cedata(:,2),'-
rs',cedata(:,1),cedata(:,4),'-
bs',cedata(:,1),cedata(:,5),'-
ks',cedata(:,1),cedata(:,7),'-gs')
74.     legend('A/D, Ce_C_F=0','A/D, Ce_C_F=max','Ce_C_F,
max','Ce_C_F, A/D=0')
75.     xlim([0.1 0.32])
76.     % ylim([0.2 1.4])
77.     grid on
78.     xlabel('Nondimensional frequency')
79.     ylabel('Parameters (-)')
80.     title('Parameters for CF excitation coefficients (VIVANA
v4.6)')

```

## Appendix B

In this section, few new sets of excitation parameters are presented with their test case numbers.

Table B.1 shows the generated new sets of excitation parameters for  $\hat{f}_{CF} = 0.13$  with amplitude modification factor range of 0.70 – 1.20 and excitation modification factor of 0.80.

**Table B.1: Sets of excitation parameters for different modification factors**

S-Test no:	$\hat{f}_{CF}$	$\left(\frac{A}{D}\right)_{C_{e,CF}=0}$	$\left(\frac{A}{D}\right)_{C_{e,CF}=\max}$	$Ce_{CF=\max}$	$Ce_{CF, \frac{A}{D}=0}$	Modification factor	
						$\gamma_{A/D}$	$\gamma_{Ce}$
1	0.13	0.63	0.301	0.64	0.32	0.70	0.80
2	0.13	0.675	0.3225	0.64	0.32	0.75	0.80
3	0.13	0.720	0.344	0.64	0.32	0.80	0.80
4	0.13	0.765	0.3655	0.64	0.32	0.85	0.80
5	0.13	0.810	0.387	0.64	0.32	0.90	0.80
6	0.13	0.855	0.4085	0.64	0.32	0.95	0.80
7	0.13	0.900	0.430	0.64	0.32	1.00	0.80
8	0.13	0.945	0.4515	0.64	0.32	1.05	0.80
9	0.13	0.990	0.473	0.64	0.32	1.10	0.80
10	0.13	1.035	0.4945	0.64	0.32	1.15	0.80
11	0.13	1.035	0.4945	0.64	0.32	1.20	0.80

Table B.2 shows the generated new sets of excitation parameters for  $\hat{f}_{CF} = 0.172$  with amplitude modification factor range of 0.70 – 1.20 and excitation modification factor of 0.95.

**Table B.2: Sets of excitation parameters for different modification factors**

S-Test no:	$\hat{f}_{CF}$	$\left(\frac{A}{D}\right)_{C_{e,CF}=0}$	$\left(\frac{A}{D}\right)_{C_{e,CF}=\max}$	$Ce_{CF=\max}$	$Ce_{CF, \frac{A}{D}=0}$	Modification factor	
						$\gamma_{A/D}$	$\gamma_{Ce}$
9505	0.172	0.63	0.301	0.76	0.38	0.7	0.95
9506	0.172	0.675	0.3225	0.76	0.38	0.75	0.95
9507	0.172	0.720	0.344	0.76	0.38	0.8	0.95
9508	0.172	0.765	0.3655	0.76	0.38	0.85	0.95
9509	0.172	0.810	0.387	0.76	0.38	0.9	0.95
9510	0.172	0.855	0.4085	0.76	0.38	0.95	0.95
9511	0.172	0.900	0.4300	0.76	0.38	1.0	0.95
9512	0.172	0.945	0.4515	0.76	0.38	1.05	0.95
9513	0.172	0.990	0.473	0.76	0.38	1.1	0.95
9514	0.172	1.035	0.4945	0.76	0.38	1.15	0.95
9515	0.172	1.035	0.4945	0.68	0.34	1.2	0.85

Table B.3 shows the generated new sets of excitation parameters for  $\hat{f}_{CF} = 0.2$  with amplitude modification factor of 1.20 and excitation modification factor range of 0.80 – 1.80.

**Table B.3: Sets of excitation parameters for different modification factors**

S-Test no:	$\hat{f}_{CF}$	$\left(\frac{A}{D}\right)_{C_{e,CF}=0}$	$\left(\frac{A}{D}\right)_{C_{e,CF}=\max}$	$C_{e,CF}=\max$	$C_{e,CF,\frac{A}{D}=0}$	Modification factor	
						$\gamma_{A/D}$	$\gamma_{Ce}$
16217	0.20	1.08	0.516	0.64	0.32	1.20	0.80
16218	0.20	1.08	0.516	0.68	0.34	1.20	0.85
16219	0.20	1.08	0.516	0.72	0.36	1.20	0.90
16220	0.20	1.08	0.516	0.76	0.38	1.20	0.95
16221	0.20	1.08	0.516	0.80	0.40	1.20	1.00
16222	0.20	1.08	0.516	0.84	0.42	1.20	1.05
16223	0.20	1.08	0.516	0.88	0.44	1.20	1.10
16224	0.20	1.08	0.516	0.92	0.46	1.20	1.15
16225	0.20	1.08	0.516	0.96	0.48	1.20	1.20
16226	0.20	1.08	0.516	1.00	0.50	1.20	1.25
16227	0.20	1.08	0.516	1.08	0.54	1.20	1.35
16228	0.20	1.08	0.516	1.12	0.56	1.20	1.40
16229	0.20	1.08	0.516	1.16	0.58	1.20	1.45
16230	0.20	1.08	0.516	1.20	0.60	1.20	1.50
16231	0.20	1.08	0.516	1.24	0.62	1.20	1.55
16232	0.20	1.08	0.516	1.28	0.64	1.20	1.60
16233	0.20	1.08	0.516	1.32	0.66	1.20	1.65
16234	0.20	1.08	0.516	1.36	0.68	1.20	1.70
16235	0.20	1.08	0.516	1.40	0.70	1.20	1.75
16236	0.20	1.08	0.516	1.44	0.72	1.20	1.8

# Appendix C

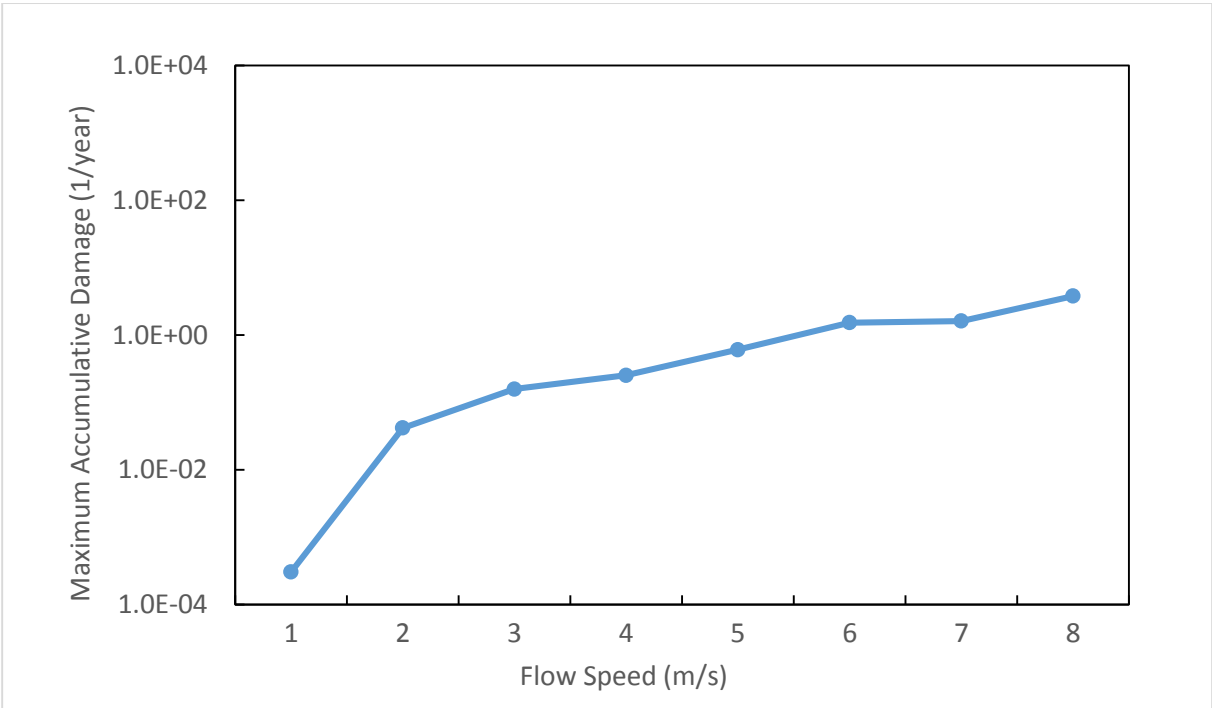
## Additional Simulation Results

### Simulation using default set of excitation parameters from VIVANA theory manual:

**Table C.1 Response values for the default set of parameters**

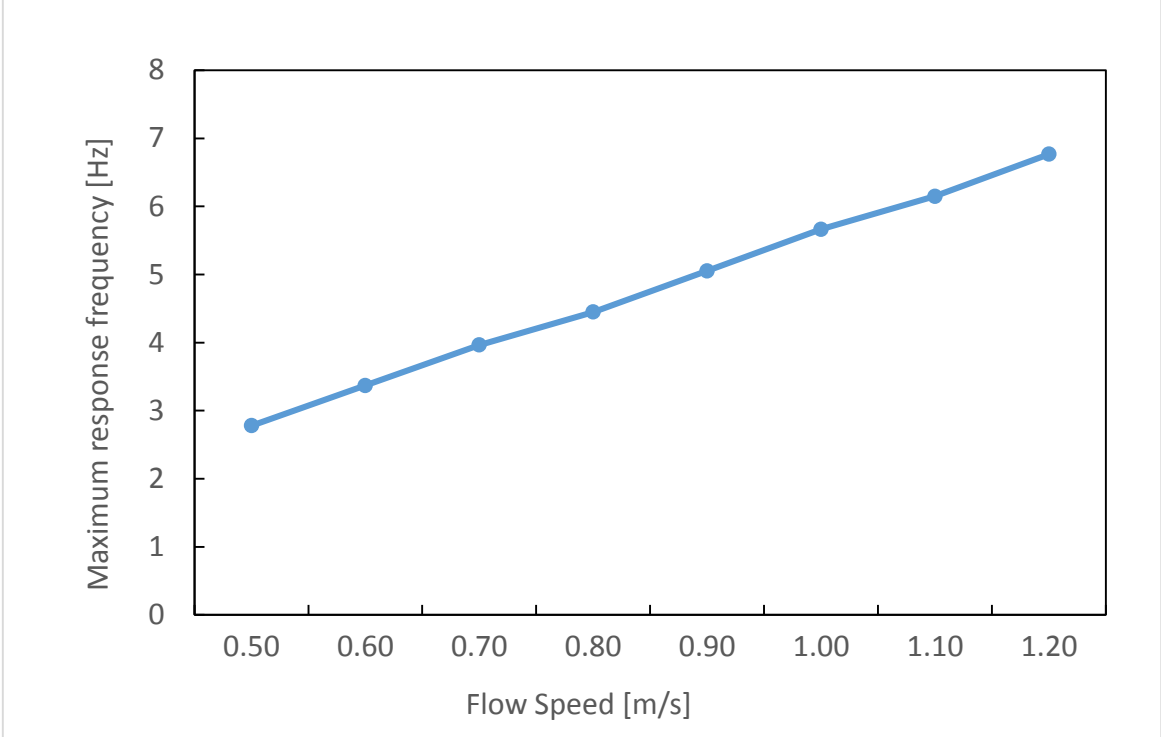
Flow speed [m/s]	Maximum accumulated damage [1/year]	Bare riser	
		Mode no.	Frequency [Hz]
0.50	3.06E-04	4	2.778
0.60	4.20E-02	5	3.369
0.70	1.58E-01	6	3.965
0.80	2.54E-01	7	4.652
0.90	6.09E-01	7	5.053
1.00	1.53E+00	8	5.663
1.10	1.62E+00	8	6.149
1.20	3.79E+00	9	6.766

Figure C.1 shows the maximum accumulated damage for bare riser for default set of excitation parameters from VIVANA.



**Figure C.1 Maximum accumulated damage for default set of excitation parameters from VIVANA theory manual – bare riser.**

Figure C.2 shows the variation of response frequency with towing speed for bare riser by using default set of parameters.



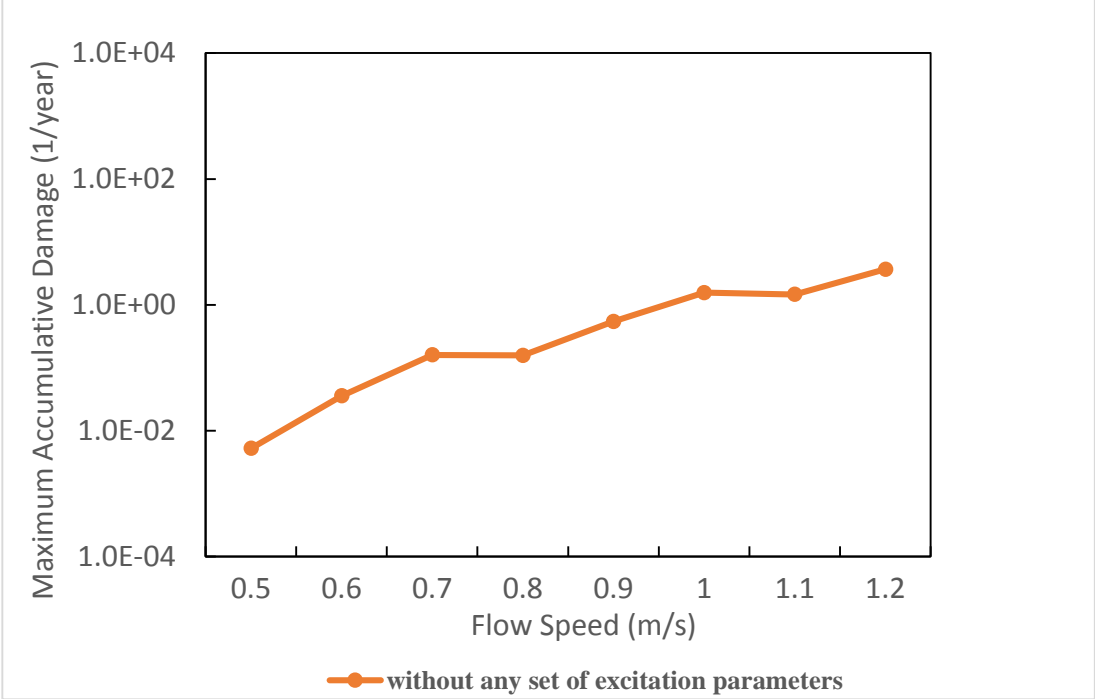
**Figure C.2 Response frequency for default set of excitation coefficients from VIVANA theory manual – bare riser.**

**Simulation without input of any set of excitation parameters:**

**Table C.2 Response values without using any set of excitation parameters**

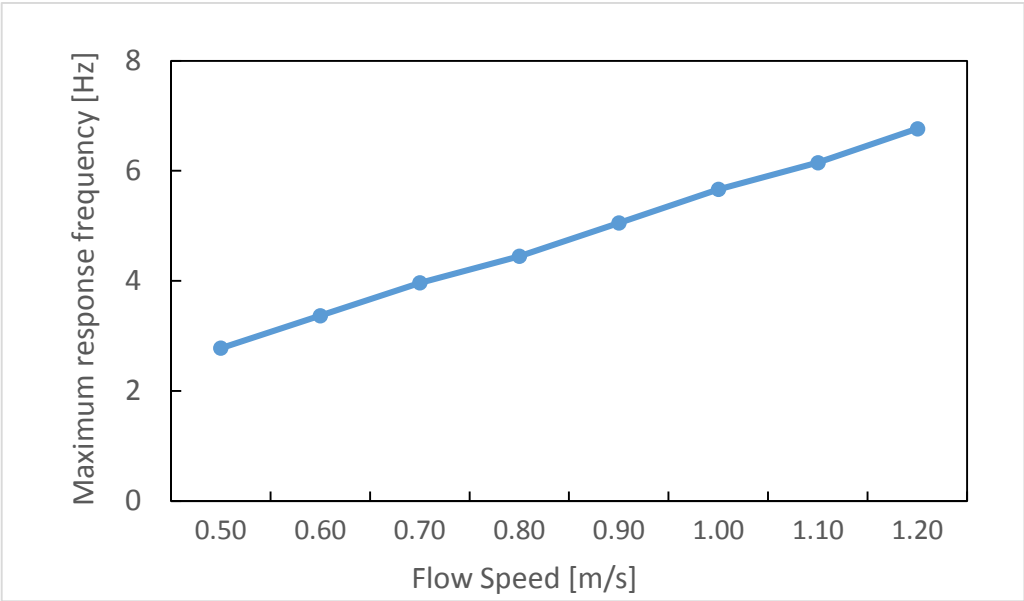
Flow speed [m/s]	Maximum accumulated damage [1/year]	Bare riser	
		Mode no.	Frequency [Hz]
0.50	5.24E-03	4	2.778
0.60	3.57E-02	5	3.369
0.70	1.60E-01	6	3.965
0.80	1.57E-01	7	4.449
0.90	5.42E-01	7	5.053
1.00	1.56E+00	8	5.663
1.10	1.46E+00	8	6.149
1.20	3.67E+00	9	6.766

Figure C.3 shows the maximum fatigue damage with towing speed for bare riser without using default set of parameters.



**Figure C.3 Maximum accumulated damage without using any set of excitation coefficients – bare riser.**

Figure C.2 shows the variation of response frequency with towing speed for bare riser by using default set of parameters.



**Figure C.4 Maximum response frequency without using any set of excitation parameters– bare riser.**